AFRL-HE-WP-TR-2002-0047

UNITED STATES AIR FORCE
RESEARCH LABORATORY

Multilayer Optical Filters for Automatic Detection of Analytes In Mixtures with Interferrants – Basic Research in Materials and Techniques

Michael L. Myrick

University of South Carolina
Office of Sponsored Programs
901 Sumter Street, Room 51
Columbia SC 29208

August 2001
Final Report - June 2000 – June 2001

20021011 000

Human Effectiveness Directorate
Deployment and Sustainment Division
Operational Toxicology Branch
Chemical and Biological Defense Group
E5183 Blackhawk Road
Aberdeen Proving Ground MD 21010-5424

DISCLIAMER

This Technical Report is published as received and has not
been edited by the Technical Editing Staff of the Air Force Research Laboratory.

TECHNICAL REVIEW AND APPROVAL

AFRL-HE-WP-TR-2002-0047

This report has been reviewed by the Office of Public Affairs (PA) and is releasable to the National Technical Information Service (NTIS). At NTIS, it will be available to the general public, including foreign nations.

This technical report has been reviewed and is approved for publication

FOR THE DIRECTOR

STEPHEN R. CHANNEL, Lt Col, USAF, BSC
Director, AF CBD Tech Base Programs
Air Force Research Laboratory

REPORT DOCUMENTATION PAGE

1. AGENCY USE ONLY *(Leave blank)*	2. REPORT DATE	3. REPORT TYPE AND DATES COVERED
	13 August 2001	Interim Report, 13 Jun 2000 - 12 June 2001

4. TITLE AND SUBTITLE

Multilayer Optical Filters for Automatic Detection of Analytes in Mixtures with Interferrants - Basic Research in Materials and Techniques

6. AUTHOR(S)

Michael L. Myrick

5. FUNDING NUMBERS

Contract: F33615-00-2-6059
PE 61384B
PR 0600
TA 060001
WU 06000101

7. PERFORMING ORGANIZATION NAME(S) AND ADDRESS(ES)

University of South Carolina
Office of Sponsored Programs
901 Sumter Street, Room 51
Columbia SC 29208

8. PERFORMING ORGANIZATION REPORT NUMBER

9. SPONSORING/MONITORING AGENCY NAME(S) AND ADDRESS(ES)

Air Force Research Laboratory, Human Effectiveness Directorate,
Deployment and Sustainment Division, Operational Toxicology Branch
Chemical and Biological Defense Group
E5183 Blackhawk Road
Aberdeen Proving Ground MD 21010-5424

10. SPONSORING/MONITORING AGENCY REPORT NUMBER

AFRL-HE-WP-TR-2002-0047

11. SUPPLEMENTARY NOTES

12a. DISTRIBUTION AVAILABILITY STATEMENT

Approved for public release; distribution is unlimited.

12b. DISTRIBUTION CODE

13. ABSTRACT *(Maximum 200 words)*

Research during the first year of the USC optical computing project demonstrated that multivariate optical elements (MOEs) could be designed, fabricated and characterized. Results of the first MOE tests revealed that near-theoretical performance could be obtained in the simple situations tested. New tools for designing MOEs were developed that bypass many anticipated problems. The limits of precision due to fabrication errors were assessed. Process control algorithms for fabrication that incorporate design tools permitted fabrication of MOEs with performance exceeding those expected theoretically for real fabricated devices; this was achieved by redesigning MOEs on the fly to offset deposition errors. Design concepts were developed for imaging tools based on MOEs, and initial demonstrations were begun for imaging applications. Mid-infrared, near-infrared and Raman spectra were acquired for nearly 50 organophosphorus compounds to explore the regions of the spectral that are most definitive for their detection.

14. SUBJECT TERMS

Organophosphorus, Optical Sensing, Standoff, Remote, Biological, Chemical, Detection

15. NUMBER OF PAGES

16. PRICE CODE

17. SECURITY CLASSIFICATION OF REPORT	18. SECURITY CLASSIFICATION OF THIS PAGE	19. SECURITY CLASSIFICATION OF ABSTRACT	20. LIMITATION OF ABSTRACT
Unclassified	Unclassified	Unclassified	SAR

THIS PAGE INTENTIONALLY LEFT BLANK

ii

TABLE OF CONTENTS

FIGURES

FIGURE   PAGE

1.0 INTRODUCTION

This report describes the first year of work conducted under this project, between 13 June 2000 and 12 June 2001. The organization of the report is as follows:

1. Aims
2. Findings of the Investigator during Y1
3. Comparison of Accomplishments with Goals
4. Chronological list of written publications
5. List of professional personnel associated with the project.
6. Related Activities: Meetings/Conferences
7. Related Activities: Discoveries and Inventions
8. Other Grants Related to F33615-00-2-6059
9. Appendixes

2.0 AIMS

Broadly, the purpose of this project is to explore the idea of using simple optical elements to do the job of more complex and costly spectroscopic hardware in measuring chemical concentrations and determining chemical composition via optical spectroscopy. Work of this type is called multivariate optical computing, a name given it in a 1998 publication in the journal Analytical Chemistry.

The underlying theme of this work is that the spectroscopic patterns that provide meaningful chemical information in complex systems can be encoded into the spectrum of a simple optical interference filter. To ascertain whether this is feasible, and if feasible then under what conditions and with what certainty, this project explores the basic theory of multivariate optical computing as well as the materials, algorithms and systems used for bringing the concept to life.

In pursuit of this aim, the USC research team undertook a wide variety of investigations. Among these were development of design algorithms, measurements of optical spectra of samples in transmittance, diffuse reflectance and grazing angle specular reflectance, process control algorithms, theoretical analysis of the limitations of our ability to fabricate optics, spectral radiometry of detectors and light sources, construction of prototype systems, construction of imaging systems, measurements of the optical constants of materials used in fabrication, literature searches and reviews, plus measurements of organic materials, thin films and other processes for making defined interference layers. The following report describes some of the salient features of the work during Year 1.

3.0 FINDINGS OF THE INVESTIGATOR DURING YEAR 1

3.1 SYNTHESIS OF MULTIVARIATE OPTICAL ELEMENTS FOR POINT MEASUREMENTS

A major focus of the USC research during Y1 was to develop and improve tools for the design of multivariate optical elements (MOEs). All initial work (prior to the beginning of this program) was aimed at spectral matching algorithms (SMAs). SMAs are used to design MOEs by attempting to design a thin-film structure whose interference-governed spectrum matches a desired target spectrum. The "match quality" of the filter spectrum to the target spectrum was characterized by a figure of merit (FOM) that generally expresses the percent transmission difference between the two across a range of wavelengths. Target spectra were derived from chemometric interpretation of sample spectroscopy. SMAs are conceptually and practically identical to design methods for any type of tailored-spectrum optical interference filter, including the very sophisticated commercially-available packages used by thin-film designers at custom coating houses. While such algorithms have been well known, they are by no means easy to implement for general MOE design. There are serious problems, both conceptual and practical, relating to how well data noise should be included in the target spectrum, for example. In addition, relating the film thickness sensitivities for layers of a MOE to the chemical prediction quality desired for an MOE is by no means straightforward or simple. Thus it was recognized at the beginning of this project that SMAs are not ideal for MOE design.

The USC team undertook software development for the synthesis of interference coatings based on a "standard error of prediction" figure of merit. This new design algorithm bypasses many of the problems associated with the old SMA approach by finding an optimal design for the MOE at each given level of MOE complexity.

This work began with a written code that calculates the transmittance of a multilayer film as a function of angle, wavelength and optical constants, including absorbance. The second stage of the work was the incorporation of this algorithm into an optimization code. This optimization code at the moment uses a pseudo-Newton gradient descent algorithm to optimize the thicknesses of materials in a multilayer that is given it as a starting point. A number of permutations on this basic theme were tried. The USC team has thus far found that random starting positions for optimization are preferable to a SMA-derived starting point. The ultimate reason behind this remains essentially unknown; one possible explanation is that an SMA-derived starting point limits the available space that can be sampled easily during optimization. Random starting points have generally produced results that outperform SMA-initiated optimizations.

The new algorithms have been the subject of both a manuscript (currently submitted) and a preliminary patent application. Both are appended to this report.

3.2   MANUFACTURING TOLERANCES

The question of how closely a fabricated filter has to match its objective, theoretical spectrum before its performance as an MOE degrades was addressed by the USC team. This question is of great importance in determining whether it is feasible to manufacture an MOE suitable for general application. Theory was developed on this topic by taking a conservative approach to tolerance. The USC team used a "bandpass selection" filter set to select the spectral region in which a MOE should work. The new theory provides an exact definition for the actual bandpass region of importance, and how the spectral tolerances where the band begins and ends. It also tells us how the tolerance changes with wavelength.

The key equations of note were found to be:

$$1. \qquad \Delta t(\lambda) = \frac{V_{co}}{V(\lambda)},$$

$$2. \qquad V_{ex} + V_{co}(\lambda_R - \lambda_L) - \frac{SEP^2}{2k} = 0$$

In equation 1, V stands for variance, Δt is the tolerance in transmittance, co means "at the cutoff wavelength", and λ is wavelength. In equation 2, SEP is the standard error of prediction in the calibration, R and L mean "at the right and left cutoffs", respectively. ex means "excluded", and k is the gain factor relating the regression vector to the predicted value. These two equations are of principal importance in determining the permissible error tolerance in filter design and manufacturing, and for determining the bandpass of the coating. Their derivation and use are described in the attached manuscript, "Fixed Tolerance Determination for Multivariate Optical Elements" which was published in Fresenius J. Anal. Chem.

The consequence of this investigation was the finding that ideal performance in an MOE would be extremely difficult to achieve in practice. In the specific example chosen for the manuscript, the designed MOE required some spectral regions to have 0.2% errors in transmittance or better for ideal performance. This level of error was found to be unachievable in practice for a fixed design. That is, the accumulated error expected in the fabrication of a fixed-design MOE would quickly mount to levels greater than the theoretical tolerance at the most critical wavelengths. This lead the USC team to the "variable-design" MOE concept that is a subject of current, ongoing research.

3.3   DEMONSTRATION OF MULTIVARIATE OPTICAL COMPUTING

The USC team completed the SEP coating synthesis programming and applied it to two simple chemical problems to determine how this solution to film design works. One of these examples is shown below as Figure 1.

3

Figure 1. Binary dye spectra corrected for source radiance detector response, and filter bandpass.
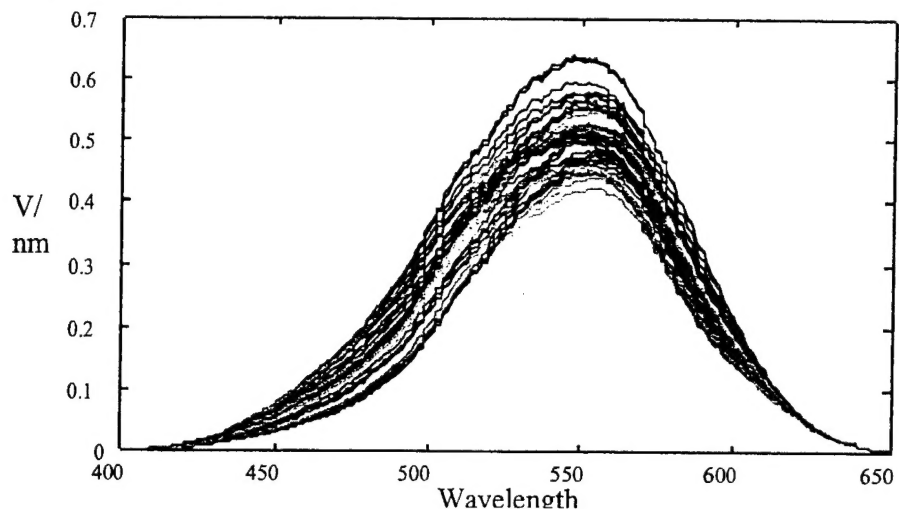
Figure 1 gives a set of optical spectra for mixtures of two dyes. The two dyes have optical spectra that overlap one another throughout the wavelength region covered. The samples were made by random generation so that the concentrations of the two dyes are independent of one another. Consequently, each dye other simulates a random interfering species for measurement of the other.

Simple bandpass filtering was found to work poorly for the measurement of the target chemical species in the mixture represented in Figure 1. The SEP approach, on the other hand, gave the spectral design illustrated in Figure 2 below.
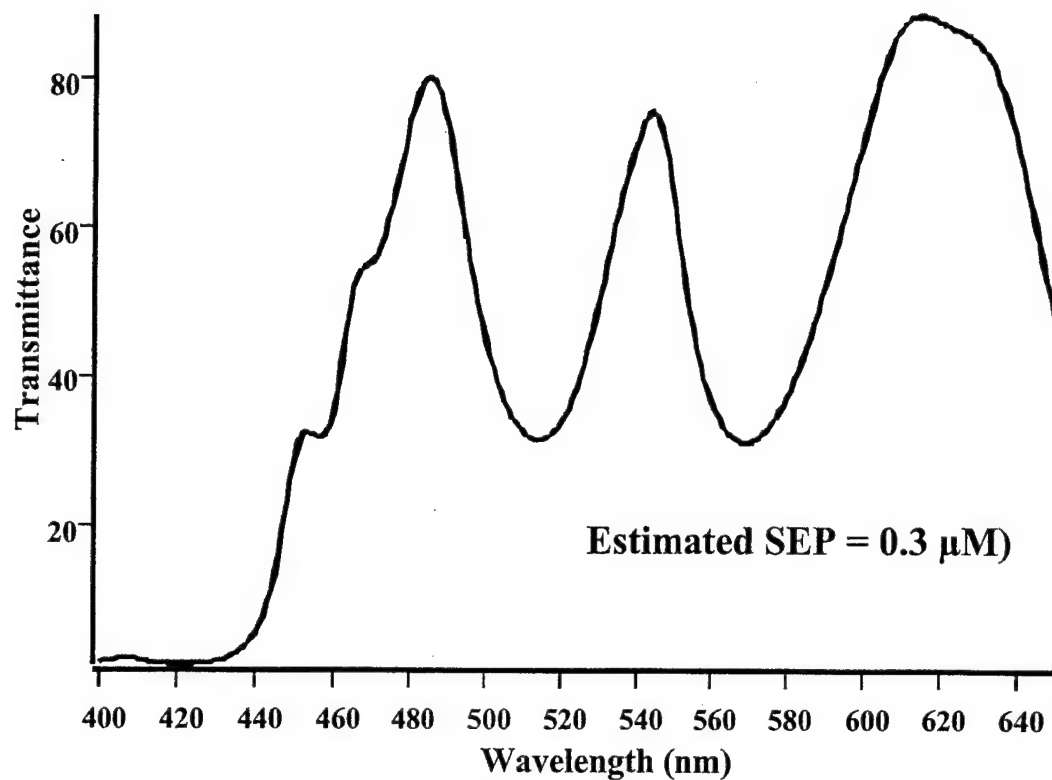
Figure 2. Theoretical transmittance spectrum of an MOE designed
for the data in Figure 1 at 45 degrees angle of incidence.

Figure 3 shows the result of actual manufacture of this coating (at normal incidence, not the 45 degrees incidence at which it would be used).
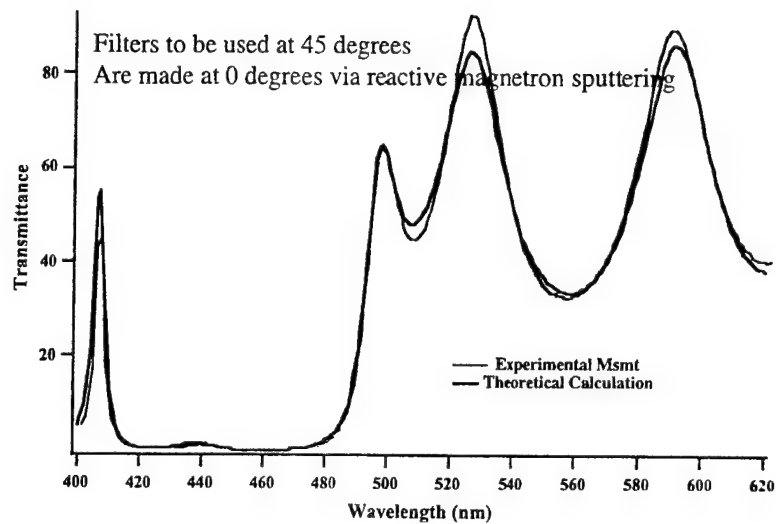
Figure 3. Real (as fabricated) and theoretical spectrum of the MOE
in Figure 2 at 0 degrees angle of incidence.

Figure 4 below shows a schematic of the point-detection system into which the Figure 3 MOE
was placed for demonstration purposes. Figure 5 shows a photograph of the actual prototype
instrument.
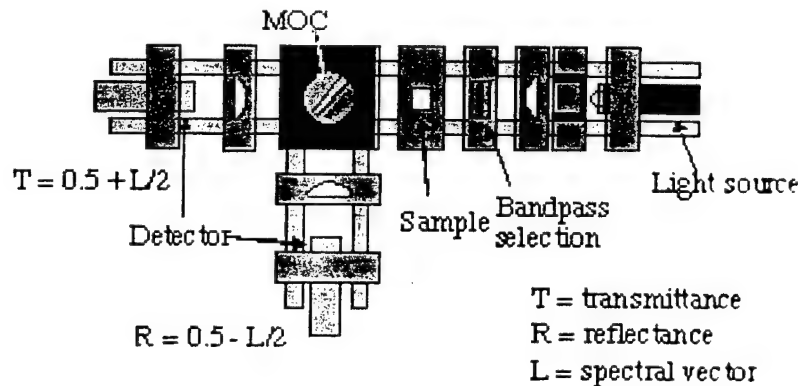
Figure 4. Schematic of Multivariate optical computing prototype
system for single-point transmission measurements.

The actual prototype is shown in the following photograph:

6
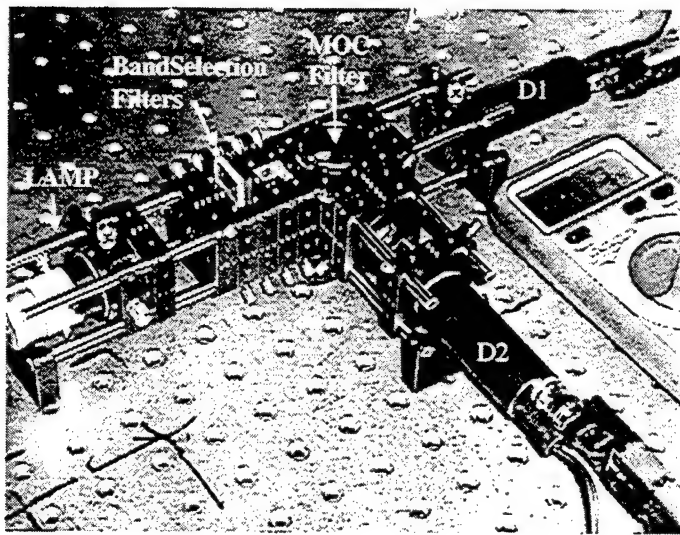
Figure 5. Photograph of prototype system illustrated in Figure 4.

Figure 6 shows that the system obtained 0.68 μM SEP rather than 0.3 μM, which was the theoretical optimum. The reduction in precision was found to be due to (a) imprecision in the manufacture of the MOE and (b) the algorithm for design that was limited to a single angle of incidence (no angular dispersion).
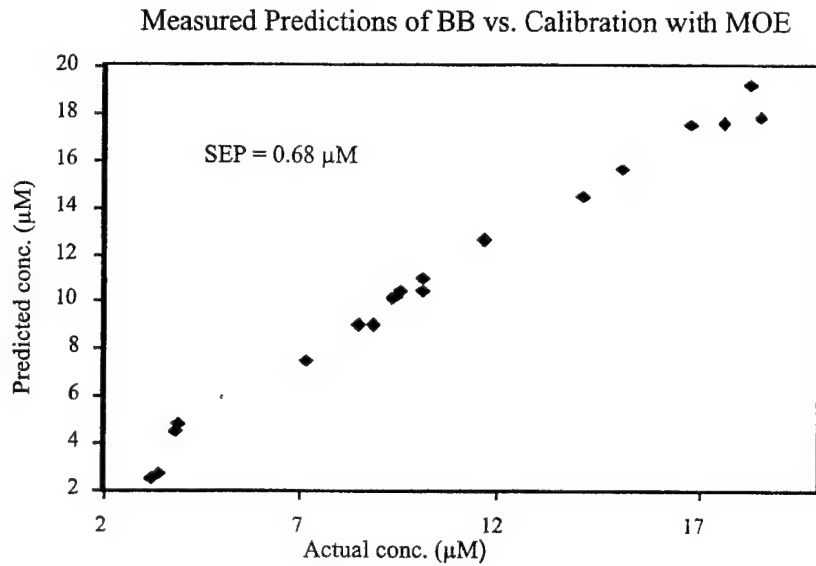
Figure 6. Results from the MOE built for demonstration purposes.

3.4 ANGLE-INVARIANT MOEs FOR IMAGING SPECTROSCOPY

As mentioned above, early forms of MOEs were designed to work with collimated light (see Figure 7 below).
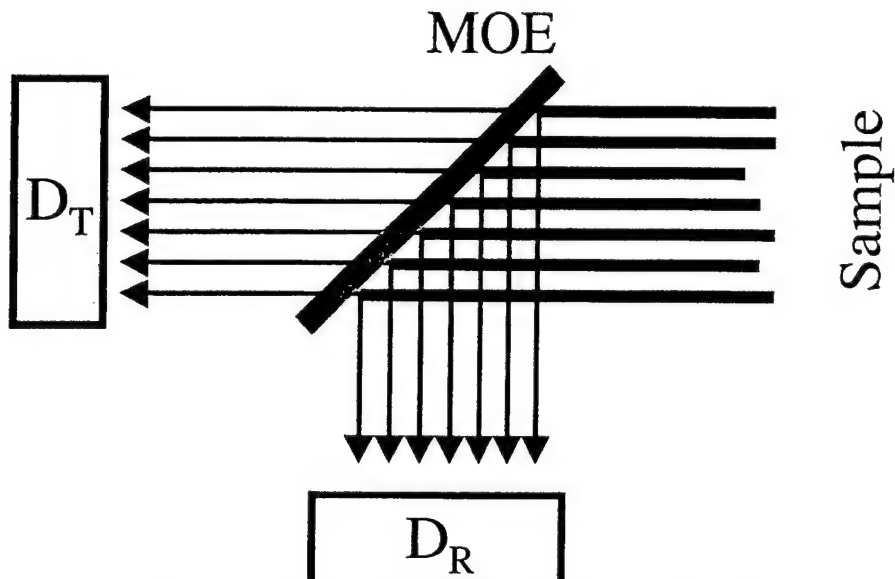
Figure 7 – Schematic of the operation of a collimated-light MOE

Imaging applications require the analysis of light from various angular positions in a field of view. This is illustrated in Figure 8 below.
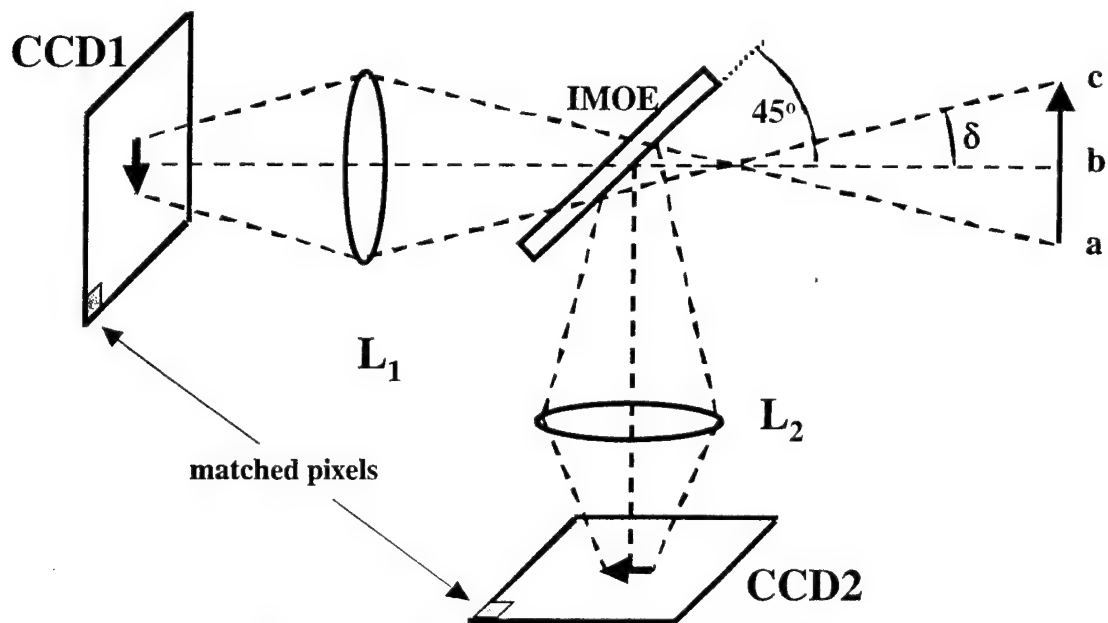
Figure 8 – angular distribution for an imaging MOE (IMOE)

In order to accomplish this, a new algorithm was developed that simulated the effects on the MOE spectrum of light impinging from different angles, and that optimizes the average prediction error over the entire angular range. The performance of this algorithm is illustrated in Figure 9, which shows the prediction error for the MOE from the last section as the angle deviates from its designed angle of 45 degrees, and compares it to an IMOE designed for the same measurement.
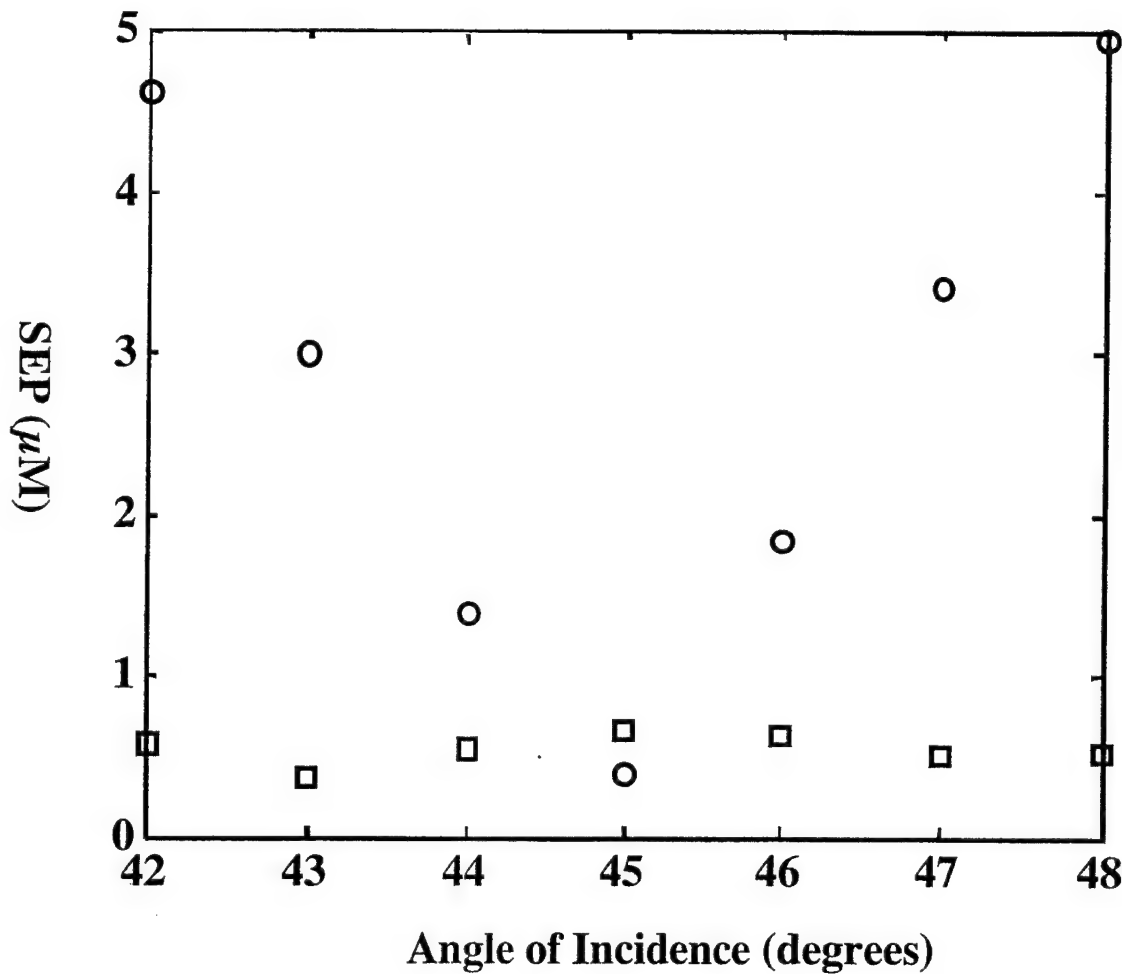
Figure 9. SEP as a function of angle for MOEs designed for 45-degree operation. (circles) SEP for the point MOE designed in the last section. (squares) SEP for an IMOE designed with the new angle-invariant algorithm.

The explanation for how a MOE can be designed for optimal performance over a range of incident angles is explained in the appended manuscript describing the algorithm.

3.5 NEAR-INFRARED AND MID-INFRARED SPECTROSCOPY OF ORGANOPHOSPHOROUS COMPOUNDS

A goal for the first year of this project was to record the near-infrared and mid-infrared spectroscopies of a number of organophosphorous compounds. 47 compounds were selected; their structures and spectra are appended to this report.

Of particular interest is the near-infrared spectral region, which contains overtone and combination band absorbances. Only two of the compounds studied this year differed in the nature of the atom doubly-bonded to phosphorous. Tetraethylpyrophosphate and tetraethyldithiopyrophosphate differ only in that the former contains oxygen, while the latter contains sulfur, doubly-bonded to phosphorous. The near-infrared spectroscopy of these com-
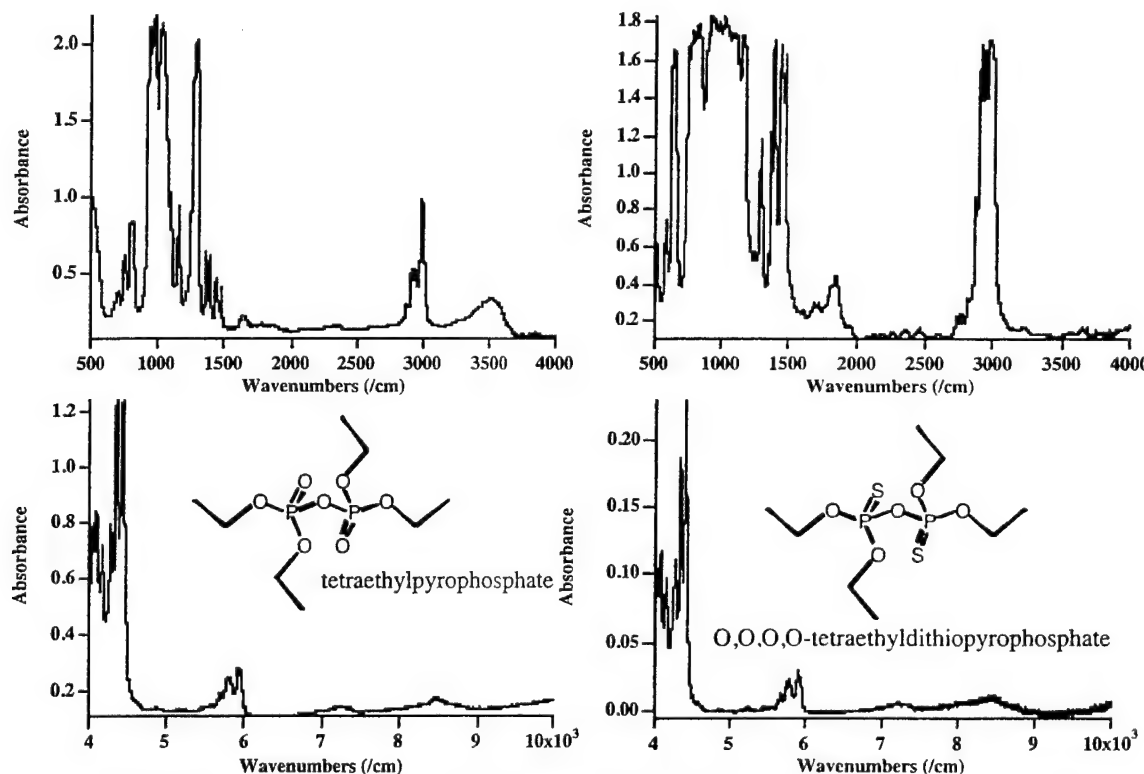
Figure 10. Spectroscopy of tetgraethylpyrophosphate (left) and tetraethyldithiopyrophosphate(right).
Top: mid-infrared absorbance. Bottom: near-infrared absorbance.

pounds exhibits a combination band that is distinctly different in the two species, and is strongly correlated with the behavior of two bands appearing in the mid-infrared spectral region. Specifically, two mid-infrared modes for the oxygen species at 1371.1 and 1445.9 cm^{-1} couple with a C-H stretching vibration at 2987.2 cm^{-1} to produce combination bands at 4345.8 and 4431.6 cm^{-1}. For the sulfur species, modes at 1367.8 and 1443.5 cm^{-1} couple with a C-H vibration at 2976.1 cm^{-1} to form combination bands at 4340.5 cm^{-1} and 4425.9 cm^{-1}. The importance of these modes is that they reproduce in the near-infrared the observed differences in the mid-infrared. The mid-IR modes (between 6.9 and 7.1 micrometer wavelength) are

10

diagnostic for the P=S and P=O assignment in these molecules. However, they occur at a wavelength that is very difficult to measure due to blackbody emission and other for other reasons. The combination bands show the same intensity differences that the fundamentals show, but appear between 2.2 and 2.3 micrometers in wavelength. This wavelength region is transparent to high-quality silica optics and can be measured with higher-quality detectors. While the intrinsic strength of these absorbances is an order of magnitude less than those in the mid-infrared region, much of that loss can be compensated by improved detector quality and the loss of the blackbody continuum background that is so troublesome in both active and passive measurement of the mid-infrared region.

Optical spectra, including Raman spectra, of all samples have been obtained, but the research is still in progress to the extent that a detailed analysis of the optical spectra is still being performed. Preliminary data is available to DOD chemical researchers on request. An appendix of this report gives the names of the compounds studied, plus the types of spectra available for them. A report detailing the optical spectra of these samples will be prepared during year 2.

4.0 COMPARISON OF ACCOMPLISHMENTS WITH GOALS DURING YEAR 1

The following figure shows the expected progress during Y1 and compares it to the actual progress.
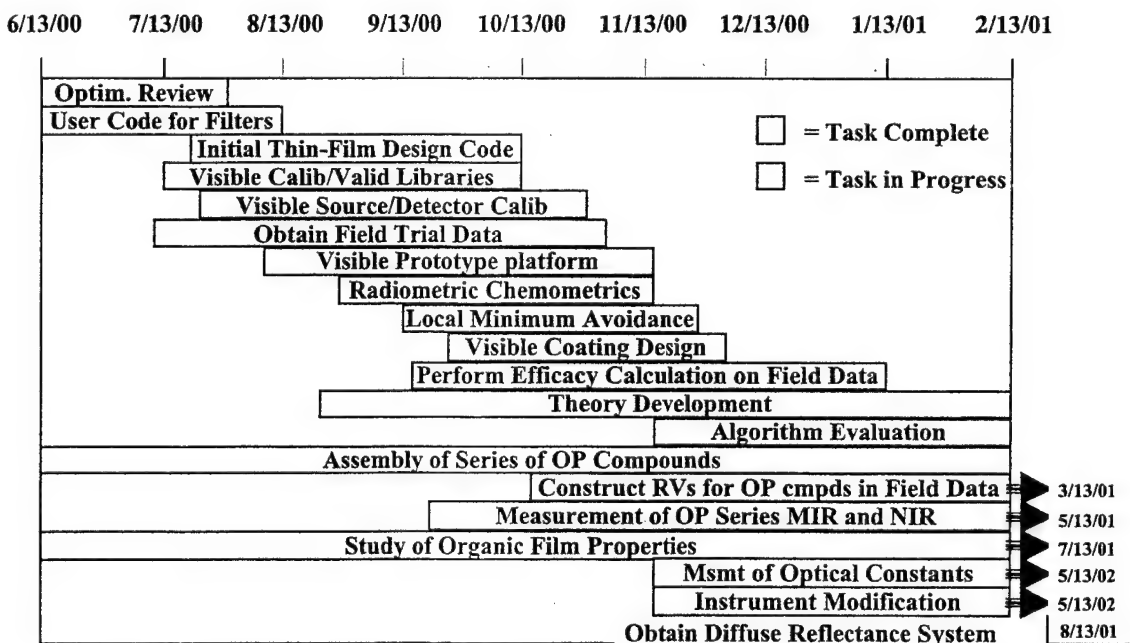
Figure 11. Estimated Schedule of task completion for Y1. All tasks listed have been completed.

All tasks scheduled for Y1 were completed on or ahead of schedule if they were (a) possible and (b) not superseded by new discoveries. Thus, some of the original parts of algorithm

development were superceded by discoveries of novel and improved methods for designing MOEs. Also, while field trial data were obtained from Air Force sources, the data were inadequate for the scheduled efficacy calculation. Nevertheless, the Myrick group was able to show for one of the data sets that a multivariate regression vector could be developed for dimethylmethylphosphonate in the field trial data that performed comparably to the algorithms used in the field test.

The setup of a diffuse reflectance system was completed during Y1, although it was not scheduled until early Y2, and it is listed in the figure.

5.0   CHRONOLOGICAL LIST OF WRITTEN PUBLICATIONS

Spectral Tolerance Determination for Multivariate Optical Element Design
    M.L. Myrick, S. Soyemi, H. Li, L. Zhang and D. Eastwood
    Fres. J. Anal. Chem. 369(2001), 351.

Spectroelectrochemical Study of the Oxidative Doping of Polydialkylphenyleneethynene using Iterative Target Transformation Factor Analysis
    Una Evans, O. Soyemi, M. Doescher, U. Bunz, L. Kloppenberg, M.L. Myrick
    Analyst 126 (2001), 508.

Field Applications of Stand-off Sensing using Visible/NIR multivariate optical computing.
    D. Eastwood, O. Soyemi, J. Karunamuni, L. Zhang, H. Li, and M.L. Myrick
    SPIE 4199 (2001), 105.

Design and Testing of a Multivariate Optical Element (MOE): The First Demonstration of Multivariate Optical Computing for Predictive Spectroscopy
    O. Soyemi, D. Eastwood, L. Zhang, H. Li, J. Karunamuni, P. Gemperline, R.A. Synowicki, M.L. Myrick
    Anal. Chem. 73 (2001), 1069.

Novel Filter Design Algorithm for Multivariate Optical Computing
    O.O. Soyemi, P.J. Gemperline, L. Zhang, D. Eastwood, H. Li, and M.L. Myrick
    SPIE 4205 (2001), 288.

Simple Optical Computing Device for Chemical Analysis
    O.O. Soyemi, P. J. Gemperline, L. Zhang, D. Eastwood, H. Li,, and M.L. Myrick
    SPIE 4284 (2001), 17.

Interference Filter Refinement for Array-Based Fluorescimetric Sensing
    J. Karunamuni, K.E. Stitzer, D. Eastwood, K.J. Albert, D.R. Walt, S.B. Brown and M.L. Myrick
    Optical Engineering 40 (2001), 888-95.

A Single-Element All-Optical Approach to Chemometric Prediction

M.L. Myrick, O. Soyemi, J. Karunamuni, D. Eastwood, H.Li, L. Zhang and P. Gemperline
Vibrational Spectroscopy (in press, 2000).

A Nonlinear Optimization Algorithm for Multivariate Optical Element Design
      O.O. Soyemi, P.J. Gemperline, L. Zhang, D. Eastwood, H. Li and M.L. Myrick
      J. Chemometrics (submitted, 2001).

Design of Angle-Tolerant Multivariate Optical Elements for Chemical Imaging
      O.O. Soyemi, P.J. Gemperline, M.L. Myrick
      Appl. Optics. (submitted, 2001).

Error Compensation in Multivariate Optical Element Fabrication via Layer-by-Layer Redesign
      F. G. Haibach, O. O. Soyemi, P.J. Gemperline, A.E. Greer, M. V. Schiza and M.L. Myrick
      (manuscript in preparation, 2001).

6.0 LIST OF PROFESSIONAL PERSONNEL ASSOCIATED WITH THE PROJECT

Michael L. Myrick, Associate Professor and Principal Investigator
J. Karunamuni, postdoctoral associate (ending 9/00)
L. Zhang, postdoctoral associate (ending 5/00)
Y. Yan, postdoctoral associate
U. Evans, postdoctoral associate (beginning 3/01)
M.V. Schiza, postdoctoral associate (beginning 5/01)
D. Eastwood, postdoctoral associate (ending 6/01)
O.O. Soyemi, postdoctoral associate (ending 7/01)
F.G. Haibach, postdoctoral associate (beginning 8/01)
A.E. Greer, graduate associate (beginning 5/01)
P.E. Colavita, graduate associate (beginning 5/01)
H. Li, graduate associate

7.0 RELATED ACTIVITIES: MEETINGS AND CONFERENCES

An All-Optical Approach to Multivariate Prediction
      M.L. Myrick
      Presented at Shedding New Light on Disease: Biodiagnostics in the New Millenium, Winnipeg, Canada, June 25-28, 2000.

A Spectroelectrochemical Study of Poly(p-Phenyleneethynylene) Based Polymers
      U.M. Evans, H. Li and M.L. Myrick
      Presented at Federation of Analytical Chemistry and Spectroscopy Societies, Nashville, TN Sept 24-28, 2000.

Optical Computing
        D. Eastwood, O. Soyemi, J. Karunamuni, L. Zhang, H. Li and M.L. Myrick
        Presented at Federation of Analytical Chemistry and Spectroscopy Societies, Nashville,
        TN Sept 24-28, 2000.

Interference Coating Design for Optical Computing Using Multivariate Nonlinear Optimization
        O. Soyemi, P. Gemperline, J. Karunamuni, L. Zhang, H.Li, D. Eastwood and M.L.
        Myrick
        Presented at Federation of Analytical Chemistry and Spectroscopy Societies, Nashville,
        TN Sept 24-28, 2000.

Novel Filter Design Method for Multivariate Optical Computing
        O. Soyemi, P.J. Gemperline and M.L. Myrick
        Presented at the Southeast Regional Meeting on Optoelectronics, Photonics and Imaging,
        Charlotte, NC, Sept. 18-19, 2000.

Preliminary Results of Stand-Off Sensing Using Visible/NIR Multivariate Optical Computing
        D. Eastwood, J. Karunamuni, O. Soyemi, H. Li and L. Zhang
        Presented at the Southeast Regional Meeting on Optoelectronics, Photonics and Imaging,
        Charlotte, NC, Sept. 18-19, 2000.

Recent Work in Multivariate Optical Computation
        M.L. Myrick, O. Soyemi, D. Eastwood, L. Zhang, H. Li, J. Karunamuni
        Presented at Southeast Association of Analytical Chemistry Conference, Greenville,
        NC, Oct. 5-7, 2000.

AFM of electrochemically doped conducting polymers
        M.S. Doescher, U.M. Evans, and M.L. Myrick
        Presented at Southeast Association of Analytical Chemistry Conference, Greenville,
        NC, Oct. 5-7, 2000.

Preliminary Results of Stand-Off Sensing Using Visible/NIR Multivariate Optical Computing
        M.L. Myrick, D. Eastwood, J. Karunamuni, O. Soyemi, H. Li and L. Zhang
        Presented at Joint Conference on Point Detection, Williamsburg, VA Oct 22-26, 2000.

Comparison of two novel approaches to designing interference coatings for multivariate optical
computing
        O. Soyemi, P. Gemperline, J. Karunamuni, L. Zhang, H. Li, D. Eastwood, M. L. Myrick
        Presented at SPIE Photonics East Conference, Boston, MA, Nov 5-9, 2000.

A Process Optimization Procedure for Mulivariate Optical Element (MOE) Manufacture
        O. O. Soyemi, P. Gemperline and M.L .Myrick
        Presented at the Pittsburgh Conference on Analytical Chemistry, New Orleans, LA,
        March 4-9, 2001.

An Electrochemical Investigation of Electroluminescent Conjugated Polymers
    U. Evans, U.H.F. Bunz, H. Li and M.L. Myrick
    Presented at the Pittsburgh Conference on Analytical Chemistry, New Orleans, LA,
    March 4-9, 2001.

Atomic Force Microscopy of Electrochemically Doped Conducting Polymers
    M.S. Doescher, U. Evans and M.L. Myrick
    Presented at the Pittsburgh Conference on Analytical Chemistry, New Orleans, LA,
    March 4-9, 2001.

Advances in Standoff Sensing Using Visible-NIR Optical Computing
    M.L. Myrick, D. Eastwood, J. Karunamuni, O. Soyemi, H. Li and L. Zhang
    Presented at the Pittsburgh Conference on Analytical Chemistry, New Orleans, LA,
    March 4-9, 2001.

Simple optical computation device for chemical analysis
O. Soyemi, R. Karunamuni, Univ. of South Carolina; P. J. Gemperline, L. Zhang, H. Li, D.
    Eastwood, M. L. Myrick
    Presented at SPIE Photonics West Conference, San Jose, CA, Jan. 20-26, 2001.

Chemical Sensing via Multivariate Optical Computing
    M.L. Myrick, O.O. Soyemi, H. Li and P.J. Gemperline
    Presented at the International Symposium on Spectral Sensing Research (ISSSR), Quebec
    City, Canada, June 10-15, 2001.

8.0   DISCOVERIES AND INVENTIONS

Novel Filter Design Algorithm for Multivariate Optical Computing
Inventors: M.L. Myrick, O. O. Soyemi, and P.J. Gemperline
Provisional Patent Application Number: 60/235,336.

9.0   OTHER GRANTS RELATED TO F33615-00-2-6059

The most recent grant to support research related to that of F33615-00-2-6059 was grant number
DOD-N-000014-97-1-0806, received by the University of South Carolina and in effect from
6/1997-6/2000. The University received a 1-year no-cost extension of this grant from the Office
of Naval Research for accounting purposes, although no new work was done that was attributed
to the ONR grant after 6/00. This is the grant that provided support for the acquisition of the
visible-light deposition system used during Y1 of the present grant. Publications that were
attributed to both DOD-N-000014-97-1-0806 AND F33615-00-2-6059 were:

Spectral Tolerance Determination for Multivariate Optical Element Design
    M.L. Myrick, S. Soyemi, H. Li, L. Zhang and D. Eastwood
    Fres. J. Anal. Chem. 369(2001), 351.

Interference Filter Refinement for Array-Based Fluorescimetric Sensing
> J. Karunamuni, K.E. Stitzer, D. Eastwood, K.J. Albert, D.R. Walt, S.B. Brown and M.L. Myrick
> Optical Engineering 40 (2001), 888-95.

Field applications of stand-off sensing using visible/NIR multivariate optical computing
> D. Eastwood, O. Soyemi, J. Karunamuni, L. Zhang, H. Li, and M.L. Myrick
> SPIE 4199 (2001), 105.

Novel Filter Design Algorithm for Multivariate Optical Computing
> O.O. Soyemi, P.J. Gemperline, L. Zhang, D. Eastwood, H. Li, and M.L. Myrick
> SPIE 4205 (2001), 288.

For these four publications, acknowledgement of DOD-N-000014-97-1-0806 was for the support of Lixia Zhang and Jeevananda Karunamuni prior to the start of F33615-00-2-6059. All research for these reports (EXCEPT the Optical Engineering report) was conducted in 6/00 and thereafter under the total support of F33615-00-2-6059. Research for the OE report was conducted prior to the beginning of F33615-00-2-6059 with ONR and DARPA support. F33615-00-2-6059 was acknowledged for supporting the salary of D. Eastwood during revision of the manuscript in the summer of 2000.

The ONR grant supported work in molecular computing and fiber-optic technique development, plus optical computing for image and data compression. Other reports totally or partially attributed to DOD-N-000014-97-1-0806, with no attribution to F33615-00-2-6059 are:

The Use of a 2D to 1D Dimension Reduction Fiber-Optic Array for Multi-Wavelength Imaging Sensors
> M. V. Schiza, M. P. Nelson, M. L. Myrick, S. M. Angel
> Appl. Spectrosc. 55 (2001), 217.

Stripping Voltammetry of Cu Overlayers Deposited on Self-Assembled Monolayers: Field Emission of Electrons Through A Phenylene Ethynylene Oligomer
> M.S. Doescher, A. Rawlett, J.M. Tour and M.L. Myrick
> J. Phys. Chem. B 105(2001), 105.

Fluorescence Fingerprint of Waters: Excitation-Emission Matrix Spectroscopy as a Tracking Tool
> Y. Yan, H. Li and M.L. Myrick
> Appl. Spectrosc. 54 (2000), 1539.

Simple Techniques for Chemical Imaging at Many Wavelengths Simultaneously, Using a Novel 2D to 1D Optical Fiber Array
> S.M. Angel, M.V. Schiza, M.L. Myrick and M.P. Nelson
> SPIE 4074 (2000), 99.

Kinetic and Spectroscopic Profiles of Pyridine Complexes at a Silver Electrode Using Surface-Enhanced Raman Scattering (SERS) and Evolving Factor Analysis
>M.A. Nicholson, J.F. Aust, K.S. Booksh, W.C. Bell and M.L. Myrick
>Vibrational Spectroscopy 24 (2000), 157.

The Lowest Electronic Excited States of poly(*para*-cyclobutadienylenecyclopentadienyl-cobalt)butadiynylene
>B. Craig Harrison, J. Seminario, U. Bunz and M.L. Myrick
>J. Phys. Chem. 104 (2000), 5937.

Simultaneous Enantiomeric Determination of Dansyl-D,L-Phenylalanine by Fluorescence Spectroscopy in the Presence of _-Acid Glycoprotein
>Yuan Yan and M.L. Myrick
>Anal. Chem. 71(1999), 1958.

Time-dependent multivariate single-frame chemical imaging spectroscopy of laser plumes using a dimension reduction fiber optic array"
>M. P. Nelson, M. L. Myrick
>SPIE 3649(1999), 92-99.

Thermodynamic Characterization of Separation Phenomena at the Silica/Polymer Interface within Glass-Reinforced Composites using Adsorption Chromatography. Part I.
>A.R. Muroski, M.P. Nelson and M.L. Myrick
>J. Adhesion Sci. Technol. 13(1999), 437.

Fabrication and Evaluation of a Dimension-Reduction Fiber-Optic System for Chemical Imaging Applications
>M.P. Nelson and M.L. Myrick
>Rev. Sci. Instrum. 70(1999), 2836.

Single-Frame Chemical Imaging: Dimension Reduction Fiber-Optic Array Improvements and Application to Laser-Induced Breakdown Spectroscopy.
>M.P. Nelson and M.L. Myrick
>Appl. Spectrosc. 53(1999), 751.

New Developments in Two-Dimensional Fluorescence Spectroscopy for Rapid Detection of Organics in Seawater
>M.L. Myrick and Y. Yan
>SPIE 3854 (1999), 65.

New Approaches to Implementing Predictive Spectroscopy
>M.L. Myrick
>SPIE 3854 (1999), 98.

Assignment of the Optical Transitions in 1,3-Diethynylcyclobutadiene (cyclopentadienyl)cobalt Oligomers
> H. Rengel, M. Altmann, D. Neher, B.C. Harrison, M.L. Myrick and U.H.F. Bunz
> J. Phys. Chem. 103(1999),10335.

High-Speed Detection of Explosives.
> K.J. Albert, M.L. Myrick, S.B. Brown, F.P. Milanovich and D.R. Walt
> SPIE 3710 (1999), 308.

Hyperspectral Imaging Sensors Using a Novel 2D to 1D Fiber Array
> M.V. Schiza, M.P. Nelson, M.L. Myrick, and S.M. Angel
> SPIE 3860 (1999), 317-325.

10.0 APPENDIXES

The appendixes include the following sections.

10.1 SPECTRAL TOLERANCE DETERMINATION FOR MULTIVARIATE OPTICAL ELEMENT DESIGN

This is a manuscript that describes the permissible error limits in design or manufacturing of optics for multivariate optical computing

10.2 SPECTROELECTROCHEMICAL STUDY OF THE OXIDATIVE DOPING OF POLYDIALKYLPHENYLENEETHYNENE USING ITERATIVE TARGET TRANSFORMATION FACTOR ANALYSIS

This manuscript describes the optical properties of an organic thin film prepared from a spin-cast polymer

10.3 FIELD APPLICATIONS OF STAND-OFF SENSING USING VISIBLE/NIR MULTIVARIATE OPTICAL COMPUTING.

This manuscript describes basic investigations at an initial stage for understanding multivariate optical computing.

10.4 DESIGN AND TESTING OF A MULTIVARIATE OPTICAL ELEMENT (MOE): THE FIRST DEMONSTRATION OF MULTIVARIATE OPTICAL COMPUTING FOR PREDICTIVE SPECTROSCOPY

This manuscript describes the USC Team's first successful demonstration of multivariate optical computing, and was featured on the cover of the journal Analytical Chemistry.

10.5 NOVEL FILTER DESIGN ALGORITHM FOR MULTIVARIATE OPTICAL COMPUTING

This manuscript describes a new concept and algorithm for designing optical elements for multivariate optical computing.

10.6 SIMPLE OPTICAL COMPUTING DEVICE FOR CHEMICAL ANALYSIS

This manuscript describes preliminary data for a multivariate optical element design and fabrication.

10.7 INTERFERENCE FILTER REFINEMENT FOR ARRAY-BASED FLUORESCIMETRIC SENSING

This manuscript describes an interference filter solution designed and constructed in the USC laboratory for application to fluorescence sensing of TNT vapors.

10.8 A SINGLE-ELEMENT ALL-OPTICAL APPROACH TO CHEMOMETRIC PREDICTION

This manuscript describes the basic concept of multivariate optical computing, and how it has evolved over the period 1998-2000 from two-filter to single-element designs.

10.9 A NONLINEAR OPTIMIZATION ALGORITHM FOR MULTIVARIATE OPTICAL ELEMENT DESIGN

This manuscript describes in detail the functioning and analysis of the novel design algorithm for multivariate optical elements reported earlier. In addition to describing the algorithm, it details how that algorithm can be used to compensate for fabrication errors during production.

10.10 DESIGN OF ANGLE-TOLERANT MULTIVARIATE OPTICAL ELEMENTS FOR CHEMICAL IMAGING

This manuscript describes a new concept for multivariate optical elements in which elements are designed to function with an angular distribution of light, such as that inherent in imaging applications.

10.11 LIST OF ORGANOPHOSPHORUS COMPOUNDS WHOSE MIR, NIR AND RAMAN SPECTRA HAVE BEEN MEASURED AT THE USC LABORATORY.

10.1 SPECTRAL TOLERANCE DETERMINATION FOR MULTIVARIATE OPTICAL ELEMENT DESIGN

SPECIAL ISSUE PAPER

M. L. Myrick · O. Soyemi · H. Li · L. Zhang
D. Eastwood

Spectral tolerance determination for multivariate optical element design

Abstract Recent reports from our laboratory have described a method for all-optical multivariate chemometric prediction from optical spectroscopy. The concept behind this optical approach is that a spectral pattern (a regression vector) can be encoded into the spectrum of an optical filter. The key element of these measurement schemes is the multivariate optical element (MOE), a multiwavelength interference-based spectral discriminator that is tied to the regression vector of a particular measurement. The fabrication of these MOEs is a complex operation that requires precise techniques. However, to date, no quantitative means of determining the allowable design/ manufacturing errors for MOEs has existed. The purpose of the present report is to show how the spectroscopy of a sample is used to define the accuracy with which MOEs must be designed and manufactured. We conclude this report with a general treatment of spectral tolerance and a worked example. The worked example is based on actual experimental measurements. We show how the spectral bandpass is defined operationally in a real problem, and how the statistics of the theoretical regression vector influence both the bandpass and the minimum tolerances. In the experimental example, we demonstrate that tolerances range continuously between 1 (totally tolerant) to approximately 10^{-3} (0.1% T) in this problem.

Introduction

Multivariate spectroscopy is a powerful tool for analytical determinations of the chemical and physical characteristics of a wide range of sample types via chemometrics. In one common approach for applying multivariate modeling to chemical problems, a spectral pattern that correlates with a dependent variable is found. In subsequent measurements of unknown samples, predictions of the dependent variable are made by computing the magnitude of this spectral pattern in the optical spectrum of the unknown [1].

A recent report from this laboratory [2] describes an all-optical approach to the last step in this procedure, the magnitude calculation given by the scalar product of a regression vector with the spectrum of an unknown sample. The first reports of a fully optical approach to multivariate chemical measurement were those of Bialkowski [3]. The all-optical approach proposed in our laboratory differs from Bialkowski's as it centers around the production of one or more optical interference coatings whose transmission spectra incorporate features of the spectral regression vector. A recently reported permutation on the original concept permits this pattern to be expressed in a single multivariate optical element (MOE) used as a 45-degree beamsplitter in a T-format instrument [4]. This permutation of the MOE based on chemometrics is most similar to a design proposed by Ryabenko and Kasparov [5].

MOEs of the type we have proposed can be designed by commercially-available software packages by assigning the desired spectral transmission profile of the MOE as a target for an iterative solution. However, these programs operate by successive approximations; exact solutions are not, in general, possible. To date, no report has been made of any method for determining the wavelength-dependent limits on spectral errors (i.e., the tolerable spectral variance) that are permissible in the design of MOEs.

The present manuscript describes the development of a general approach to determining the spectral tolerance of MOEs. The approach taken here is to define lower and upper wavelength limits beyond which tolerances are unnecessary, and then to distribute the prediction errors caused by coating misfit even between these limits. Because no *a priori* knowledge of the final iterative solution can be available at the start of the design process, the authors take the conservative approach of assuming that all spectral errors will sum in the result in the worst possible way. All computations are developed for numerical solution in real problems,

M. L. Myrick (✉) · O. Soyemi · H. Li · L. Zhang · D. Eastwood
Department of Chemistry and Biochemistry,
University of South Carolina, Columbia, SC, 29208, USA

352

as opposed to computations that depend on analytical expressions for spectral shapes and variances. This work is completed with an example application based on real data.

There are two main applications for the equations developed here. First, they provide tolerance criteria for the design of MOEs via spectral matching. That is, in some permutations of MOE design, a spectral pattern can be defined from standard chemometric approaches which the MOE must faithfully reproduce. The criteria developed here specify how closely the design must reproduce the target spectrum of an MOE synthesized in this way. The second application for these equations is to define manufacturing tolerances. Regardless of how an MOE is designed, fabrication must produce an actual device that reproduces the design within the limits set by these equations if there is to be no degradation of prediction compared to theory.

Experimental

A Hewlett-Packard UV-Vis diode array spectrophotometer Model 8543 was used to collect transmission and absorption data on binary dye mixtures for this study. A compact prototype field instrument (Fig. 1) was designed and constructed for this project to show proof of concept using Linos Photonics (Milford MA) optical components. The characteristics of bandpass filters, lamps and detectors in the prototype instrument were used to convert transmittance spectra of calibration samples into detector spectral responses.

A 6 V/6 W tungsten filament lamp with 1×1.2 mm active filament area was used as a light source in the Fig. 1 instrument. The spectral radiance of the lamp was measured in W per (steradian $\times$ cm^2 $\times$ nm) with a CCD spectrometer system (consisting of a Chromex 250IS spectrometer with 300 lines/mm grating and a Princeton Instruments 1100×300 pixel CCD camera, model TE/CCD-1100-PE). The input optics of the spectrometer system were duplicates of the Fig. 1 system. For these measurements, the operating voltage for the lamp was fixed at 5.76 V. The wavelength range of the CCD camera/spectrometer system was calibrated with a standard mercury penray lamp and a standard neon lamp. The spectral radiance of the lamp under these conditions was calibrated against an OL series 455 integrating sphere calibration standard lamp (Optronic Laboratories, Inc.) operated under standard conditions.

The two Si photodiode active detectors were type BPW21 with a sensitive area of 2.7×2.7 mm^2, spectral range 320–820 nm and
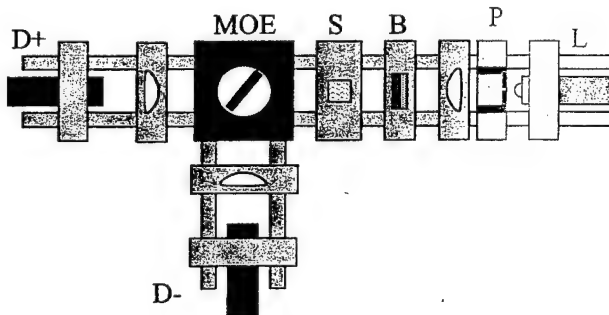

Fig.1 Layout of a single-element system in which a multivariate optical element acts as a 45-degree beamsplitter. *MOE* is the optical element, *L* is a lamp, *P* is a spatial filtering pinhole. *S* is a sample, *B* is a bandpass selection filter set, *D+* and *D−* are detectors for the transmitted and reflected light from the MOE

radiant sensitivity at the peak wavelength (550 nm) of 3.8 V/mW. The relative signal intensity (detector response) vs. wavelength was estimated from a Linos Photonics data sheet with values measured at 25 degrees C and 12 V DC supply voltage.

The bandpass filter set, used to isolate the spectral region between 400 nm and 650 nm, consisted of two 3 mm thick Schott glass filters (Duryea, PA) BG-39 and GG400.

The binary dye mixtures used for initial testing of our MOC filter design were prepared from two water-soluble dyes obtained from Aldrich Chemical Company, Bismarck Brown Y (BB) (max 457 nm, dye content 50%) and Crystal Violet (CV) (max 590 nm, ACS reagent dye content 95%). Stock solutions in distilled water of BB at 6.72×10^{-5} M and CV at 1.64×10^{-5} M were prepared. Then random numbers were generated and applied to the concentrations of the dyes with dilution to determine that the relative concentrations of the two dyes were varied independently. In the dilution process transmission values were kept between 10% and 90% in the mixtures. In this manner 40 binary dye solutions were prepared and their transmittance spectra were measured. Twenty-five of these spectra were used to generate a regression vector and 15 were kept as a test set.

Discussion

Prediction error

Figure 1 shows a schematic of the optical layout for a single-MOE measurement system, illustrating that both transmittance through and reflectance from the MOE are detected. The estimated prediction, C'_{pred}, for a quantity in an unknown sample is given by Eq. (1):

$$C'_{pred} = k(\mathbf{T'} - \mathbf{R'}) \times \mathbf{S} + O. \tag{1}$$

In this equation, $\mathbf{T'}$ and $\mathbf{R'}$ are vectors representing the real transmittance and reflectance of the MOE, $\mathbf{S}$ is a vector for the spectrum of the unknown, k is a scalar gain factor and O is a constant scalar offset.

For interference filters made from non-absorbing or approximately non-absorbing materials, the transmittance and reflectance sum to unity at each wavelength. Under this approximation, we can write the vector difference in parentheses in Eq. (1) as:

$$\mathbf{T'} - \mathbf{R'} = 2\mathbf{T'} - \mathbf{1} \tag{2}$$

where $\mathbf{1}$ represents a column vector of dimension equal to the number of wavelengths that contains all ones.

The error in prediction due to errors in the spectrum of the MOE can be determined by inserting the definition $\mathbf{T'} = \mathbf{T} + \Delta\mathbf{T}$ into Eq. (2), which can be rearranged into the form of Eq. (3):

$$C'_{pred} = k(2\mathbf{T} - \mathbf{1}) \times \mathbf{S} + O + 2 k \Delta\mathbf{T} \times \mathbf{S} \tag{3}$$

where $\mathbf{T}$ is the intended transmittance, or target transmittance, of the MOE and $\Delta\mathbf{T}$ is the spectral error vector.

The first two terms on the right-hand side of Eq. (3) constitute the "ideal" prediction which an ideal, error-free MOE would have produced. Note that the "ideal" prediction is not the same as the "true analytical variable" whose value we can only know via the reference method for the underlying chemometrics, but only our usual chemometric prediction of that variable.

Expressing the difference between the actual prediction and the ideal prediction as ΔC_{pred}, we can write:

$$\Delta C_{pred} = 2\,k\sum_i \Delta t_i s_i. \qquad (4)$$

In Eq. (4) the scalar product has been rewritten in the form of a summation of the individual wavelength-dependent terms. We are interested in the dependence of ΔC_{pred} on the spectrum of the unknown since, once fabricated, the spectral errors in the MOE are fixed. In particular, we are interested in the variance of ΔC_{pred} with the spectral variance, because constant offsets in ΔC_{pred} can be accounted for easily in operation. By a constant offset, we mean any component of prediction error that does not vary from sample to sample. In the basic multivariate optical computing approach, the measurement device is operated much like a pH meter is used: a couple of standard samples are inserted into the device to set a gain and offset factor. Constant components of the offset are implicitly removed by this procedure. Eq. (5) can be used to evaluate the dependence of the prediction variance with respect to the spectral variance.

$$\partial\Delta C_{pred} = 2\,k\sum_i \Delta t_i \partial s_i \approx 2\,k\int_{\lambda_L}^{\lambda_R} \Delta t(\lambda)\partial s(\lambda)d\lambda \qquad (5)$$

In Eq. (5), λ_R and λ_L, are the bandpass cutoff wavelengths. There is a fine point to be made here. The effect of MOE errors at different wavelengths on prediction can be either positive or negative. One can imagine conditions in which the spectral errors in an MOE offset one another more or less exactly. An example would be two MOEs that code for different valid regression vectors for the same measurement. One of these MOEs could be pictured as an erroneous version of the other that just happens to give completely valid results. However, since we cannot know the patterns of spectral variance in the original data a priori, we will assume they all sum as random error. The partial derivatives on each side of this equation can then be identified with the variance in prediction error, V_c, and the variance in the spectral intensity at each wavelength, $V(\lambda)$.

Tolerance as a function of wavelength

A simple relationship between the tolerable error in MOE transmittance and the spectral variance at each wavelength can be obtained by integrating by parts (Eq. (6)):

$$\int_0^\infty V(\lambda)d(\Delta t(\lambda)) = [V(\lambda)\Delta t(\lambda)]_0^\infty - \int_0^\infty \Delta t(\lambda)d\,V(\lambda) \qquad (6)$$

In this equation, the spectral variance and MOE error vector (spectral tolerance) are treated as continuous functions of wavelength. Figure 1 shows that the spectral window over which the MOE is calculated is determined largely by a bandpass filter set (or equivalently by a combination of a long-wavelength pass filter and a detector cutoff, or by a light source spectrum and detector spectrum, etc.).

By using limits of integration in Eq. (6) that are far to the left or right of the spectral bandpass, we assure that the first term on the right, the difference between the variance-error function at the limits of integration, is zero. This is because the error in transmittance is limited to unity since MOEs have transmittance values limited to the range $0 \le t \le 1$. Since the spectral intensity outside the bandpass is always zero, the spectral variance falls to zero there as well. This simplifies Eq. (6) to the form:

$$\int_0^\infty V(\lambda)d(\Delta t(\lambda)) = -\int_0^\infty \Delta t(\lambda)d\,V(\lambda) \qquad (7)$$

Taking the derivative of both sides, we can easily rearrange the result and reintegrate to show that:

$$\Delta t(\lambda) = \frac{G}{V(\lambda)}, \qquad (8)$$

where G is a constant of integration. Eq. (8) relates the permissible error in transmittance at a particular wavelength to the spectral variance at the same wavelength. For the small values of variance typically found outside the bandpass of the measurement, the permissible error in transmittance can reach as much as unity. This provides a rational basis on which to determine the effective bandpass. The bandpass can be defined as the wavelength region over which the allowable error in transmittance is less than unity.

Finding the effective bandpass

Returning to Eq. (5), the integral on the right-hand side can be separated into integrals over wavelengths above and below the bandpass cutoff wavelengths, λ_R and λ_L, plus an integral over the bandpass between those limits. Below λ_L and above λ_R, the allowable transmittance error can be assumed to be fixed at 1. In an operational sense, this means that outside the spectral bandpass, the transmittance of the MOE no longer matters. As a result, the integrals below and above the cutoff wavelengths become integrals of the excluded variance alone, V_{ex}. Eq. (8) provides a substitution for $\Delta t(\lambda)$ in the region between the cutoff wavelengths that permits integration to give:

$$\frac{\partial\Delta C_{pred}}{2\,k} \approx V_{ex} + G(\lambda_R - \lambda_L) \qquad (9)$$

This equation can be used to determine the effective bandpass by noting that G is the value of $V(\lambda)$ at which $\Delta t(\lambda)$ equals unity. G is thus the bandpass cutoff spectral variance, represented by $V_{co} = V(\lambda_L) = V(\lambda_R)$. The permissible variance in prediction error can be reasonably identified with the square of the standard error of prediction in the original regression analysis, $(SEP)^2$. Making these insertions and rearranging, we get:

$$V_{ex} + V_{co}(\lambda_R - \lambda_L) - \frac{SEP^2}{2\,k} = 0 \qquad (10)$$

Eq. (10) provides a direct route for determining λ_L and λ_R. To understand how this is done, consider a simple data set

in which $V(\lambda)$ passes through a single maximum, V_{max}, and falls toward zero on either side. At values of $V(\lambda)$ between zero and V_{max}, every line of constant variance crosses the spectral variance curve at two different wavelengths. The integrated variance outside these wavelengths gives V_{ex}, the spectral variance at these wavelengths is V_{co}, the two wavelengths are λ_L and λ_R, and the remaining factors in Eq. (10) are constants. In a real data set, values of spectral variance can be chosen that define a curve with a single root. This root is a solution that defines the important parameters V_{co} ($\equiv G$), λ_L and λ_R. Outside this spectral range the allowable error in transmittance is assumed to be 1, while inside the spectral window it is given by Eq. (8).

A minor reinterpretation of Eq. (10) is adequate to extend the model to cases in which the spectral variance is not unimodal and where the bandpass encloses one or more bandblocks. In these cases, V_{co} is the cutoff value of spectral variance at any single channel, V_{ex} integrates variance over all channels with variance below this cutoff value, and the difference in cutoff wavelengths is replaced by an summation of the number of wavelengths with variances above the cutoff variance. This interpretation is simple to implement with most spreadsheet programs by sorting the variances and calculating the left-hand side of Eq. (10) for each value of variance to locate the root of the equation.

One further point remains to be made regarding Eqs. (8) and (10). These two equations set the spectral tolerances in design or manufacturing based on the SEP of the conventional measurement. This implies that if an MOE is produced with errors equal to the tolerances at all wavelengths, we should anticipate the SEP for the measurement might degrade by $\sqrt{2}$. Put another way: the fundamental SEP of the measurement due to errors in the regression model represents a lower-bound to the SEP that can be produced by an MOE system. SEPs with magnitudes that result from low signal strengths (e.g., counting statistics) could be improved by an MOE system since the light-gathering and light-analyzing power of the optical computing approach is much better than most conventional instruments. But if the model itself is the limiting factor in error, then an MOE cannot improve it but can only degrade it. The challenge is to make that degradation as small as possible.

A worked example

Consider the data for spectral intensity through a series of Bismarck Brown/Crystal Violet dyes shown in Fig. 2. A calculation of the spectral variance in this data set, $V(\lambda)$, is shown in Fig. 3. A regression analysis of the dye data in Fig. 2 gives an SEP of 0.3 µM for the prediction of Bismarck Brown at concentrations up to 16 µM, and a regression vector that, when transferred to an MOE, gives $k = 40$ µM–nm/V. Using these values, the left-hand side of Eq. (10) varies with the spectral variance as shown in Fig. 5. This figure indicates that the cutoff spectral variance is nearest 5.52×10^{-6} V²/nm. This value of V_{co} oc-
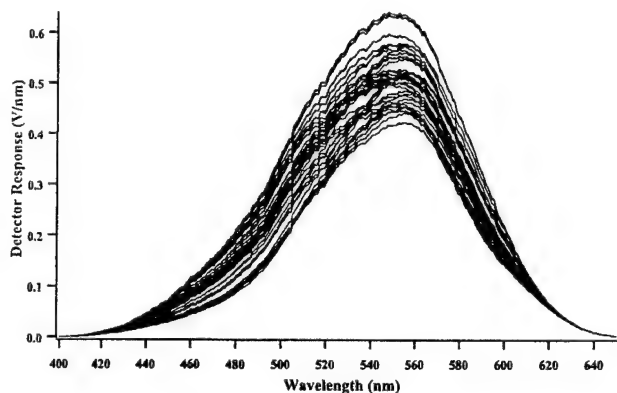
Fig. 2 A series of 40 spectra for a two-dye mixture consisting of Bismarck Brown and Crystal Violet with uncorrelated concentrations. These spectra are produced as described in the text
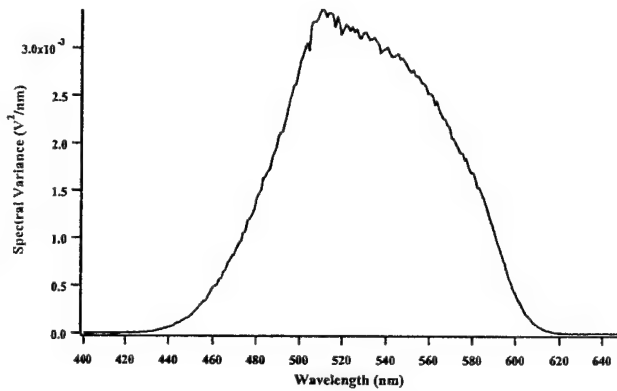
Fig. 3 The spectral variance in the data sets of Fig. 2
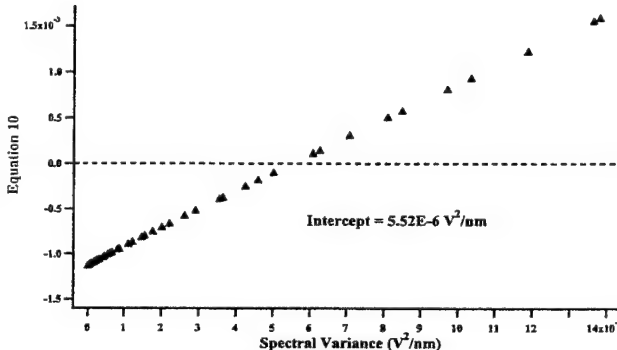
Fig. 4 An equation 10 plot based on the data in Fig. 3 giving the root of the equation as 5.52×10^{-6} V²/nm

curs on the left of Fig. 3 nearest $\lambda = 424$ nm, and on the right of Fig. 4 nearest $\lambda = 622$ nm. These limits then define spectral bandpass over which tolerances are required. The tolerances outside this range are set to 1, while those in this range are set to $V_{co}/V(\lambda)$. The tolerances thus vary over about 3 orders of magnitude, from unity to near 1×10^{-3}, as shown in Fig. 5. The region of tolerances less than about 0.005 (0.5% transmittance) extends from 474 nm to 590 nm. To aid in visualizing these tolerances, Fig. 6
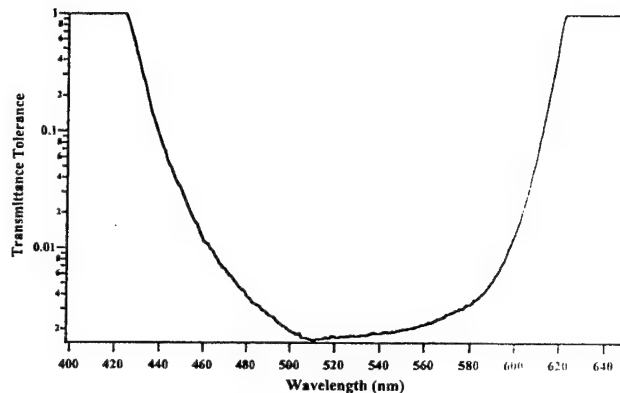
Fig. 5 Calculated tolerances for an MOE based on Figs. 3 and 4. Units are based on a maximum transmittance of 1
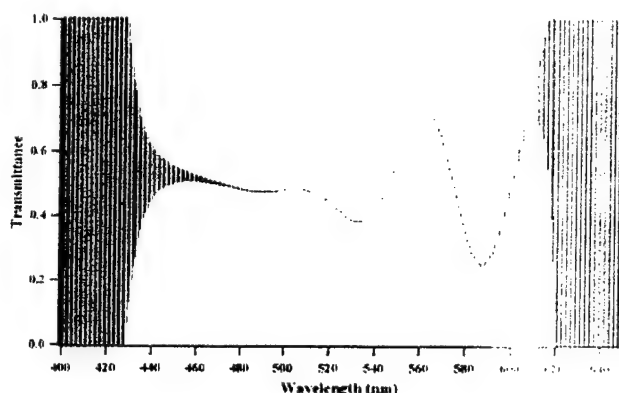
Fig. 6 A proposed spectrum for an MOE for the Bismarck Brown/ Crystal Violet samples. Error bars are taken from the tolerances in Fig. 5. Any MOE with a spectrum falling within the limits defined by these error bars will perform approximately the same

shows the regression vector (obtained from PCR for the data of Fig. 2 based on 4 principal factors) with these tolerances provided as error bars. These tolerances are sufficient for a thin-film design program to achieve a usable solution via iteration. In some cases, the tight tolerances required in the central portion of the MOE spectrum are readily achievable, while in others they are not. In general, complex MOE structures reduce the likelihood of achieving the most restrictive tolerances. An approach to solving this problem is to redesign the MOE following each material layer deposition; this problem will be addressed in a future report.

Conclusions

From the preceding equations and the example we can draw several conclusions. First, wide bandpasses will necessitate tight tolerances. The narrower the bandpass is permitted to be, the looser the fit. This is because of the wavelength factor in Eq. (10), which is the major factor offsetting the constant factor in the equation on the edges of the bandpass. For example, with a bandpass equal to

100 nm instead of 200 nm, the cutoff variance would have been approximately twice the value obtained here, which would double all the tolerances and make MOE production easier. Likewise, peaked variance distributions such as the one given here will give rise to regions of very low tolerance to design error and manufacturing defects in a single-element MOE design. Another consideration is that the transfer of a regression vector to the target spectrum of an MOE coating is very flexible in the sense that any amplification factor is permissible. The modulation of the spectral function can be made larger or smaller depending on this factor, provided that one keeps the hypothetical MOE spectrum within the limits of physicality. However, small modulations will yield large values of k, the gain factor. The result will be smaller values of V_{co}, leading to a wider bandpass and lower tolerances throughout the spectral bandpass.

The development of MOEs and multivariate optical computing as an alternate method for implementing multivariate prediction is only at its inception. Within limits (whose bounds are not fully determined at present), one can imagine using MOEs to perform many types of multivariate spectroscopic calculations. The application of MOEs is not to perform measurements that cannot be performed by conventional spectroscopy, but to perform them faster, with less complex instrumentation and at far lower costs. To place this in context, recent work in our laboratory has shown that we can produce 50+ identical $1/4 \leq$ -square MOEs in a single run. Extrapolated to a true commercial facility, the cost of producing MOEs could be as little as a few \$US per element. The devices that could be produced from them might look and feel a lot like a "tricorder" from the Star Trek television series. But these simple-looking devices would use the power of complex multivariate spectroscopy to perform necessary tasks in medicine (e.g., glucose measurement), agriculture (ripeness, moisture content, etc.), industry (e.g., fuel quality) and combat (e.g., chemical detection). Our laboratory is currently exploring the practical design and fabrication of MOEs. From an optimistic viewpoint, these tools could bring multivariate spectroscopy to the mass consumer market.

References

1. Malinowski ER (1991) Factor Analysis in Chemistry, 2nd ed. John Wiley and Sons, New York
2. Nelson MP, Aust JA, Dobrowolski JA, Verly PG, Myrick ML (1993) Anal Chem 70: 73–82
3. Bialkowski S (1986) Anal Chem 58: 2561–2570
4. Myrick ML, Nelson MP, Soyemi O, Karunamuni J, Eastwood D, Li H, Zhang L (2000) Vib Spectrosc (in press)
5. Ryabenko A, Kasparov V (1991) Pattern Recognition and Image Analysis 1: 347–54

10.2 SPECTROELECTROCHEMICAL STUDY OF THE OXIDATIVE DOPING OF POLYDIALKYLPHENYLENEETHYNENE USING ITERATIVE TARGET TRANSFORMATION FACTOR ANALYSIS

Spectroelectrochemical study of the oxidative doping of polydialkylphenyleneethynylene using iterative target transformation factor analysis

U. Evans, O. Soyemi, M. S. Doescher, U. H. F. Bunz, L. Kloppenburg and M. L. Myrick*

Department of Chemistry and Biochemistry, University of South Carolina, Columbia, SC 29201, USA

Iterative target transformation factor analysis (ITTFA) was used to determine the spectra of the individual species generated during the oxidative p-doping of films of poly(para-phenyleneethynylene) (PPE). UV-visible spectra of PPE films on transparent electrodes were obtained in-situ during an anodic sweep. ITTFA identified 4 species present during the oxidation, which we assign as neutral polymer, polaron species, bipolaron species, and a species formed by further bipolaron reaction. The region of electrochemical stability for each of these species was identified and their potential-dependent profiles were obtained. This work is the first deconvolution of conjugated polymer spectroelectrochemistry.

Introduction

Electronically conducting polymers with π-conjugated backbones have been actively studied in recent years.[1] The conjugated backbone of these polymers leads to extensive electron delocalization; nevertheless, the quantum-confined nature of the structure leads to large bandgap energies, making the polymers insulators or weak semi-conductors in their neutral (undoped) state.[2] Electrochemical oxidation (p-doping) of conjugated polymers can create mobile charge-carrying defects that result in increased conductivity; these charged sites are balanced by anions that migrate into the polymer. Doping introduces new defect-centered electronic states that exhibit distinctive optical transitions. Undoped polymers exhibit the characteristic $\pi-\pi^*$ transitions of conjugated organic molecules; the new mid-gap states introduced by doping generally result in new red-shifted absorbances. Two major defect types can be formed on oxidation. The first of these are polarons, molecular radical cations, which are formed at low doping levels. Bipolarons, dicationic defects delocalized over a number of repeat units, may be formed at higher doping levels.[3]

In our laboratory, we have recently studied conductivity and charge-carrier mobility in polyphenyleneethynylene-based polymers. Phenylenevinylene and the related phenyleneethynylene polymers constitute an important class of conducting polymers with applications in optoelectronic devices and materials.[4,5]

In this work the spectroelectrochemistry of a novel 2,5-dialkyl(paraphenyleneethynylene) polymer, synthesized by us, has been investigated. This polymer has been shown to emit light blue shifted from poly(p-phenylenevinylene), (PPV) and has been investigated as an emitting layer in organic electroluminescent (OEL) devices.[6,7] Efficiency in OEL devices is directly related to the oxidation and reduction potential of the emitting layers.[8,9] Wrighton et al.[10] examined the cyclic voltammetry of a dialkoxy-poly(para-phenyleneethynylene)-derivative in solution and found that it is irreversibly oxidized at 1.05 V (vs. calomel) in liquid SO_2. However, to date the electrochemistry of poly(para-phenyleneethynylene)s (PPEs), especially in solid-state films, is largely unexplored.

Spectroelectrochemistry is a powerful technique for the determination of the intermediates in conjugated polymer oxidation.[11] Rapta et al. studied the oxidation of polypyrrole by in-situ EPR/UV-vis spectroscopy and determined the UV-vis spectra of the neutral, polaronic and bipolaronic states. In-situ spectroelectrochemical studies of p-doped PPV have identified the polaronic and bipolaronic states of this polymer.[12,13] Unfortunately, spectroelectrochemistry of conducting polymers is complicated by overlapping spectra for the different charge-carrying defects possible in each material. Factor-analysis-based approaches to interpretation such as iterative target transformation factor analysis (ITTFA) have the power to provide insight into the number of species present, and how their concentrations vary with time and potential. However, to date factor analysis has been used only once to deconvolute spectroelectrochemical data: by Keesey and Ryan who studied the reduction of E. coli sulfite reductase hemoprotein and a Mo–Fe–S cluster.[14] In this report, we explore the spectroelectrochemistry of a PPE-based polymer using ITTFA. Using this approach, we obtain the distinct optical spectra of two charged-defect states that we assign as the polaron and bipolaron states on the basis of their potential and doping level dependence.

Experimental

Thin films of **1** and **2** on indium tin oxide (ITO)-coated slides were used for a spectroelectrochemical study.

The polymers **1** and **2** were synthesized according to a literature procedure[15]. Thin films of **1** and **2** were made by spin-coating 150 μl of a 25 mg ml⁻¹ chloroform solution of the polymer onto ITO at a speed of 770 rpm for 50 s. In some cases, the film was removed from a portion of the ITO coating with a chloroform-soaked swab prior to making electrical contact with an alligator clip. In other cases, no cleaning protocol was used and a direct connection via an alligator clip was made through the film. No difference in the behaviors of these connection types was observed. Film thickness was determined using contact-mode atomic force microscopy by scoring the polymer film with a blade and measuring step heights from the top of the polymer film to the substrate.

The experimental instrumentation for the electrochemical set-up consisted of an EG&G PARC Model 263 potentiostat, connected with a GPIB interface (National Instruments) to a

Gateway 2000 Model P5-60 computer with EG&G PARC Model 270 Research Electrochemistry Software. Cyclic voltammetry (CV) of the films was performed with 0.1M tetrabutylammonium perchlorate (TBAP) supporting electrolyte in dichloromethane (DCM). DCM was obtained as reagent-grade from Fischer Scientific and was used without further purification. The polymer coated ITO was used as the working electrode in a standard 3-electrode electrochemical set-up, platinum was the counter electrode and the potential was measured against a platinum wire pseudo-reference electrode. Ferrocene was used as a standard for oxidation potential. All experiments were performed in air. During electrochemical studies outside the spectrometer, the solvent was purged with nitrogen gas.

Spectroelectrochemistry was carried out using a quartz cuvette as an electrochemical cell. A Hewlett Packard UV-visible spectrometer was used. The 'Automation' option of the chemstation software enabled spectra to be recorded at 30 s intervals. Spectral data were exported as ASCII files for further use. Continuous nitrogen purging was not possible during these studies, but thoroughly de-aerated solutions were prepared and transferred to the spectrometer for immediate use.

Results and Discussion

Polymers 1 and 2 showed identical electrochemical behavior. Typical cyclic voltammograms of 1 in a 0.1 M TBAP–DCM electrolyte solution at a sweep rate of 50 mV s^{-1} and at different potential limits are shown in Fig. 1. When the upper voltage limit is 1.45 V vs. Fc/Fc$^+$ an anodic peak is seen at 1.19 V vs. Fc/Fc$^+$. There is also a small anodic peak at 0.59 V vs. Fc/Fc$^+$. One reduction peak is observed at −0.26 V vs. Fc/Fc$^+$. This redox reaction is accompanied by a reversible color change — the polymer originally has a yellow–green color. At applied potentials above 1 V this changes to a deep red color, which persists until the applied potential is cycled back past −0.26 V vs. Fc/Fc$^+$, where the original yellow–green color reappears.

However when the upper voltage limit is set at 0.85 V vs. Fc/Fc$^+$ a new cathodic peak emerges. The small oxidation peak observed at 0.59 V vs. Fc/Fc$^+$ exhibits a corresponding reduction at 0.54 V vs. Fc/Fc$^+$. In this case there is a color change to brown, which is reversible upon cycling past the 0.54 V cathodic peak. No cathodic peak at −0.26 V vs. Fc/Fc$^+$ is observed in this case. At an intermediate voltage limit in the region of 1.1 V vs. Fc/Fc$^+$ both cathodic peaks are observable on the cathodic sweep, but the magnitude of the 0.54 V cathodic peak decreases relative to its peak height at the 0.9 V limit, and the red color persists until cathodic cyclic past 0.26 V vs. Fc/Fc$^+$.

It seems most probable that the first peak at 0.59 V vs. Fc/Fc$^+$ is due to polaron (radical cation) formation, which is initially reversible. The second oxidation at 1.19 V vs. Fc/Fc$^+$ induces
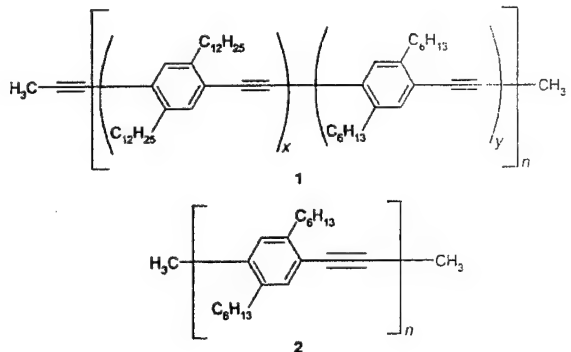
conversion of polarons to bipolarons, a process that is irreversible in that the bipolaron cannot be reduced to the polaron. Therefore, although the overall oxidation reaction can be reversed, the process is thermodynamically irreversible, at least under the conditions of our experiment. The redox reactions of dialkyl(paraphenyleneethynylene) can be summarized as follows: PPE − e$^-$ ↔ PPE^{o+}, reversible radical cation formation; PPE^{o+} → PPE2$^+$, radical cation oxidation to form bipolaron, irreversible; PPE2$^+$ + 2e$^-$ → PPE, bipolaron reduction to neutral polymer. Upon continuous cycling of the polymer between 0.34 and 0.85 V vs. Fc/Fc$^+$ there is no decrease in observed current with cycle number, subsequent cyclic voltammograms are superimposable. Upon continuous cycling of the polymer between −0.5 and 1.35 V vs. Fc/Fc$^+$, however, there is a sharp decrease in observed current with cycle number. This occurs for both the anodic and cathodic peaks although the qualitative behavior of the films remains constant and the corresponding color change remains.

We made an effort to determine n, the number of ClO$_4^-$ ions incorporated into the polymer matrix on polaron formation and on complete oxidation. To do this, a number of assumptions were made. It was assumed that the molar absorptivity of the polymer in solution is equal to that of the polymer in the film. The measured absorbance per unit film thickness was used to calculate the concentration of polymer in the film. The absolute absorbance of the film was then used to determine the number of polymer molecules in the film. Chronoamperometry was used to determine the total number of electrons removed from the film. A value of n at an applied potential of 1.2 V vs. Fc/Fc$^+$ of between 20 and 30 was calculated, i.e. an electron is removed from the polymer chain every 3 to 4 repeat units, near 100 C cm^{-3}. Further increasing the applied potential to 1.5 V vs. Fc/Fc$^+$ does not affect the n value obtained. This is comparable to the faradic charge of 120 C cm^{-1} reported for fully oxidized polypyrrole films used as battery electrodes.[16] The variation in n values between experiments was attributed to inhomogeneity of the spin-coated polymer film. Therefore the overall electrochemical reaction can be defined as PPE + 20 ClO$_4^-$ ↔ [PPE^{20}ClO$_4^-_{20}$] + 20e$^-$. For polaron formation only, at applied potentials of 0.6 V vs. Fc/Fc$^+$, n was calculated to be approximately 1.

The observed decrease in current upon polaron formation is attributed to polymer delamination upon doping, leading to decreased polymer concentration in contact with the electrode. This delamination may be the result of decreased polymer
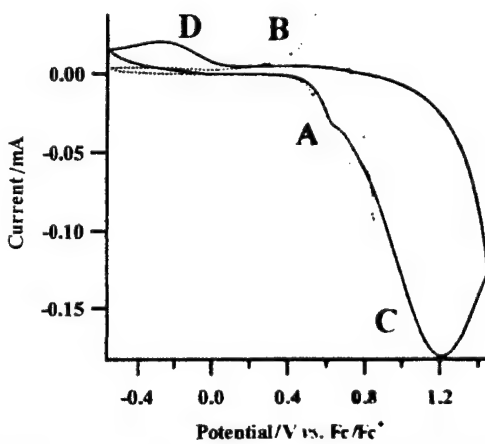

Fig. 1 Representative cyclic voltammogram for the oxidation of 1 at 50 mV s^{-1} in a 0.1 M TBAP–DCM solution, showing the effect of upper potential limit on the cyclic voltammogram characteristics. Peak A: Neutral PPE oxidation to form polaron. Peak B: Polaron reduction. Peak C: Polaron oxidation to form bipolaron. Peak D: Bipolaron reduction to neutral polymer.

29

flexibility coupled with swelling/shrinkage during heavy doping.

The spin-cast polymer films adhere well to the ITO substrate. Atomic force microscopy (AFM) results show that polaron formation at low doping levels does not significantly change the polymer morphology. At this low doping level, delamination does not occur and therefore current peak heights do not change upon continuously cycling to the point where only polarons are formed. After heavy doping, however, it was observed that the films crack and shrink and are more easily removed from the underlying ITO. A possible explanation for delamination is that upon oxidation the large concentration of positive defects (at least one per 4 polymer repeat units) leads to structural perturbation of the polymer, such as increased planarization. The irreversibility of the radical cation to bipolaron formation may also be due to these inferred structural changes at high doping levels. Some evidence exists to support the notion of doping-induced micro- and nano-structural changes in polymer morphology. For example, the decreasing rate of polaron decay to bipolaron with increasing oxidation level in the conducting polymer polybithiophene has been attributed in the scientific literature to increasing polymer stiffness upon oxidation.[17] Our own AFM studies show that, while polaron formation does not significantly affect polymer morphology, bipolaron formation at high doping does. We have also performed force modulation microscopy (FMM) on the PPE films. Results of FMM studies indicate that the fully doped polymer is much more rigid than the undoped polymer.[18]

Spectroelectrochemistry

Cyclic voltammetry was carried out on 1 at 1 mV s^{-1} and the UV-visible spectrum of the film was collected at 30 s intervals, *i.e.* at potential intervals of 30 mV, from 0.34 to 1.43 V *vs.* Fc/Fc$^+$ on the forward sweep. The cyclic voltammogram recorded during the experiment was not perturbed by the optical measurement. As before, two peaks appeared on the forward sweep: polaron formation at 0.6 V *vs.* Fc/Fc$^+$ and bipolaron formation at 1.19 V *vs.* Fc/Fc$^+$. The polymer film was considerably delaminated at the end of the experiment. The degradation was probably enhanced by the relatively long time the doped film was in solution.

The spectra obtained during the electrochemistry are shown in Fig. 2. They correlate to spectra obtained during preliminary
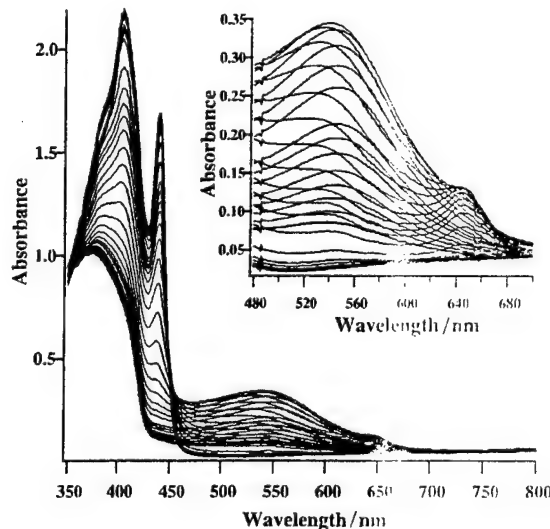

Fig. 2 The 37 spectra obtained during a linear sweep voltammogram at 1 mV s^{-1}. Spectra were taken at 30 mV intervals and represent applied potentials of 0.352 V, 0.382 V, ..., 1.432 V *vs.* Fc/Fc$^+$.

work, where chronoamperometry was used to apply a fixed potential to the polymer and UV-visible spectra were obtained in this potentiostatic manner.[19]

The undoped polymer film has absorption maxima at 404 nm (3.07 eV) and 440 nm (2.82eV). In solution, the phenyl rings of PPEs are known to be relatively rotationally free. The 404 nm peak is the only one observed for polymer in solution, and is attributed to the relatively short conjugation lengths that exist due to rotational motion. The peak at 440 nm appears only in films. This latter peak has been attributed to an intrachain effect in which spin-coating leads to increased planarization and thus improved conjugation with a lower band-gap.[20]

At an applied potential of 0.65 V *vs.* Fc/Fc$^+$, a new absorption centered at 645 nm (1.92 eV) appears and reaches a maximum absorption as a function of potential at approximately 0.9 V. This absorption is assigned to polaron formation. At potentials above 0.76 V *vs.* Fc/Fc$^+$, a stronger, broad peak with λ_{max} = 545 nm (2.27 eV) appears. Both peaks coexist in the 0.7 to 1 V range. The 540 nm peak reaches a maximum with respect to potential at 1.07 V *vs.* Fc/Fc$^+$, at which potential the 645 nm peak has disappeared. The 540 nm absorbance is assigned to the bipolaron defects in the polymer. The peaks at 404 nm and at 440 nm diminish until ~ 1.1 V *vs.* Fc/Fc$^+$. As the applied potential is increased the peak at 404 nm maximum undergoes a hypsochromic shift to 379 nm.

Iterative target transformation factor analysis

(ITTFA) was carried out using a modified version of a Matlab (version 5.1.0, MathWorks, Inc.) program written by Paul Gemperline at East Carolina University.[21]. ITTFA is a powerful mathematical tool to deconvolute spectra with broad overlapping spectral features. ITTFA works by finding two factors C_{pred} and E_{pred} that are related to the original data matrix, A, *via*: $A = C_{pred}E_{pred}$. Transformation analysis is carried out by finding a transformation matrix, M, such that $C_{pred} = UM$ where C_{pred} is the prediction of the new ordinate system. The eigenvectors E_{pred} of the new coordinate system are found from the inverse of M. $E_{pred} = M^{-1}SV^T$. Target transforms are performed by selecting test vectors for M and minimizing the difference between C_{pred} and C_{test}.

Principal component analysis (PCA) was carried out to identify the number of significant factors. PCA is a multivariate dimension reduction method which takes m spectra with n independent variables and produces a new set of orthogonal eigenvectors that are a linear combination of the original variables. Principal component one describes the greatest variability in the data set. Subsequent PCs, ranked by decreasing eigenvalue, describe successively less variability until only noise is being accounted for. In our example the number of significant factors was found to be 4, see Fig. 3. 98.25% of the total cumulative variance was accounted for by these four PCs.

The data input to the ITTFA program was the 37 × 750 matrix of absorption data exported from the Varian software, where the 37 rows represent complete spectra at individual scan numbers or applied potentials and the 750 columns represent individual wavelengths from 351 to 1100 nm. The data was not preprocessed. The result of the iteration was two matrices, called [cpred] and [epred]. [cpred] is a 37 × 4 matrix which represents the concentration profile with respect to applied potential for each of the 4 species identified. [epred] is a 4 × 750 matrix which represents the spectra of these 4 components.

The ITTFA program allows certain variables to be specified, namely the number of components to identify, the convergence tolerance and the maximum number of iterations. From PCA it was known that four species were present. ITTFA is a convergent program so it is necessary to choose a maximum

number of iterations greater than the number needed to converge. The convergence tolerance has a large effect on the number of iterations.

The deconvolution yielded four separate factors, corresponding to the main species present during the positive sweep. Fig. 4 shows the deconvoluted spectra and Fig. 5 shows the concentration profile of the four species. These are the results obtained when the convergence tolerance was selected as 0.0004. 71 iterations were needed to reach convergence in this case.

The deconvolution shows that the partially-planarized neutral polymer in the film is the only species present initially, consistent with expectation. The production of polarons begins to occur at 0.55 V *vs.* Fc/Fc$^+$ with a maximum at 0.89 V *vs.* Fc/Fc$^+$. Polaron formation is characterized by the emergence of an associated spectral peak at 650 nm. The neutral polymer peaks at 404 nm and 440 nm remain, but are reduced in magnitude. The fact that the 440 nm 'planarization' peak remains at these potentials lends credence to the claim that polaron formation does not significantly alter the polymer morphology. At 0.77 V the spectrum of a third species, the bipolaron, emerges, showing a characteristic broad band centered at 550 nm. This absorption reaches a maximum at 1.07 V *vs.* Fc/Fc$^+$. The 440 nm peak due to planarized regions of polymer disappears completely. The 404 nm absorbance characteristic of the dissolved polymer with short conjugation lengths has decreased hugely. This agrees with our chronoamperometry data. If on average each polymer chain has lost 20 electrons then it is to be expected that there will be an insignificant number of neutral segments remaining, and hence insignificant absorption at 404 and 440 nm.

Species 4 emerges at potentials above 0.9 V *vs.* Fc/Fc$^+$. The main absorbance for this species is at 380 nm. From both cyclic voltammetry and chronoamperometry we know that there is no electrochemical reaction occurring on the positive sweep following bipolaron formation and therefore the emergence of this species is not fully understood. We know that once the polymer films are freed from an applied potential, they gradually lose their red coloration, possibly due to reaction with atmospheric gases. The fact that species 4 shows both bipolaron and neutral characteristic spectra may mean that it was doped but is unstable in solution and is converting back to the insulating state. Another possible explanation is that after formation, the bipolaron defects undergo a further potential-dependent structural relaxation to another form with distinctive spectroscopy.

The result of the deconvolution were found to be affected by the tolerance limit. Decreasing the tolerance limit increases the number of iterations required to reach convergence. For example decreasing the tolerance limit by a factor of 10 from the example discussed above, to 0.000004, increases the number of iterations required to reach convergence to 207. This also affects the relative height of the 380 nm peak of species 4, which increases with decreasing tolerance. Conversely, raising the tolerance to 0.0004 lowers the amount of iterations needed to 21 and affects the spectrum of species 3 in that a 380 nm peak is also present in this case. The spectra of species 1 and 2 are not affected by these factors. This indicates that species 3 and 4 are not well separated by ITTFA.

To summarize, the ITTFA concentration profile shows that with increasing applied potential PPE is oxidized to form polarons, which initially are the only charged species present. Further increasing the applied potential leads to bipolaron formation. There is a potential window in which both coexist, but at 1.07 V *vs.* Fc/Fc$^+$ the bipolaron reaches a maximum concentration and all of the polaron has been converted. This corresponds to the PPE cyclic voltammetry, where the current maximum for bipolaron formation is 1.19 V *vs.* Fc/Fc$^+$.

Without deconvolution of the data it would appear that the fully p-doped polymer consists of both neutral and bipolaron segments, with a hypsochromic shift of the 404 nm to 380 nm. Using ITTFA to deconvolute the spectra obtained during dialkylpoly(paraphenyleneethynylene) oxidation enables us to obtain the spectra of the polymer polaron and bipolaron separately and to show that there are clear regions of stability for
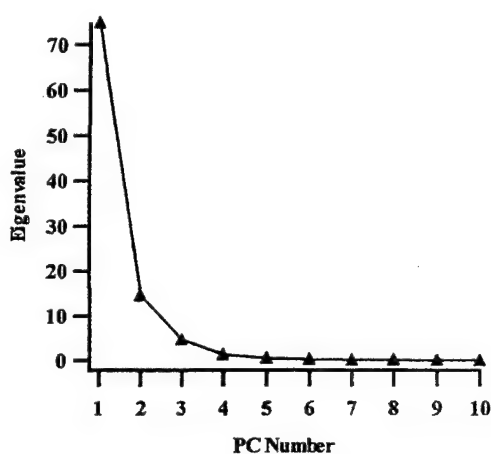
Fig. 3   Principal component analysis.
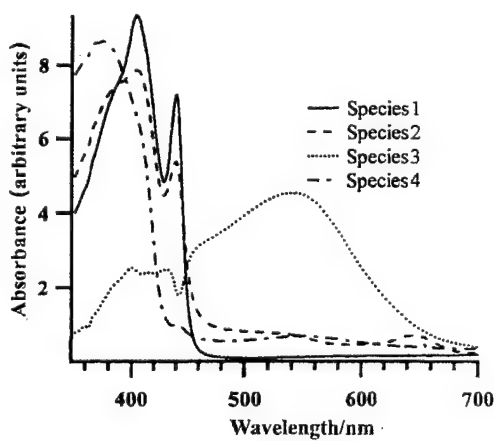
Fig. 4 Deconvoluted spectra showing the four significant species identified by the ITTFA program, where species 1 is the neutral polymer, species 2 is the polaron species, species 3 is the bipolaron species and species 4 is the final delaminated species.
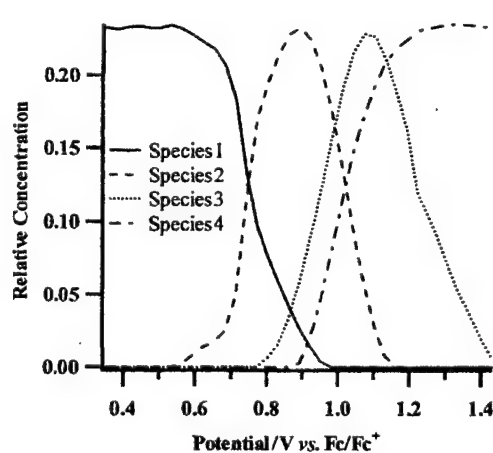
Fig. 5 Concentration profile showing species relative concentration as a function of applied potential. Species 1–4 are as detailed in Fig. 4.

Analyst, 2001, **126**, 508–512   **511**

31

each species. We find that the species only coexist over narrow ranges of potential. Iterative target transformation factor analysis also shows the presence of a fourth species, closely related to the bipolaron, which was not observable without spectral deconvolution.

Acknowledgement

References

1   *Handbook of Conducting Polymers*, T. A. Skotheim, R. L. Else-nbaumerand J. Reynold, Marcel Dekker, New York, 2nd edn., 1998.
2   M. S. Doescher, A. M. Rawlett, J. M. Tour and M. L. Myrick, *J. Phys. Chem. B*, 2001, **105(1)**, 105.
3   M. E. G. Lyons, *Electroactive Polymer Chemistry, Part 1: Fundamentals*, Plenum Press, New York, 1994.
4   U. H. F. Bunz, *Chem. Rev.*, 2000, **100(4)**, 1605.
5   R. H. Friend, R. W. Gymer, A. B. Holmes, J. H. Burroughes, R. N. Marks, C. Talani, D. D. C. Bradley, D. A. Santos, J. L. Bredas, M. Loglund and W. R. Salaneck, *Nature*, 1999, **397**, 121.
6   H. Li and M. L. Myrick, unpublished results.
7   A. Montali, P. Smith and C. Weder, *Synth. Met.*, 1998, **97**, 123.
8   J. L. Bredas, R. Silby, D. S. Boudreaux and R. R. Chance, *J. Am. Chem. Soc.*, 1983, **105**, 6555.
9   S. Janietz, D. C. C. Bradley, M. Grell, C. Giebeler, M. Inbasekaran and E. P. Woo, *Appl. Phys. Lett.*, 1998, **73(17)**, 2453.
10 D. Ofer, T. M. Swager and M. S. Wrighton, *Chem. Mater.*, 1995, **7(2)**, 418.
11 P. Rapta, A. Neudeck, A. Petr and L. Dunsch, *J. Chem. Soc., Faraday Trans.*, 1998, **94(24)**, 3625.
12 M. Baitoul, J. Wery, B. Dulieu, S. Lefrant, J. P. Buisson and M. Hamdoune, *Synth. Met.*, 1999, **101**, 173.
13 M. Baitoul, J. P. Buisson, S. Lefrant, B. Dulieu, J. Wery and M. Lapowski, *Synth. Met.*, 1997, **84**, 623.
14 R. L. Keesey and M. D. Ryan, *Anal. Chem.*, 1999, **71**, 1744.
15 L. Kloppenburg, D. Jones and U. H. F. Bunz, *Macromolecules*, 1999, **32**, 4194.
16 T. Yeu and R. E. White, *J. Electrochem. Soc.*, 1991, **137(5)**, 1327.
17 G. Zotti and S. Zecchin, *Synth. Met.*, 1997, **87(2)**, 115.
18 M.S. Doescher, U. Evans and M.L. Myrick, unpublished results.
19 U. Evans, M. S. Doescher, U. H. F. Bunz and M. L. Myrick, *Synth. Met.*, , submitted.
20 T. Miteva, L. Palmer, L. Kloppenburg, D. Neher and U. H. F. Bunz, *Macromolecules*, 2000, **33**, 652.
21 P. G. Gemperline, *Anal. Chem.*, 1986, **58**, 2656.

10.3 FIELD APPLICATIONS OF STAND-OFF SENSING USING VISIBLE/NIR MULTIVARIATE OPTICAL COMPUTING

Field applications of stand-off sensing using visible/NIR multivariate optical computing

DeLyle Eastwood, Olusola Soyemi, Jeevanandra Karunamuni, Lixia Zhang, Hong Li
Michael Myrick*

Department of Chemistry and Biochemistry,
University of South Carolina
Columbia, SC 29208

ABSTRACT

A novel multivariate visible/NIR optical computing approach applicable to standoff sensing will be demonstrated with porphyrin mixtures as examples. The ultimate goal is to develop environmental or counter-terrorism sensors for chemicals such as organophosphorus (OP) pesticides or chemical warfare simulants in the near infrared spectral region. The mathematical operation that characterizes prediction of properties via regression from optical spectra is a calculation of inner products between the spectrum and the pre-determined regression vector. The result is scaled appropriately and offset to correspond to the basis from which the regression vector is derived. The process involves collecting spectroscopic data and synthesizing a multivariate vector using a pattern recognition method. Then, an interference coating is designed that reproduces the pattern of the multivariate vector in its transmission or reflection spectrum, and appropriate interference filters are fabricated. High and low refractive index materials such as Nb_2O_5 and SiO_2 are excellent choices for the visible and near infrared regions. The proof of concept has now been established for this system in the visible and will later be extended to chemicals such as OP compounds in the near and mid-infrared.

Keywords: Sensors, optical computing, multivariate analysis, visible/NIR, remote sensing, standoff sensing

* - myrick@mail.chem.sc.edu

1.INTRODUCTION

A novel multivariate visible/NIR optical computing approach has been established in the visible spectral region based on a theoretical assessment performed in 1998.[1] Spectra of mixtures of 4 porphyrins in solution were used as examples. The long-term objective is to develop environmental or counter-terrorism sensors for field use by the military for chemicals such as organophosphorus (OP) pesticides or OP chemical warfare simulants. These sensors would be used in the near infrared (NIR) or, after instrumental improvements and substitution of appropriate infrared optical materials, in the mid-IR.

After the acquisition of appropriate spectra, chemometric approaches are used to extract a spectral pattern (or regression vector) that is correlated to the property of interest but orthogonal to interferences. The magnitude of the spectral pattern is calculated by taking the direct "scalar" product between a spectrum and the predetermined regression vector. In this paper we used visible transmission spectra of 4 porphyrins, treating one as an analyte and three as interferents as proof of concept for chemicals of military interest in the near and mid IR spectral region. Porphyrin solutions were prepared using mixtures generated with random numbers to make sure that the components were varied independently. The resulting transmission spectra were spectrally corrected and used to calculate a regression vector and to design an appropriate target filter.

The all-optical approach we describe centers on the production of an interference coating whose transmission spectrum incorporates features of the spectral regression vector.[2] The concept of using interference coatings for chemical measurement vectors in spectroscopy was pioneered by Bialkowski more than a decade ago.[3] The interference filter was produced in house using reactive magnetron sputtering of multilayers of niobia and silica (high and low refractive indices, respectively) using software in house software.

The resulting interference filter produced in-house is used as a beam-splitter in a prototype, rugged, compact field instrument shown in Figure 1. In this sensor the difference between the transmitted and reflected beams will be proportional to the regression vector. The device containing the actual filter was tested with random mixtures of porphyrin solutions. The random error of prediction for the experiments on the actual filter value was found to be greater than the theoretical error for that filter design, as expected. The error was still much less than would have been expected from a conventional notch filter covering the same spectral region.

2. EXPERIMENTAL

The experimental approach and apparatus have been described elsewhere. Briefly, a Hewlett-Packard UV-Vis diode array spectrophotometer Model 8543 was used to collect transmission and absorption data on quaternary porphyrin mixtures for this study. A compact prototype field instrument (Figure1) was designed and constructed to show proof of concept in the visible using Linos Photonics (Milford, MA) optical components.

The characteristics of bandpass filters, lamps and detectors in the prototype instrument were used to convert transmittance spectra of calibration samples into detector spectral responses.

A 6V/6W tungsten filament lamp with 1 x 1.2mm active filament area was used as a light source in the prototype instrument. The spectral radiance of the lamp was measured in watts per (steradians x cm^2 x nm), with a charge coupled device (CCD) spectrometer system consisting of a Chromex 250IS spectrometer with 300 grooves/mm grating and a Princeton Instruments 1100 x 300 pixel CCD camera, (Model TE/CCD-1100-PE). The input optics on the spectrometer system are shown in figure 1. For these measurements, the operating voltage the lamp was fixed at 5.76V. The wavelength range of the CCD camera/spectrometer system was calibrated with a standard mercury Pen-Ray lamp and a standard neon lamp. The spectral radiance of the lamp under these conditions was calibrated against an OL series 455 integrating sphere standard lamp (Optronic Laboratories Inc.) operated under standard conditions.

The two Si photodiode active detectors were type BPW21 with a sensitive area of 2.7 x 2.7 mm^2, spectral range 320-820 nm and radiance sensitivity at the peak wavelength (550 nm) of 3.8 V/nm. The relative signal intensity (detector response) versus wavelength was estimated from a Linos Photonics data sheet with values measured at 25 degrees and 12 V DC supply voltage.

The filter bandpass set used to isolate the region from 400 nm to 650 nm consisted of two 3 mm thick Schott glass filters (Duryea, PA) BG-39 and DG-400.

The quaternary porphyrin mixtures for testing multivariate optical element (MOE) filter design were prepared from four uroporphyrins I (free base or H_2, Cu (II), Ni (II), and Sn (IV)Cl_2) dissolved in 1M ammonium hydroxide. These uroporphyrins were obtained from the Porphyrin Products division of Frontier Scientific Inc. (Logan, UT). The stock solutions were H_2 at 106, Sn (IV)Cl_2 at 57.4,Cu at 62.6, and Ni at 56.1 micromoles, respectively. Random numbers were generated and applied to stock solutions of the porphyrins with dilution so that the relative concentrations of the four porphyrins varied independently. The random numbers were also chosen to make sure that the transmittance spectra of the diluted mixtures were between 30% and 70%. Forty quaternary porphyrin solutions were prepared and their transmission spectra were measured. These spectra after appropriate corrections were used to design the filter. When the filter was designed and produced, 20 additional solutions were prepared in a similar manner. Ten of these were used to calibrate the instrument, and 10 were used as a validation set. The Cu uroporphyrin was selected as the analyte and the other three uroporphyrins were regarded as uncorrelated interferents whose concentrations varied randomly.

The MOE filter was manufactured via reactive magnetron sputtering (RMS). The sputtering system (Model CV 5.1) was custom-manufactured by Corona Vacuum Coaters of Vancouver, B. C. Operating at room temperature, the system utilizes a 40 kHz mid-frequency RF supply to power four water-cooled planar magnetrons positioned in pairs

around a drum that rotates about a horizontal axis. The coating chamber contains 4 inch x 10 inch magnetron targets, two containing niobium (99.95 %, high index) and two containing silicon (99.9999% pure, low index). Each magnetron target is powered at about 0.7 kW, although the power is varied during deposition for fine control over the deposition rate. The RMS process was used to deposit alternating layers of niobium pentoxide (Nb_2O_5) and silicon dioxide (SiO_2) films by reaction with oxygen in the gas mixture. Deposition was carried out on a 1-inch BK-7 glass substrate according to prescribed multilayer coating thicknesses.

TFCalc, a commercial software product from Software Spectra Inc. (Portland, OR), was used to synthesize multilayer thin film designs to match a spectral target. An in-house thin film design program written in the MATLAB programming environment (MathWorks Inc., Natick MA) was used to design simpler multilayer structures for chemical prediction. The details of the chemometric/software approach will be reported elsewhere.[4]

3. RESULTS AND DISCUSSION

Figure 1 shows the experimental setup for implementing the single filter design in a simple transmission measurement. In this system, a spatial filter and collimating lens are used to restrict the angular dispersion of light reaching the bandpass filter set and then through a 10 mm I.D. fused silica cell containing a porphyrin mixture solution. The light, after passing through the sample cell, then hits the multivariate optical element (MOE) interference filter employed in a beam splitter arrangement at approximately 45 degrees with part of the light being reflected to a detector and part being transmitted to a similar detector.

The spectrum of the 45-degree MOE is designed to be

$$T(\lambda) = 0.5 +/- L(\lambda),$$

where T is the filter transmittance function and L. The reflectance may be represented by R (wavelength) = 0.5 -/+ L (wavelength). The difference between these values is proportional to the spectral regression vector, while the sum of the two is independent of the spectral vector.

Figure 2 shows the transmission spectra for a series of 40 mixtures of these porphyrins, mixtures in which the concentration of the 4 porphyrins are varied independently of one another based on a random number generator. Cu(II) uroporphyrin I was chosen as the analyte and the other 3 uroporphyrins were taken as interferents. Before calculation of a regression vector, the transmission spectra are converted into system units by measuring the spectral radiance of the light source to be used for illumination of the sample, the transmittance of a spectral bandpass filter set, and the spectral sensitivity of the detector selected for the measurement. The product of these factors as described elsewhere with the sample transmittance spectra gives the system-corrected spectra shown in Figure 3.

An interference filter was designed using our in-house software to minimize the standard error of prediction (SEP). Figure 4 shows the transmission spectra of the actual filter compared with the theoretical filter transmission spectra. The theoretical SEP for the system, assuming a filter with the exact spectrum of the theoretical filter, is 0.59 μM. We should expect some degradation in the SEP as a result of spectral mismatch (reference 4 describes how spectral tolerance in a coating is obtained from the spectral variance).

We used 10 uroporphyrin mixtures as a test set to determine the optimum value of C in the following equation: Pred = k (T-CR). C in this equation is a correction for the differing responsivities of two different detectors due to factors such as gain resistor variation, etc. k in this equation is the gain factor for prediction (Pred). 10 more uroporphyrin samples were used to validate the system. Figure 5A shows the actual concentration of Cu(II) uroporphyrin I as a function of the measured value of T-CR for the data set used to determine C, while figure 5B shows the validation set. The calculated SEP from these data is 0.86 μM, only slightly worse than the theoretical best value of 0.59.

ACKNOWLEDGEMENTS

38

REFERENCES

1.   M.P. Nelson, J.F. Aust, J.A. Dobrowolski, P.G. Verly, and M.L. Myrick, Anal. Chem. 58(1986), 2561.

2.   J.A. Dobrowolski, P.G. Verly, J.F. Aust, M.P. Nelson and M.L. Myrick in Proceedings of the SPIE Annual Meeting on Optical Science and Engineering, San Diego, California, July, 1997, 232.

3.   S. Bialkowski, Anal. Chem. 58(1986), 2561.

4.   M.L. Myrick, S. Soyemi, H. Li, L. Zhang and D. Eastwood, Fres. J. Anal. Chem. (submitted, 2000).

5.   O. Soyemi, H. Li, L. Zhang, D. Eastwood, P. Gemperline, and M.L. Myrick, Anal. Chem. (submitted, 2000)
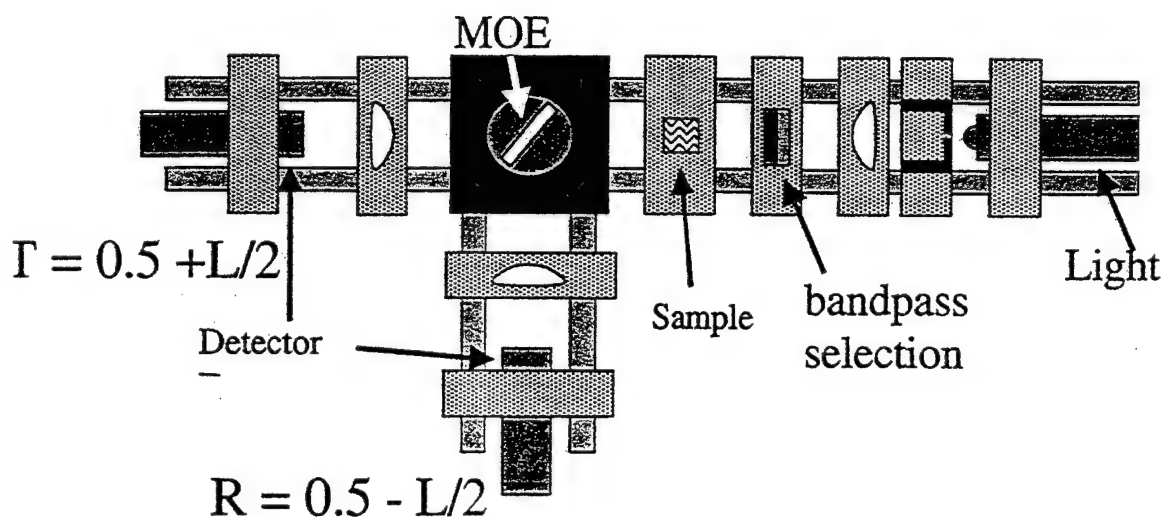
Figure 1: Prototype field Instrument utilizing multivariate optical element (MOE) interference filter as beam-splitter. T = transmittance, R = reflectance, L = spectral vector
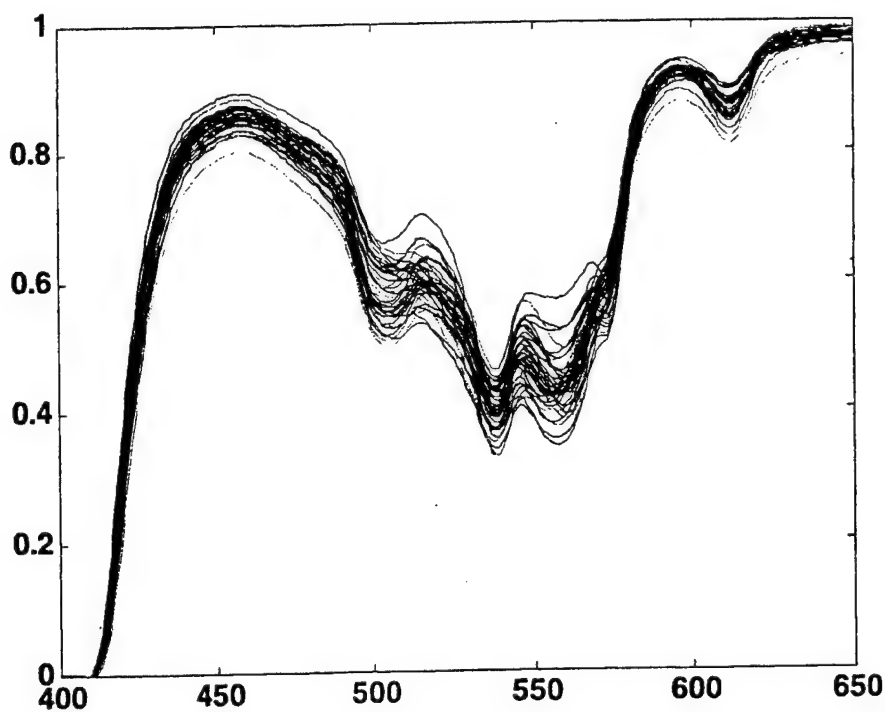
Figure 2: Transmission spectra of 40 uroporphyrin mixtures in 1M NH₄OH
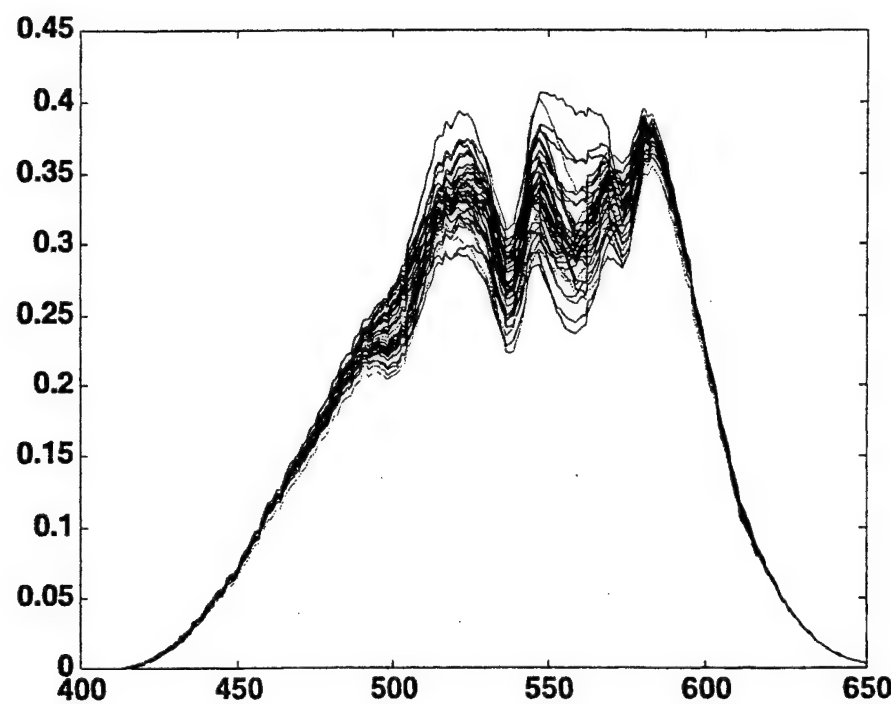
Figure 3: Detector response (corrected transmission spectra) of uroporphyrin mixtures.

41

Comparison of the theoretical filter spectrum and the experimental filter spectrum for the quaternary porphyrin mixture MOE
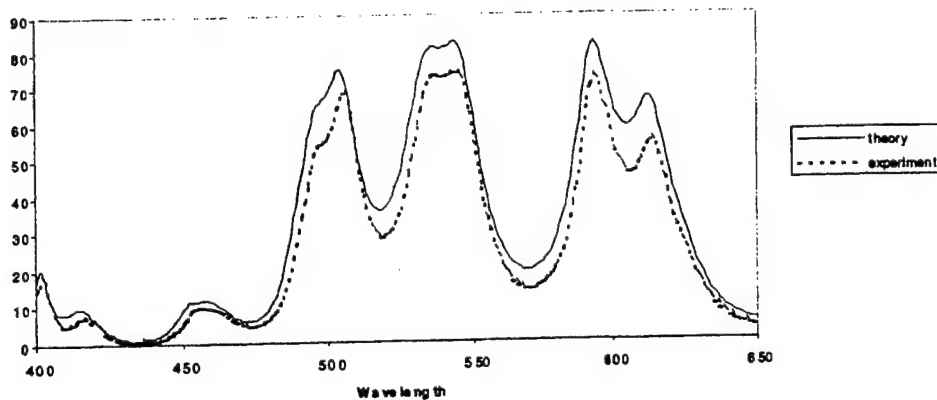
Figure 4: Comparison of the theoretical filter spectrum and the experimental filter spectrum for the quaternary porphyrin mixture multiple optical element (MOE) filter.

42
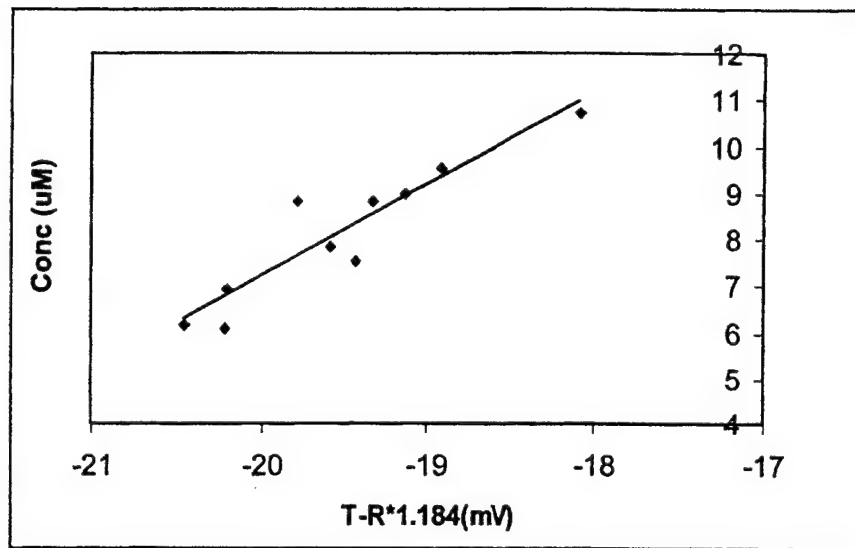
Figure 5A: Concentration of Cu (II) uroporphyrin in ten test uroporphyrin mixtures vs. T-R (the difference between the two detector readings) multiplied by a correction factor.
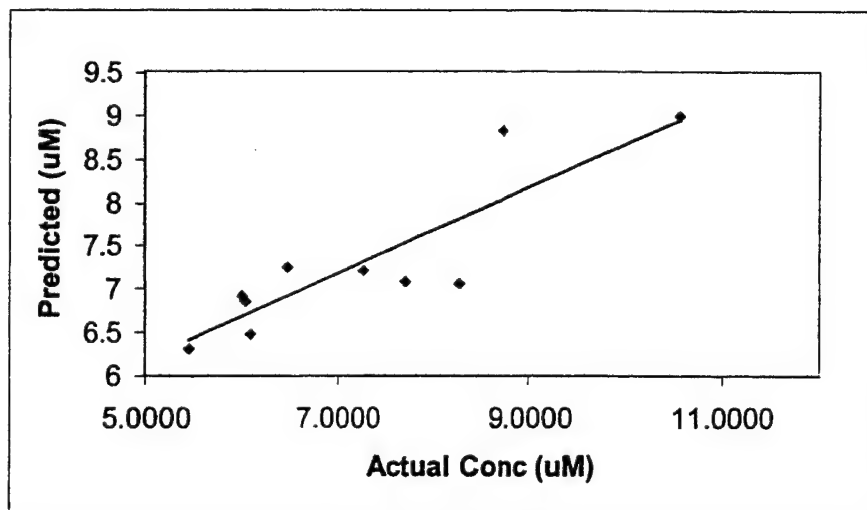
Figure 5B: Predicted vs. actual concentrations for the Cu (II) uroporphyrin in ten validation uroporphyrin mixtures.

43

10.4 Design and Testing of a Multivariate Optical Element (MOE): The First Demonstration of Multivariate Optical Computing for Predictive Spectroscopy
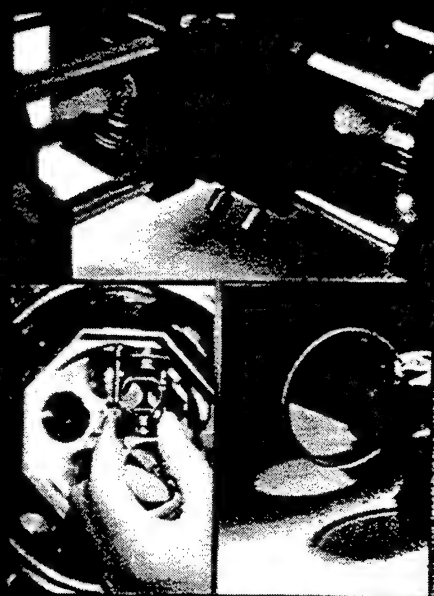
Accelerated Articles

Design and Testing of a Multivariate Optical Element: The First Demonstration of Multivariate Optical Computing for Predictive Spectroscopy

O. Soyemi,[†] D. Eastwood,[†] L. Zhang,[†] H. Li,[†] J. Karunamuni,[†] P. Gemperline,[‡] R. A. Synowicki,[§] and M. L. Myrick*,[†]

Department of Chemistry and Biochemistry, University of South Carolina, Columbia, South Carolina 29208, Department of Chemistry and Biochemistry, East Carolina University, Greenville, North Carolina 27258, and J. A. Woollam Company Inc., 645 M Street, Suite 102, Lincoln, Nebraska 68508

A demonstration of multivariate optical computing is presented using binary dye mixtures consisting of Bismarck Brown and Crystal Violet. Bismarck Brown was treated as the analyte, while Crystal Violet was treated as a random interfering species. First, a multilayer multivariate optical element (MOE) for the determination of Bismarck Brown was designed using a novel nonlinear optimization algorithm. Next, the MOE was fabricated by depositing alternating layers of two metal oxide films (Nb_2O_5 and SiO_2) on a BK-7 glass substrate via reactive magnetron sputtering. Finally, the MOE was tested on 39 binary dye mixtures using a simple T-format prototype instrument constructed for this purpose. For each sample, measurements of the difference between transmittance through the MOE, and the reflectance from the MOE were made. By setting aside some of the samples for instrument calibration and then using the calibration model to predict the remaining samples, a standard error of prediction of 0.69 μM was obtained for Bismarck Brown using a linear regression model.

Multivariate calibration is an established tool in chemometrics for the correlation of a physical or chemical property of interest to information spanning multiple wavelength channels in optical spectroscopy.[1–3] The conventional application of this tool in chemical analysis entails first the acquisition of optical spectra in the appropriate wavelength region (typically from the ultraviolet to the mid-infrared). Next, chemometric tools are used to extract a spectral pattern (the regression vector) which is correlated to the property of interest but orthogonal to interferences.[4] Prediction of the property in an unknown sample is then carried out by determining the magnitude of the spectral pattern in the optical spectrum of the sample. More specifically, the magnitude is calculated by taking the inner product of the regression vector and the optical spectrum of the unknown sample. A major drawback in the widespread use of multivariate calibration, especially for field applications, is its dependence on expensive and bulky laboratory-type equipment for data acquisition and analysis.

A recent publication from our laboratory[5] addressed from a theoretical standpoint the feasibility of using optical computing in predictive spectroscopy to simplify and harden the apparatus necessary for chemical prediction. The first reports of a related hypothetical optical approach to multivariate chemical measurement were those of Bialkowski.[6] The use of a single multivariate optical element (MOE) in a beam splitter configuration has also

---

* To whom correspondence should be addressed. Telephone: (803)-777-6018. Fax: (803)-777-9521. E-mail: myrick@psc.sc.edu.
† University of South Carolina.
‡ East Carolina University.
§ J. A. Woollam Company Inc.

(1) Aust, J. F.; Booksh, K. S.; Myrick, M. L. *Appl. Spectrosc.* 1996, 50, 382–387.
(2) Thomas, E. V.; Haaland, D. M. *Anal. Chem.* 1990, 62, 1091–1099.
(3) Ruyken, M. M. A.; Visser, J. A.; Smilde, A. K. *Anal. Chem.* 1995, 67, 2170–2179.
(4) Martens, H.; Naes, T. *Multivariate Calibration*; John Wiley & Sons: New York, 1989; Chapter 3.
(5) Nelson, M. P.; Aust, J. F.; Dobrowolski, J. A.; Verly, P. G.; Myrick, M. L. *Anal. Chem.* 1998, 70, 73–82.
(6) Bialkowski, S. *Anal. Chem.* 1986, 58, 2561–2563.

46
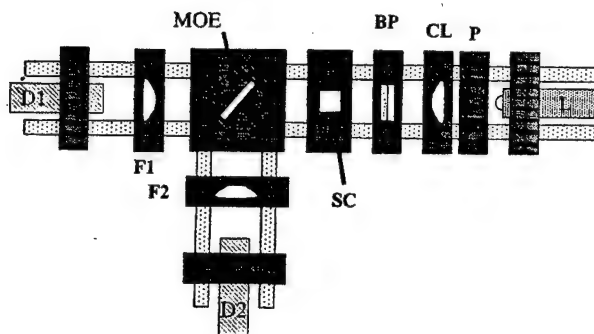
Figure 1. Schematic of a multivariate optical computing system for the measurement of BB in a binary dye mixture. Key: MOE, multivariate optical element; SC, quartz sample cell; OB, optical block; BP, band-pass filter set consisting of two 3-mm Schott glasses; CL, achromatic collimating lens; L, tungsten halogen lamp; P, pinhole; D1/D2, Si photodiode detectors for light radiation transmitted through and reflected from the MOE; F1/F2, focusing lens.

been described for the same purpose,[7] a permutation most similar to that proposed by Ryabenko and Kasparov.[8] The all-optical approach proposed by our laboratory differs from previous work by centering around the production of one or more optical interference coatings whose transmission spectra incorporate features of a spectral regression vector. Such interference filters based on multivariate spectroscopy will be referred to as MOEs. MOEs have never been demonstrated as a tool for actual chemical measurement, however.

This report details the first demonstration of multivariate optical computing (MOC) using an MOE. Simple binary dye mixtures of Bismarck Brown (BB) and Crystal Violet (CV) were selected to design a MOE that would test the concept of all-optical prediction. The experiments reported below consist of several elements. First, the optical properties of all the pertinent components of a simple T-format spectroscopic system were evaluated. Second, spectra of a series of binary dye mixtures were recorded and converted to a spectral radiance scale for chemometricinterpretation. Third, a theoretical design for a MOE suitable to this measurement was generated. Fourth, the MOE was fabricated in-house. Finally, the MOE was installed in our T-format instrument and measurements of calibration and validation samples were performed.

EXPERIMENTAL SECTION

Owing to the possible confusion between dimensions for wavelength and layer thicknesses, in the following we will uniformly employ the units "nanometer" for dimensions of wavelength and "angstroms" for units of film thickness.

Demonstration of the MOC technique was carried out on a compact T-format instrument (Figure 1), which was constructed using Linos Photonics (Milford, MA) optical components.

A 6-V/6-W tungsten filament lamp (Linos Photonics) with 1×1.2 mm active filament area was used as a light source for the test instrument. The spectral radiance of the lamp was measured

in W/sr·cm²·nm with a CCD spectrometer system consisting of a Chromex 250IS spectrometer with a 300 line/mm grating blazed at 500 nm and a Princeton Instruments 1100×300 pixel CCD camera, model TE/CCD-1100-PE. The input optics on the spectrometer system were duplicates of the Figure 1 system. For these measurements, the operating voltage for the lamp was fixed at 5.76 V. The wavelength range of the camera/spectrometer system was calibrated with a standard mercury pen lamp and a standard neon lamp. The spectral radiance of the lamp under these conditions was calibrated against an OL series 455 integrating sphere calibration standard lamp (Optronic Laboratories Inc.) operated under standard conditions.

The two Si photodiode active detectors were type BPW21 (Linos Photonics) with a sensitive area of 2.7 mm², spectral range of 320−880 nm, and radiant sensitivity at the peak wavelength (550 nm) of 3.8 V/mW. The relative spectral sensitivity of the detector wavelength was estimated from a Linos Photonics data sheet giving values measured at 25 °C and 12-V dc supply voltage.

A band-pass filter set was used to isolate the spectral region between 400 and 650 nm in which the visible absorbances of the two dyes are found. The band-pass set consisted of two 3-mm-thick Schott glass filters (Duryea, PA) BG-39 and GG400.

Water-soluble dyes obtained from Aldrich Chemical Co. The dyes were Bismarck Brown ($\lambda_{max} = 457$ nm, dye content 50%) and Crystal Violet ($\lambda_{max} = 590$ nm, ACS reagent grade, dye content 95%). Stock solutions in distilled water of BB at a concentration of 82.3 μM and CV at a concentration of 37.7 μM were prepared.

Forty mixtures of BB and CV were prepared by dilution of the stock solutions in order to obtain data for multivariate calibration. These mixtures were made with known random concentrations of each dye to ensure that the concentrations of the two dyes were varied independently. The ranges over which the concentrations of BB and CV were varied were chosen to ensure that the minimum transmittance of the diluted mixtures in the 400−650-nm window were between 30 and 70%. BB was selected as the analyte because the spectrum of CV was an interference at all wavelengths over which BB absorbed. CV was treated as an uncorrelated interference. Optical spectra were recorded on a Hewlett-Packard UV−visible diode array spectrometer (model 8543). The samples were measured in a 1-cm fused-silica cell (Starna Cells Inc., Atascadero, CA).

Following data collection and radiometric corrections for lamp intensity, detector response, and band-pass, design of MOE coatings was performed in two different ways. First, a spectral vector based on a principal components regression (PCR) model with four components was defined, and an iterative spectral-matching synthesis was performed. This procedure used TFCalc, a commercial software product from Software Spectra, Inc. (Portland, OR). The second approach began by synthesizing a crude filter design based on spectral matching to the PCR vector. The result of the crude spectral match was then used to initialize a nonlinear least-squares optimization routine to produce the final filter design.[9] The nonlinear least-squares algorithm was written in-house in the MATLAB programming environment. More detail is provided in the discussion below.

(7) Myrick, M. L. Soyemi, O.; Karunamuni, J.; Eastwood, D.; Li, H.; Zhang, L.; Gemperline, P. *Vib. Spectrosc.,* in press.

(8) Ryabenko, A.; Kasparov, V. *Pattern Recognit. Image Anal.* 1991, *1*, 347−354.

(9) Soyemi, O.; Gemperline, P. J.; Zhang, L.; Eastwood, D.; Li, H.; Myrick, M. L., in preparation.

47
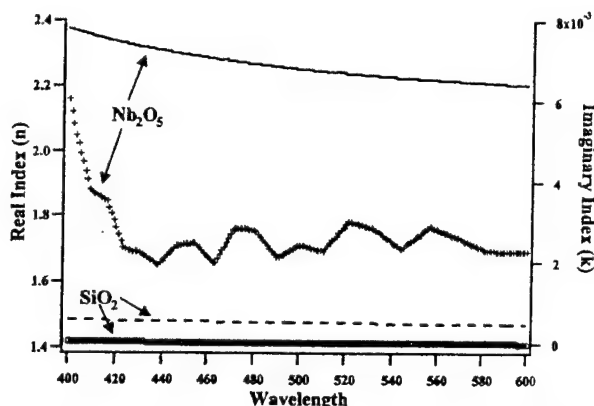
Figure 2. Real refractive indices of Nb_2O_5 (solid line) and SiO_2 (dashed line) deposited in the USC deposition chamber in the wavelength region between 400 and 600 nm as determined from variable-angle spectroscopic ellipsometry. The left axis gives values for real indices. Imaginary refractive indices are indicated by + (Nb_2O_5) and o (SiO_2) on the right axis.

The MOE was manufactured via reactive magnetron sputtering (RMS). Our sputtering system (model CV 5.1) was custom-manufactured by Corona Vacuum Coaters of Vancouver, BC. The system operates at room temperature and utilizes a 40-kHz midfrequency rf supply to power four water-cooled planar magnetrons positioned in pairs around a drum that rotates about a horizontal axis. The coating chamber is 55.9 cm in diameter and 50.8 cm deep and contains 10.1 cm × 25.4 cm magnetron targets, two containing niobium (99.95% pure, high index) and two containing silicon (99.9999% pure, low index). Each magnetron target is powered at ~0.7 kW, although the power is varied during deposition as one method of controlling deposition rate. The RMS process was used to deposit alternating layers of niobium pentoxide and silicon dioxide films by reaction with oxygen in the gas mixture. MOE designs require accurate knowledge of the optical constants of the coating materials. Figure 2 shows experimental measurements of the real and imaginary refractive indices of Nb_2O_5 and SiO_2 deposited in our chamber as determined by variable-angle spectroscopic ellipsometry.

The MOE tested here was fabricated on a 2.54-cm BK-7 glass substrate. Layer deposition was optically monitored on-line with a 1200 line/mm grating monochromator (model 9030, Sciencetec, London, ON, Canada) blazed at 250 nm. Light detection was achieved using a photomultiplier tube (model H5784-03, Hamamatsu, Japan). Visible light was obtained from a tungsten filament lamp (Gilway Technical Lamps, Waltham, MA). After MOE design was completed, the interference effects on transmission for each layer were computed at all accessible monitoring wavelengths. The system can currently monitor wavelengths between 420 and 600 nm with ~1-nm resolution, and thus ~180 different "monitor curves" were produced for each layer. From the 180 possible curves, the optimum wavelength for monitoring and controlling the deposition of each layer was selected based on a set of criteria developed as a result of experience in our laboratory. Process control of the deposition process was performed with in-house software written in the LabVIEW 5.1 programming environment that operated in concert with the system control software provided by Corona Vacuum Coaters. The two software packages used the

selected monitor curves to deposit each filter layer as accurately as possible. More detail is provided in the discussion below.

After the production of the MOE as described above, it was installed in the T-format instrument shown in Figure 1. A total of 39 new samples of BB and CV were prepared using the random number generation described above. The difference between the signal due to light transmission through the sample followed by transmission through the optical filter (aligned at ~45°) and light transmission through the sample followed by reflection from the surface of the optical filter was measured for each sample. Twenty of these measurements were used for calibrating the instrument (determining the optimum relative gain factor for the two detectors, vide infra), while the remaining 19 samples were used to validate the calibration model.

The relative gain factor described above is used to correct for the fact that the two detectors illustrated in Figure 1 have slightly different responsivities. These different responsivities can result from variance in the electronics of the two detectors or from other causes. When performing calculations using two detectors in our setup, we used a set of calibration samples to obtain measurements of transmittance and reflectance and then varied an empirical relative gain factor (called K in the discussion below) until the best correlation was obtained. This optimum gain factor was then used for future experiments.

RESULTS AND DISCUSSION

Single MOEs can be designed for chemometric prediction by using them in a beam splitter arrangement as shown in Figure 1.[7] Consider the optical transmission spectrum of an MOE to be $T(\lambda) = 0.5 + L(\lambda)$, where $L(\lambda)$ is a spectral pattern that can also be represented in vector form as l. Assuming negligible absorbance in the MOE, the difference between the intensity of light transmitted through the MOE ($\mathbf{t} \cdot \mathbf{x}_i$) and light reflected from it ($\mathbf{r} \cdot \mathbf{x}_i$) is proportional to the scalar product of the vector l with the sample spectrum vector for the ith sample, $\mathbf{x}_i$

$$\mathbf{t} \cdot \mathbf{x}_i - \mathbf{r} \cdot \mathbf{x}_i = (\mathbf{t} - \mathbf{r}) \cdot \mathbf{x}_i =$$
$$((0.5 + \mathbf{l}) - (0.5 - \mathbf{l})) \cdot \mathbf{x}_i = \mathbf{l} \cdot \mathbf{x}_i \quad (1)$$

In this measurement paradigm, l can be chosen to be proportional to a regression vector for a dependent sample variable. Because an MOE must have transmittance values between 0 and 1 inclusive, l can have a magnitude no greater than 0.5 at any wavelength. For reasons of improving signal-to-noise ratio, the magnitude of l should be made as large as possible, subject to this limitation. Thus, the scalar product of this vector with the spectral vector is proportional to the value of the dependent variable ($\hat{y}_i$), with a proportionality constant we will represent by G/m (where m is the number of wavelength channels in the vectors) and an offset (off):

$$\hat{y}_i = (G/m)(\mathbf{l} \cdot \mathbf{x}_i) + \text{off} \quad (2)$$

To achieve this, the spectrum of the 45° filter (the MOE in Figure 1) must be designed such that an optimal multivariate regression vector can be derived from it that results in the best possible standard error of sample prediction (SEP). This regression vector, according to equation two, is the vector $\mathbf{R} = (G/m)\mathbf{l}$.

48

1. Selection of the Spectral Window and Spectral Mode. Although MOC should function in many linear types of spectroscopy, the most convenient and most basic multivariate measurement to set up is spectral absorbance. MOC should also function in any spectral range where good optical elements can be produced. However, in our laboratory, our experimental system lends itself most conveniently to measurements in the visible spectroscopic region. This is because our MOE fabrication system is presently process-controlled using an optical monitor between 420 and 600 nm. We elected to make measurements of mixtures of visible-absorbing dyes in the spectral window between approximately 420 and 600 nm.

Absorbance is nominally linear in concentration within the limits over which Beer's law holds. A radiometric measurement, however, is more directly related to transmittance of the sample than absorbance, and transmittance is logarithmically related to concentration. Nevertheless, a number of studies correlating single-beam and radiometric measurements to chemical properties using linear chemometric models have been performed with some success.[10,11] In the limit of low absorbances, transmittance varies linearly with concentration; even for high absorbances, transmittance can be considered piecewise linear with concentration. Also, it has been shown that linear multivariate calibration methods such as PCR and partial least-squares regression (PLS) can satisfactorily model nonlinear responses by the inclusion of extra factors or latent variables in the calibration model.[12] In the following discussion, the raw data from which an MOE is designed will be analyzed in both transmittance and absorbance modes for comparison purposes to evaluate how the nonlinearity of transmittance with concentration affects the resulting prediction error.

Since measurement by an MOE-based instrument is inherently radiometric in nature, a number of factors not normally considered in absorption measurements must be quantitatively evaluated. These include the following: (a) the spectral radiance of the source, (b) the transmittance of the samples, (c) the transmittance of any band-pass-selection filter, (d) the spectral sensitivity of the detector, and (e) the determination of the effective band-pass. Once these factors are known, the design of an MOE must be conducted via iterative thin-film synthesis subject to suitable starting, optimization, and stopping criteria. Following thin-film design, the precision of the fabrication process must be extreme. This requires a real-time monitoring system with suitable control software and accurate knowledge of the optical constants of materials involved in fabrication. Only after all these issues have been dealt with and concluded satisfactorily can the final system be evaluated. The following sections describe each of these basic considerations in detail.

2. Radiometric Correction of Spectral Data. A realistic representation of the MOC instrument detector signal must include a convolution of the following radiometric quantities: the detector sensitivity, the spectral radiance of the source, the spectral band-pass, and the sample transmittance, all of which are functions of wavelength. Figure 3 shows the transmittance spectra of 40 mixtures of the two dyes in the region between 400 and 650

(10) Ding, Q.; Small, G. W.; Arnold, M. A. *Appl. Spectrosc.* 1999, *53*, 402–414.
(11) Hazen, K. H.; Arnold, M. A.; Small, G. W. *Anal. Chim. Acta* 1998, *371*, 255–267.
(12) Gemperline, P. J.; Long, J. R.; Gregoriou, V. G. *Anal. Chem.* 1991, *63*, 2313–2323.
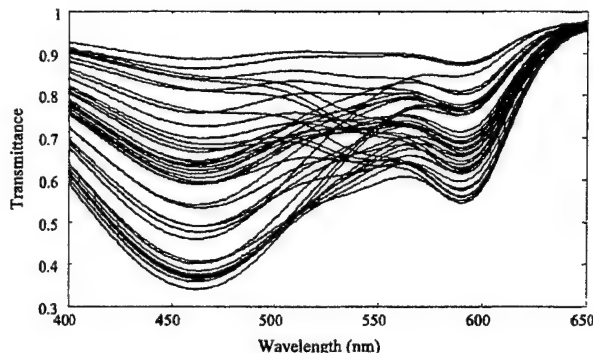
Figure 3. Transmittance spectra of 40 binary mixtures of Bismarck Brown and Crystal Violet acquired on a UV–visible diode array spectrometer.

nm (with concentration and wavelength ranges similar to those described above).

In ordinary chemometric applications, out-of-band light can be eliminated by simply ignoring it. That is, light from the sample that is not in the range over which the chemometrics is performed does not have to be sampled. In the MOC measurement, however, band selection filters must be used to obtain this result. To ensure that light from outside the wavelength range of our targeted response window is not transmitted through the MOE onto the detector, a colored-glass band-pass filter set whose transmittance profile is shown in Figure 4A was used.

Si photodiode detectors were selected for the dual-channel measurement system (Figure 1). Figure 4B shows a plot of the detector spectral sensitivity versus wavelength as estimated from a manufacturer-provided graph. The sensitivity reaches a maximum at ~550 nm and tapers off in the short-wavelength near-infrared region (not shown in the figure).

A tungsten filament lamp was selected to serve as a light source for the measurement. These lamps are approximately blackbody-type emitters, with a spectral radiance maximum in the near-infrared. Figure 4C shows the spectral flux (in W/nm) of our tungsten filament lamp after passing through a 1-mm pinhole. The spectral flux profile was obtained by correcting the measured spectral radiance profile for the active solid angle $(=(3/4)\,(r^2/f^2)$ sr, where r and f are the radius and focal length of the focusing lens in the calibration system, respectively) and the active pinhole area $(=\pi r_p^2$, where r_p is the radius of the pinhole).

Figure 4D shows the sample transmittance spectra corrected for the radiometric quantities described above, and they represent the spectral signal for each sample.

3. MOE Design. An initial permutation of the MOC technique was proposed which involved the reproduction of the positive and negative lobes of the PCR regression vector on two separate filter elements.[5] In this original conception, the light transmitted through two MOEs is separately detected to give a difference signal that is proportional to the sample concentration. The MOC configuration used in the study requires only a single MOE in a T-format configuration in which the MOE acts as a 45° beam splitter. Because of this, the MOE is designed to operate at this angle. Coatings at nonnormal incidence are prone to strong polarization effects. However, our calculations assumed completely unpolarized light since the light source for the instrument is an on-axis tungsten lamp. The algorithm thus designs a coating for

49
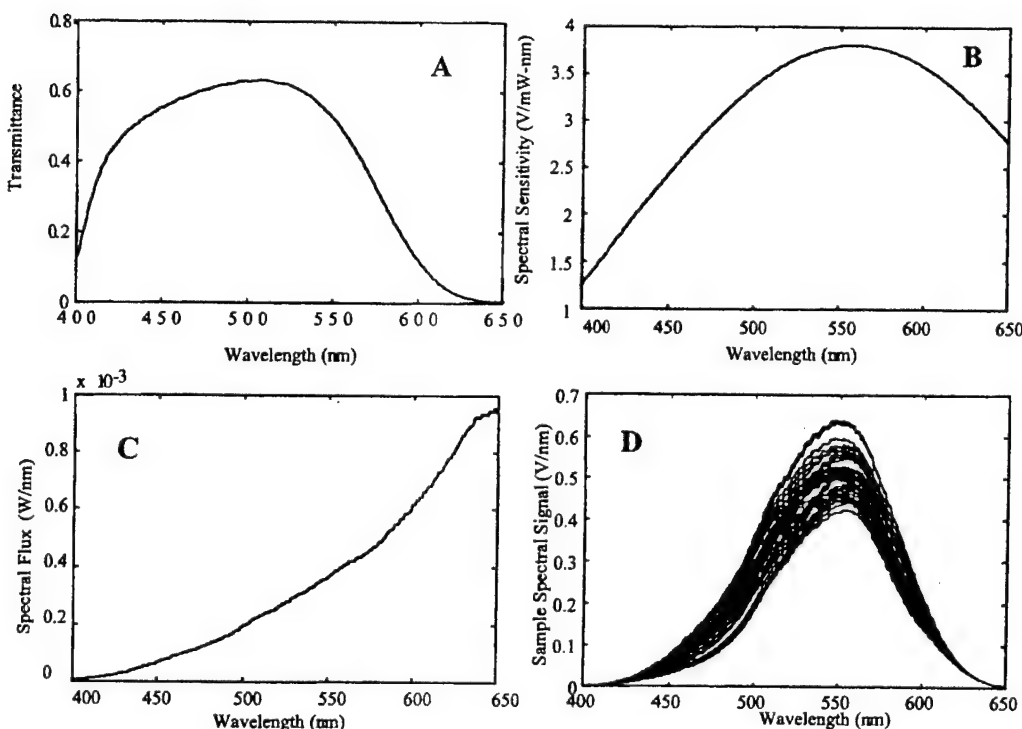
Figure 4. (A)–(C) are the characteristics of selected radiometric quantities for the T-format measurement system in Figure 1: (A) Band-pass of two 3-mm Schott glass filters versus wavelength, (B) detector sensitivity of two Si photodiode detectors versus wavelength, and (C) source radiance of the tungsten filament lamp versus wavelength. (d) shows the sample spectra in Figure 3 corrected for the three radiometric quantities in (A)–(C).

light with equal magnitudes of *s*- and *p*-polarized light; our unpolarized light source provides such light to a very good approximation as long as the lamp is on the optical axis of the system. For the same reason, the detectors must be kept on axis as well.

The corrected detector response profiles (corrected transmittance spectra) in Figure 4D were used for MOE design. Two possibilities exist for designing a viable MOE, both of which use iterative solving approaches. In each, calculation of the MOE spectrum from the design utilizes a matrix formulation that is based on the solutions to Maxwell's equations.[13] The spectrum of a hypothetical coating is obtained and then evaluated subject to various criteria and then modified in ways that improve the criteria for evaluation. The criteria are the main points of differentiation between the two methods for design we will describe below. The first entails the transfer of the structure of a PCR regression vector onto a filter element via spectral matching using the established needle optimization technique.[14–16] The evaluation criteria in this case are "goodness of spectral match". The second method of MOE design referred to in the Experimental Section above uses a novel algorithm that synthesizes the best filter solution based on the constraint of minimizing the standard error in sample prediction.

Effective Band-Pass. As Figure 4A shows, the band-pass defined by our colored-glass filters is not clear-cut. The transmission band of the filters is far from a rectangular function of wavelength. An operational definition of the band-pass can be proposed, however, as the wavelength range over which the transmittance function of the MOE must be defined. In other words, outside the operational band-pass, all values of transmittance for the MOE are permissible because the variance of the signal strength is so small that it has a negligible impact on prediction. Determination of the operational band-pass limits has recently been examined in a discussion of spectral tolerance for MOE design.[17] The lower and upper wavelength limits of the spectral band are given by solving the following equation:

$$V_{ex} = V_{co}(\lambda_R - \lambda_L) - \frac{SEP^2}{2(G/m)} = 0 \qquad (3)$$

where V_{ex} is the excluded variance of the spectroscopic samples at all wavelengths outside the band-pass, V_{co} is the variance cutoff value at wavelengths defining the edges of the band-pass, λ_R and λ_L are the right and left wavelength limits of the band, SEP is the standard error of prediction for the calibration model, and (G/m) is the proportionality factor defined in eq 2. Based on the original 40-sample calibration set, the effective band-pass was determined to be between 424 and 622 nm for these data.

Spectrum Matching. Reference 5 describes needle optimization as a method by which spectral transmission targets can be

(13) Liddell, H. M. *Computer-Aided Techniques for the Design of Multilayer Filters*; Adam Hilger Ltd.: Bristol, U.K., 1983; Chapter 1.

(14) Dobrowolski, J. A.; Lowe, D. *Appl. Opt.* **1978**, *17*, 3039–3050.

(15) Tikhonravov, A. V. *Vest. Mosk. University, Ser 3: Fiz., Astron.* 1982, *23*, 91–93.

(16) Verly, P. G.; Tikhonravov, A. V.; Trubetskov, M. K. *Appl. Opt.* 1997, *36*, 1487–1495.

(17) Myrick, M. L.; Soyemi, O.; Li, H.; Zhang, L.; Eastwood, D. *Fresenius J. Anal. Chem.* **2001**, *369*, 351–5.

50
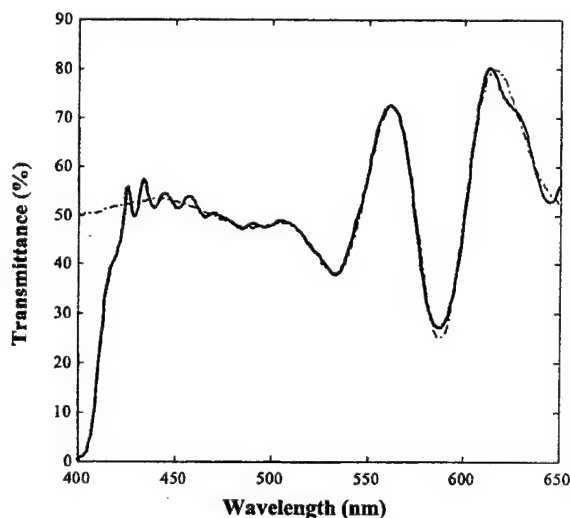
Figure 5. Comparison of the spectral target generated from the 4-factor PCR regression vector for the determination of BB generated from a calibration set of 20 binary dye transmittance spectra (dashed line), to the transmittance spectrum of a MOE designed by spectral matching with permissible tolerances (solid line).

approximated through iterative synthesis of an interference coating.[15] It is the basis for several commercial thin-film design programs that are presently available.[18,19] Using needle optimization, the MOE design that best matches the spectral profile of the PCR vector is iteratively synthesized by minimizing a merit function, F, which describes the difference between a calculated spectrum (based on the MOE layer thicknesses in each iteration) and the target spectrum (represented by the spectral profile of the PCR vector). F for a spectral-matching synthesis routine can be defined by

$$F = \left(\frac{1}{m} \sum_{j=1}^{m} \frac{|Z_j^D - Z_j|^k}{\text{Tol}_j} \right)^{1/k} \qquad (4)$$

where Z_j^D is the calculated response (e.g., transmittance) value at wavelength j, Z_j is the target value, Tol_j is the design tolerance at that wavelength, m is the number of wavelength targets, and k is an algorithm gain factor used to weight the relative importance of mismatched regions. Design tolerances can be selected for each wavelength channel, which specify the minimum allowable deviation from the target at that wavelength. The design process involves the insertion of a zero-thickness layer (needle) into the MOE refractive index profile at each iteration of the optimization routine. The insertion results in the adjustment of existing layer thicknesses as well as that of the new layer to give a better (lower) estimate of the merit function. The process continues until the merit function can no longer be minimized. The periodic application of a "tunneling" function helps in achieving a global minimum for the optimization process by regularly perturbing the system as a means of escaping local minimums. Figure 5 shows a comparison of the transmittance spectrum of a MOE element

(18) TFCalc, Software Spectra Inc., Portland, OR.
(19) FilmWizard, Scientific Products and Services Inc., Carlsbad, CA.

produced by spectral matching to the target spectrum. The target spectrum was created from the 4-factor PCR regression vector that resulted from the calibration of 20 binary dye detector profiles with corresponding BB concentrations. Although the spectrum (the solid line in Figure 5) varies from the target (the dashed line) in some wavelength regions, the result is within the allowable tolerances for the design. The main complication of this approach to designing MOEs is that the PCR regression vector is not necessarily the basis for the simplest MOE.

For example, this MOE designed by spectral matching using spectral tolerances determined as reported elsewhere[17] consists of 46 alternating layers of Nb_2O_5 and SiO_2, with a total coating thickness of 3.7 μm. The deposition system we use for depositing these coatings (vide infra) would require ~2 days to produce this coating. Further, the accuracy with which a spectrum can be created in an actual MOE is related to the number of layers in the coating; more layers provide increased opportunity for manufacturing errors. The MOE designed by spectral matching was not fabricated. Instead, we pursued an alternative method to MOE design developed in our laboratory with the aid of P.G. Conceptually, this new approach could be called "spectral vector relaxation" (SVR). The basis for SVR is that many vectors satisfy the criteria for good regression vectors in addition to the ones that are found via PCR. Some of these vectors will be easier to fabricate in the MOE form than others; we seek a general method for locating those that are the simplest to fabricate.

MOE Design via Least-Squares Minimization of Sample Prediction Error: SVR. Even with the careful selection of design tolerances, there is no guarantee that needle optimization will produce a design that matches a spectral target *and* can be readily fabricated. For example, in cases where the target spectrum has many high-frequency components (e.g., noise), it is quite likely that a MOE design will result with many layers and a large value of total layer thickness. Such coatings are difficult to fabricate using conventional thin-film deposition techniques because manufacturing errors accumulate with each layer and because stress builds between the coating and its substrate with increasing coating thickness. Such stress will generally lead to coating delamination when the coating thickness exceeds ~10–25 μm. In addition, economic considerations of long deposition cycles argue for simplified, thinner coatings.

Instead of trying to match a PCR regression that represents a fixed SEP, an alternative algorithm has been developed that combines design with optimization of the SEP.[9] This algorithm is based on a nonlinear least-squares optimization technique and attempts to synthesize the optimum MOE design at a given level of complexity of the coating. In other words, instead of creating an MOE design whose spectrum matches a regression vector, an MOE design is created with a fixed upper-bound level of complexity (numbers of layers and layer thicknesses). Among all the possible MOE designs with a fixed maximum level of complexity, the one whose spectral profile results in an optimal value of the SEP can then be obtained.

Unlike the previous design method, which starts from a single layer and gradually builds up the coating, the SVR filter design algorithms are initialized with a specified number of layers with either random or predetermined layer thicknesses.

Table 1. 26-Layer MOE Design for the Determination of Bismarck Brown in a Binary Dye Mixture with Crystal Violet Showing the Individual Layer Thicknesses (in Nanometers)[a]

layer no.	material	layer thickness (Å)	layer no.	material	layer thickness (Å)
1	Nb_2O_5	279	14	Nb_2O_5	675
2	SiO_2	2099	15	SiO_2	374
3	Nb_2O_5	702	16	Nb_2O_5	675
4	SiO_2	796	17	SiO_2	493
5	Nb_2O_5	477	18	Nb_2O_5	795
6	SiO_2	657	19	SiO_2	309
7	Nb_2O_5	434	20	Nb_2O_5	2024
8	SiO_2	723	21	SiO_2	1023
9	Nb_2O_5	328	22	Nb_2O_5	796
10	SiO_2	664	23	SiO_2	1539
11	Nb_2O_5	304	24	Nb_2O_5	921
12	SiO_2	1405	25	SiO_2	881
13	Nb_2O_5	577	26	Nb_2O_5	720

[a] Layer 1 is the layer closest to the substrate (BK-7 optical glass).

If n is the number of layers in the coating, optimization using the SVR algorithm can be visualized in an $n + 2$ dimensional space. The additional two dimensions in the space are scaling (G/m) and offset (off) factors relating the spectral vector to the dependent variable in the sample. The figure of merit in this optimization is the SEP for prediction of the dependent variable using the design of the coating at each iteration. The steps to calculating the SEP at the end of each iteration is as follows; first, the current optical transmission spectrum ($T(\lambda)$) spanning m wavelength channels is scaled to a regression vector (R) as in

$$\mathbf{R} = (G/m)[2\mathbf{t} - 1] \tag{5}$$

Next, an estimate of the concentration of sample i ($\hat{y}_i$) is determined as the offset scalar product of its spectrum ($\mathbf{x}_i$) with the regression vector (R), where t represents the vector transpose.

$$\hat{y}_i = \mathbf{x}_i\mathbf{R}^t + \text{off} \tag{6}$$

By substituting eq 5 into eq 6, the SEP for N validation samples is calculated thus:

$$\text{SEP} = \frac{\sum_{j=1}^{N}\left\{\left\{\mathbf{x}_i\left[\frac{G(2\mathbf{t} - 1)}{m}\right]^t + \text{off}\right\} - y_i\right\}^2}{N} \tag{7}$$

During optimization, layer thicknesses that fall below a specified threshold value are deleted because extremely thin layers are difficult to deposit accurately in our current apparatus. Because the final MOE design that results from SVR can have less than, or equal to, the starting number, this novel algorithm creates designs with smaller overall coating thicknesses than those created with needle optimization. In practice, we have found that this can often be achieved without sacrificing predictive ability.

The starting point of the optimization routine is important since the SVR algorithm can converge to a nonglobal optimum. The choice of an appropriate starting point usually produces a rapid descent to the global optimum for a given upper-bound level of complexity.

Figure 6. Results for a MOE produced by SVR. Comparison of the measured MOE spectrum at 45° (dashed line) to the calculated SVR MOE spectrum at 45° (solid line). Polarization effects in the measured spectrum are uncorrected.

There are currently two variants of the SVR MOE design algorithm that differ in their modes of initialization. The first one initializes the optimization process with a specified number of layers with random thicknesses, which are then modified to give the best MOE design. Starting with a random number of layers or layers with fixed thicknesses, the second variant to the design algorithm creates a partial design by crudely matching the PCR regression vector using standard spectral matching. With this partial design as the starting point, the MOE spectrum is then further refined. The SVR approach does not add new layers but instead deletes layers that fall below a specified minimum permissible thickness during iteration. For comparison to the 46-layer spectral-matching design described above, we initialized a SVR design beginning from a partial needle design consisting of 30 layers. The final SVR result is shown in Table 1. This design, which corresponds to an SEP of 0.31 μM, has 26 layers with total thickness of 2.1 μm (solid line in Figure 6) and was selected for fabrication and testing, as described in the following sections.

4. MOE Fabrication. The multilayer thin-film coating as synthesized by the filter design algorithm consists of alternating layers of Nb_2O_5 and SiO_2 deposited on a glass substrate (Corning

BK-7). These materials have well-defined refractive indices as shown in Figure 2 and are suitable for use between the near-UV and the long-wavelength mid-infrared spectral regions. Only one set of targets, either of elemental niobium or elemental silicon, is operated at a given time during deposition, producing films of exclusively one or the other material.

During the RMS process,[20] argon atoms are ionized and entrained in a magnetic field. The argon ions strike the elemental targets and eject atoms from the targets by momentum transfer. Oxide films form on the substrate as a result of the reaction of the metal atoms and oxygen in the chamber gas. This reaction occurs exclusively on the substrate under the conditions of deposition. The placement of the substrate on a 35.6-cm-diameter octagon-shaped rotating drum ensures a uniform coating as the drum sweeps through the deposition zone.

Process Control. The layer thicknesses of the coating materials must be controlled very precisely during deposition to ensure that the MOE spectrum accurately matches the design. The progress of the MOE fabrication is optically monitored by keeping track of the evolving filter spectrum as each layer is deposited. This is done with monitor curves, which are single-wavelength transmittance spectra of the evolving MOE spectrum for individual layers (i.e., transmittance versus layer thickness). In an ideal situation, experimentally measured monitor curves are compared with calculated values to determine the end point of layer deposition. The facilities that are currently available to us for process monitoring do not allow us to directly measure the true transmittance as the layers are coated, but instead only the power transmitted through the coating. The relationship between the observed monitor values and the predicted monitor curves is found by normalizing the experimental monitor curves to the theoretical curves at turning points in their transmission as a function of layer thickness. Layer deposition is terminated when normalized values of the transmittance match the value expected for the target thickness as closely as possible. In our experience, the fairly complex normalization routines we have built into our LabVIEW process control engine only work well when the monitor curve wavelengths are selected subject to the following criteria:

(1) The monitor curve should have adequate curvature with well-defined maximums or minimums. This is because maximums and minimums provide the most stable points for normalization of the experimental transmitted power measurements to the predicted transmittance monitor curves.

(2) The monitor curve should cover a fairly wide range in transmittance values because the rate of transmittance change per unit deposition thickness is directly related to the precision with which the layer can be deposited.

(3) Slight changes in the monitor wavelength should not result in rapid changes in either the shape of the monitor curve or the range in transmittance values that are covered by the monitor curve. This is because errors inevitably accumulate, shifting the monitor curves to higher or lower wavelengths by small amounts. Monitor wavelengths at which the monitor curves experience large changes with small errors in wavelength lead to irreproducible results and frequently to serious errors in fabrication.

(20) Parsons, R. Sputter Deposition Processes. In *Thin Film Processes;* Vossen, J. L., Kern, K., Eds.; Academic Press: San Diego, 1991.

As an example, Figure 7 shows the calculated (transmittance versus physical thickness) and experimental (transmitted power versus number of deposition cycles) monitor curves for the first 2 layers of the 26-layer SVR MOE. Deposition is closely monitored by matching the two curves for each layer. The two layers correspond to a total thickness of 2400 Å. After the selection of appropriate monitor curves, the software program generates a recipe file which contains the chamber operating conditions for the initial deposition of all the individual layers. Since these conditions are based purely on the approximate deposition rate of the materials, they are only accurate to within about ±5%. Consequently, the system is designed to automatically deposit only 80% of each layer initially to avoid overdepositing the layer before the process control algorithm comes into play. The parameters entered into the recipe file include the Ar and O_2 flow rates (controlled by mass flow controllers), predetermined monitor wavelengths for each layer, the number of deposition cycles required for ~80% deposition of each layer, the magnetron power, predeposition sputtering time (to clean the targets of contaminants), and the detector gain. After each layer is 80% deposited, new commands are entered into the recipe file by our process control engine to make adjustments to the process parameters until the layer deposition is complete. These updates to the recipe file are fully automated. The experimental curves, particularly for the first layer (Figure 7B), do not appear to faithfully reproduce the theoretical curve. This is only due to the operation of the process control engine, which adjusts the rate of deposition so that the final layer thickness is achieved as nearly as possible. This gives the experimental measurements a "stuttered" appearance as the process control engine iterates to a physical end point.

Deposition rates are rarely constant due to slight fluctuations in power as well as the values of the optical constants (i.e., layer absorption coefficients and refractive indices as functions of wavelength) of the two materials at room temperature over a period of time. Also certain layers are more sensitive to errors than others due to a lack of adequate monitor curves at the available wavelengths. These factors combine to introduce minor errors in the MOE spectrum. Despite this we have been able to routinely produce filter elements with better than 95% accuracy. Figure 6 shows a comparison of the measured MOE spectrum at 45° to the design (theoretical) spectrum. Much of the error between the two curves is an offset due to polarization in the spectrometer that recorded the measurement. Even so, there is a reasonably good fit between the two spectra.

5. Installation and Tuning of the MOE in the Measurement System. The optical spectra of the original samples from which the MOE was designed were recorded on a UV–visible diode array spectrometer. However, the deposition of the coating is controlled with a different spectrometer. If these two spectrometers are not exactly calibrated in wavelength with one another, the result will approximately be a fixed wavelength offset between the actual MOE spectrum at the desired angle of incidence and the designed MOE spectrum at the same angle. Provided that this error is small, it can be corrected by slightly tuning the angle of the MOE in the measurement system. That is, instead of using the MOE at exactly 45°, the optimum angle might be slightly more or less than 45°, depending on the wavelength calibrations of the two spectrometers. The best spectrometer for making this
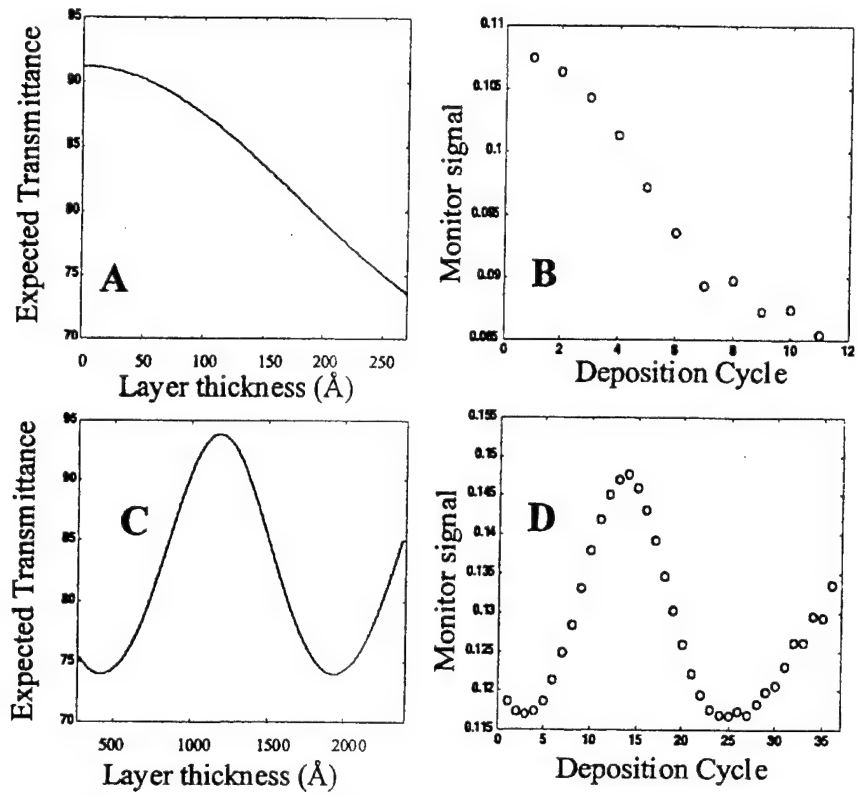
Figure 7. Theoretical and experimental monitor curves for layers 1 and 2. (A) Theoretical layer 1 monitor at 420 nm; (B) experimental layer 1 monitor at 420 nm; (C) theoretical layer 2 monitor at 450 nm; (D) experimental layer 2 monitor at 450 nm.

determination is clearly the one on which the original samples were measured. For this reason, a device to adjust the filter angle prior to sample measurements was built. This device consists of a micrometer-driven adjustment for the MOE angle. When the MOE was installed in the optical block shown in Figure 1, the optical block was transferred to the original spectrometer and adjusted with the micrometer-driven tool to match the wavelength axis with the design as closely as possible. After adjustment, the MOE was locked in place and transferred back to the optical system for measurements.

6. Analysis of Crystal Violet/Bismarck Brown Dye Mixtures. *Conventional PCR Regression on Absorbance and Transmittance Data.* To gauge the results of the MOC measurements (using the apparatus in Figure 1 fitted with the fabricated MOE) against conventional multivariate calibration, conventional PCR regression analysis was carried out on the same data set used for MOE design. A PCR calibration of the BB concentration (requiring two factors) was initially carried out with absorbance spectra that are obtained by the conversion of the measured transmittance spectra ($A = -\log T$). This produced a SEP of 0.2 μM in BB. Next, a PCR calibration (requiring four factors) was done with the corrected detector intensity response. Despite the nonlinearity between the detector response and concentration, a linear calibration was obtained with an SEP of 0.26 μM. This is slightly worse than the results obtained from calibrating the absorbance spectra; nevertheless, the results are reasonably comparable as shown in Figure 8. The corresponding SEP for the radiometrically corrected spectra and our theoretical 26-layer MOE is slightly higher at 0.31 μM.
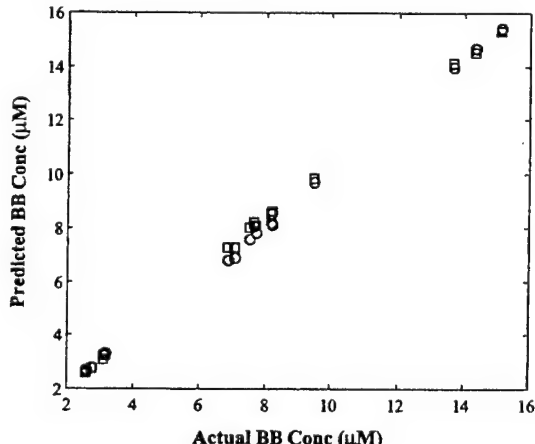
Figure 8. Calibration in absorbance vs transmittance modes. Comparison of PCR calibration of BB in a binary dye mixture using absorbance spectra (squares) with PCR calibration using radiometrically corrected transmittance spectra (circles).

Expectations versus Realities. The theoretical SEP for our 26-layer SVR MOE is based on spectra obtained on a conventional spectrometer. To evaluate the way in which a real MOE will operate, we should consider the source of the SEP. If, for instance, 0.31 μM is an SEP attributable to model or reference errors (as is probably the case here), then a real MOE-based device could produce an actual SEP no better than this value. In other words, if model or reference errors are responsible for the SEP, then the theoretical (model) SEP is a lower bound for the real SEP. Errors in the production of the MOE or errors in the calculations

54
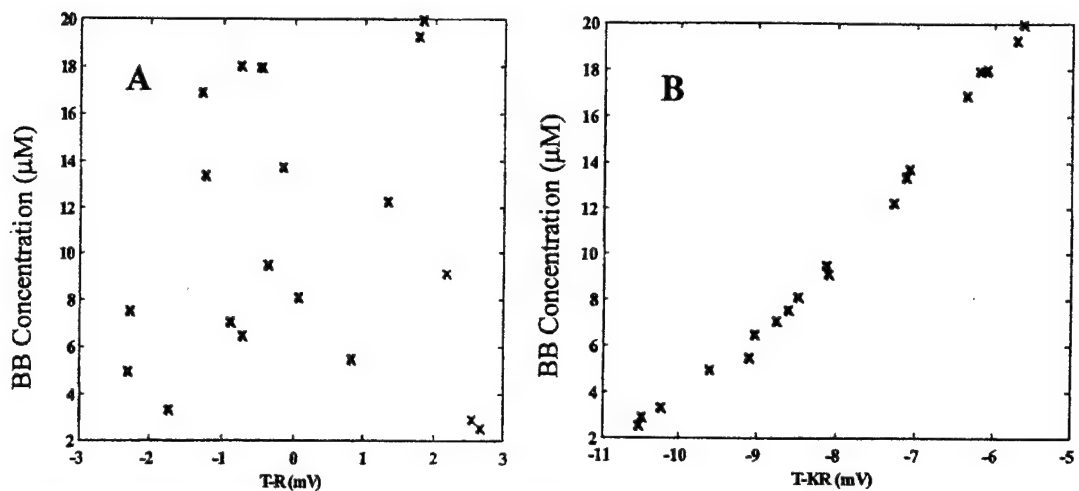
Figure 9. Effect of the detector relative gain factor. $T - KR$ vs the calibrated concentration of BB with unscaled vs optimized scaled detector sensitivities. T and R are the measured transmitted and reflected intensities, respectively, and K is the relative gain factor. (A) $K = 1$. (B) $K = 1.18$ (optimum).

preceding the model could negatively impact the result but probably not improve it. On the other hand, if the SEP is not limited by model or reference error but by signal-to-noise ratio in the original measurements on conventional instruments, an MOE could conceivably improve the result. As described in ref 5, MOEs are far less sensitive to detector noise contributions and low light levels than are conventional spectrometry systems. In general, UV−visible spectroscopy and modeling is not limited by noise but by model or reference errors. Thus, we should anticipate that our actual MOE will not miraculously reduce the expected SEP.

Determination of Bismarck Brown with the MOC Approach. The difference (in millivolts) in detector signals between detectors viewing MOE-reflected versus MOE-transmitted light that first passed through validation samples was measured for 39 samples. These samples were different from those samples that were used for MOE design, but were designed with a similar spread of concentration values. A total of 20 of these samples were used to evaluate the relative responsivities (the relative gain factor) of the two detection arms of the measurement system. To understand why this is necessary, consider that the two detectors shown in Figure 1 are physically different devices and thus can have slightly different relative responses. Since the MOC measurement is given by the difference in the two detector responses, a correction factor is necessary to give them the same overall gain. If this relative gain factor is called K, to ignore it assumes $K \approx 1$. Figure 9A shows the result of ignoring K. With an incorrect value of K, correlation between the detector differences and the BB concentration is seriously degraded. Figure 9B shows the optimum correlation obtained between the detector differences and BB concentration by giving $K = 1.18$ in the MOC equation,

$$C = 3.64 \ (T - KR) + 39.57 \tag{8}$$

where C is BB concentration in micromolar and T and R are the detector outputs in millivolts.

The calibration model was tested by using the linear regression model in eq 1 to predict the concentrations of the remaining 19 samples. Figure 10 (square points) shows a plot of the predicted
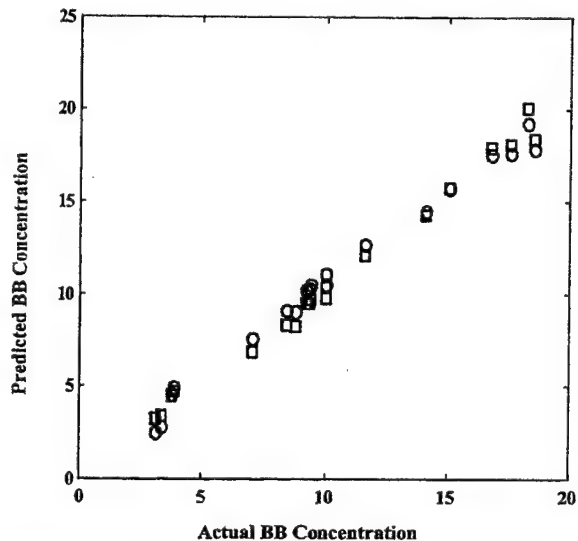
Figure 10. Predicted BB concentration vs actual BB concentration from detector difference measurements with optimum relative gain factor. Squares: linear model, SEP = 0.69 μM. Circles: third-order polynomial model, SEP = 0.60 μM.

BB concentrations versus the actual BB concentrations using this model. The SEP was determined to be 0.69 μM. On the basis of the appearance of nonlinearity in the calibration data, different nonlinear models were constructed from polynomial fits of increasing order. These nonlinear models were developed by assuming a polynomial correlation between $(T - KR)$ and concentration instead of the linear relation given in eq 8. Thus, the first 20 samples were used to obtain each of the possible models, and predictions based on these models were made for the remaining 19 samples. We observed that a third-order polynomial model provided the best improvement to the SEP (=0.6 μM). The improvement obtained by using these nonlinear models was relatively minor.

Discussion of Results. A number of factors exist to explain the disparity between the estimated linear SEP (0.69 μM) for MOC in this example and the expected SEP of 0.31 μM. First, we were

55

unable to calibrate the detectors because of instrumental limitations. Instead, data from the manufacturer's specifications were relied upon in determining detector spectral response. This information is of a general nature and better results are expected when all the individual optoelectronic components used in assembling the MOC measurement system are fully calibrated.

Second, fabrication errors resulting in the mismatch between the measured MOE spectrum and the theoretical spectrum can play an important role in the final results. An accurate reproduction of the MOE coating layers as specified by the design is necessary to achieve a value of the SEP that is comparable with that predicted for the design. The current process control system for the fabrication of MOEs does not provide the most effective means of monitoring the deposition process to produce layers with accurate thicknesses. Fortunately, many of the shortcomings of our current process control system can be rectified. These improvements will be the subject of future reports.

Third, normalization of the data was not performed. The acquisition of the test data in our laboratory was performed over the course of two 2-h sessions, so slight drift in the detectors probably contributes to our error. Normalization is an aspect of multivariate optical computation that will be the subject of a future report. A brief description of normalization and its hypothetical use in multivariate optical computing is given in ref 5. In brief, eqs 1 and 2 provide that the difference between transmitted and reflected rays in the Figure 1 instrument is related to the magnitude of a spectral vector (the regression vector) in the sample spectrum. The summation of the two responses, however, is directly proportional to the total magnitude of the spectrum. Corrections to the calibration data can be made so that they are suitable for measurement by calculating the ratio of the difference between T and R to the summation of T and R. This forms an implicit "normalization" of the spectrum during the prediction step and can be used to correct for prediction errors associated with power fluctuations and detector drifts.

Fourth, the lamp whose calibration we show in Figure 4C burned out early in our testing. Although a new lamp of the same type was installed and operated at the same voltage, there is no guarantee that the color temperature of the new lamp matched that of the old. This is an interesting problem that is common to many spectrometry systems using lamps and one that is ultimately addressable with MOC technology: a spectral vector for color temperature can be produced that will enable lamps to be controlled for color temperature. This problem is one that we are currently beginning to address and will also be the subject of a future report.

CONCLUSION

The concept of multivariate optical computing has been demonstrated with the successful design and testing of an MOE for the analysis of a binary dye mixture. The results obtained compare quite favorably with conventional PCR regression despite the nonidealities in sample measurement using the current prototype instrument, as well as those stemming from MOE manufacture. Measurements will be extended to the determination of chemical species in more complex systems with a greater number of interfering agents.

There exist several areas of theory that still need to be explored in order to gain a better understanding of MOC. For example, no theory has been developed covering the susceptibility of this technology to manufacturing errors. Also, the application of chemometrics to radiometric data has not been fully developed, so that there is currently no way to quantitatively predict the errors accumulated from nonlinearities in radiometry. All these areas are subjects of further study.

In general, we think it is important to keep in mind the following truth about multivariate optical computing: It is not a panacea. It is subject to all the same problems to which conventional multivariate spectroscopy is prone. In the case of weak signals or noisy detectors, it can hypothetically produce better SEPs than conventional spectroscopy; but it is no less sensitive to model or reference errors than conventional measurement techniques. Instead, MOC trades one set of problems for another. At the cost of a complex design and manufacturing process and the loss of some experimental flexibility, one gains a far simpler instrument with dramatically lower cost and maintenance. In our laboratory, for example, we estimate that the cost of producing the 26-layer MOE used here is much less than $100 per element when 50 or more are made. In some instances, multivariate optical computation is a tool that could make complex spectroscopic measurements accessible to a mass market.

56

10.5 NOVEL FILTER DESIGN ALGORITHM FOR MULTIVARIATE OPTICAL COMPUTING

Novel Filter Design Algorithm for Multivariate Optical Computing

Olusola O. Soyemi[a*], Paul J. Gemperline[b], Lixia Zhang[a], DeLyle Eastwood[a], Hong Li[a], Michael L. Myrick[a]

[a]Dept. of Chem. and Biochem., University of South Carolina, Columbia SC 29208

[b]Dept. of Chem. and Biochem., East Carolina University, Greenville, NC 27858

ABSRACT

A new algorithm for the design of optical computing filters for chemical analysis otherwise known as Multivariate Optical Elements (MOEs), is described. The approach is based on the nonlinear correlation of the MOE layer thicknesses to the standard error in sample prediction for the chemical species of interest using a modified version of the Gauss-Newton nonlinear optimization algorithm. The design algorithm can either be initialized by random layer thicknesses or by a pre-existing design. The algorithm has been successfully tested by using it to design a MOE for the determination of copper uroporphyrin in a quaternary mixture of uroporphyrin (freebase), nickel uroporphyrin, copper uroporphyrin, and tin uroporphyrin.

Keywords: optical computing, thin films, chemometrics, spectroscopy, multivariate

1. INTRODUCTION

Multivariate calibration is a well-established tool in chemometrics for the correlation of a physical or chemical property of interest to multiple wavelength channels of optical spectra. (1-3) The conventional application of this tool in chemical analysis entails the acquisition of optical spectra in the appropriate wavelength region (typically from the ultraviolet to the mid-infrared). Next, chemometric tools are used to extract a spectral pattern (or regression vector), which is correlated to the property of interest but orthogonal to interferences (4). Prediction of the property in an unknown sample is carried out by determining the magnitude of the spectral pattern in the optical spectrum of the sample. More specifically, the magnitude is calculated by taking the inner product of the spectral pattern and the optical spectrum of the unknown compound. A major drawback in the widespread use of multivariate calibration, especially for field applications, is its dependence on expensive and bulky laboratory-type equipment for data acquisition and analysis.

In Multivariate Optical Computing (MOC), spectral patterns are encoded into the transmission spectrum of optical interference filters for the purpose of detecting spectral signatures for chemical prediction. Earlier reports by Myrick et al. (5,6), have shown that the prediction step can be optically mimicked by passing light of a fixed bandwidth (which has interacted with the sample either by transmittance through the sample or reflectance from the surface of the sample), through two optical filters whose transmission profiles combine to give a structure that accurately describe the positive and negative portions of the spectral pattern. A more recent study (7) has described a new approach to this method of optical computation, which uses a single filter for prediction.

A typical interference filter (coating) design consists of alternating layers of high- and low-refractive index materials with specified thicknesses. Interference coatings with irregular transmittance profiles are fabrication through the process of reactive magnetron sputtering (8). As was originally envisaged, the

---

profile of a pre-determined spectral pattern is transferred to the optical coating by a process of iterative synthesis (9). This design technique systematically synthesizes a multilayer coating subject to minimizing a merit function which describes the difference between the target spectral pattern, and the calculated spectrum within specified tolerance limits. However, complex spectral patterns necessitate filters of high complexity with more layers than can be realistically fabricated, effectively limiting the widespread use of this design technique in MOC.

As a way of overcoming this limitation in filter design, we present the description of an alternative design algorithm, (based on a nonlinear least-squares optimization technique), which synthesizes an optical coating that also results in the lowest possible error in sample prediction for the chemical species of interest. In other words, instead of creating an optical coating design whose spectrum matches a pre-determined spectral pattern, a design is created whose spectral profile can be scaled into a spectral pattern or regression vector that results in an optimal value of root mean squared calibration error (RMSQ).

A demonstration of this algorithm is presented in which a MOE for the determination of copper uroporphyrin in a quaternary porphyrin mixture has been designed.

2. DESCRIPTION OF FILTER DESIGN ALGORITHM

2.1. Calculation of filter transmittance

The application of a fast and efficient method of calculating filter transmittance is crucial to developing an algorithm for designing optical filters. The matrix method for calculating the transmittance and reflectance of multilayer optical thin films meets these criteria (10), and was therefore incorporated into the design algorithm. This method is easily implemented on a digital computer and has become the mainstay of most filter design algorithms. In this method, each layer of a thin film stack is represented by a 2x2 characteristic matrix (Equation.1), which describes the layer properties at particular wavelengths of incident light and at specified angles of incidence These properties include layer thickness, refractive index and the absorption coefficient.

$$Y_l = \begin{vmatrix} Y1+iY2 & Y3+iY4 \\ Y5+iY5 & Y7+iY8 \end{vmatrix} = \begin{vmatrix} \cos\delta & i/\eta\sin\delta \\ i\eta\sin\delta & \cos\delta \end{vmatrix} \quad (1)$$

Y_l is the characteristic matrix for the lth layer, η is the complex refractive index (= n_l+ik$_l$), where n_l is the real refractive index and k_l is the absorption coefficient. δ is the phase factor, which is given by

$$\delta = \frac{2\pi n_l k_l x}{\lambda}\cos\theta_l \quad (2)$$

where λ is the wavelength, x is the layer thickness, and θ_l is the interior angle of propagation in medium l. For normally incident light, $\cos\theta_l$ =1. However, for tilted filters in which the incident angle is oblique,

$$\cos\theta_l = \sqrt{1-\frac{n_0^2\sin^2\theta_0}{n_l^2}} \quad (3)$$

where n_o is the refractive index of the incident medium (air), and θ_o is the angle of incidence (in radians). The characteristic matrix of the entire film stack (M) is determined by multiplying the matrices of individually layers, i.e.;

$$M = [Y(layer1)*Y(layer2)*...*Y(layerL)] \quad (4)$$

Layer 1 is the layer that is closest to the substrate. Light transmitted through the film layers consists of an electric vector component (E) and a magnetic vector component (H). The characteristic matrix relates the electric and magnetic fields at individual layer boundaries in the following manner:

$$\begin{bmatrix} E \\ H \end{bmatrix} = [M] \begin{bmatrix} 1 \\ n_s + ik_s \end{bmatrix}$$

(5)

where n_s and k_s are the refractive index and absorption coefficient of the substrate respectively. The propagation of light through a single thin film coating is illustrated by Figure 1. As is shown in the diagram, there are multiple reflections of the incident light at the air/film and substrate/air interfaces. The transmittance and reflectance at the air/film interface, is given by equations 6 and 7.
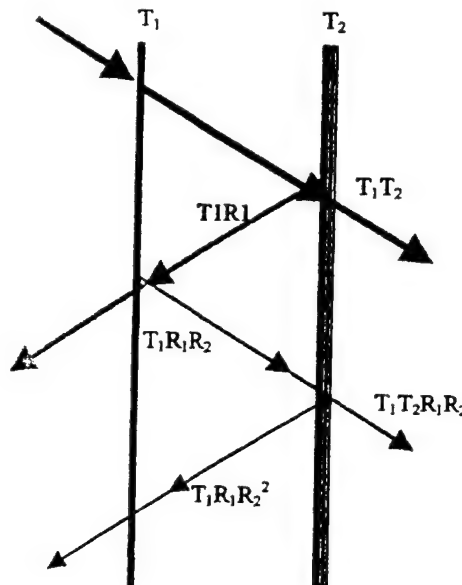
Figure 1: Transmission of light through a one-layer interference coating

$$T_1 = \frac{4n_s n}{(n + n_s)^2}$$

(6)

$$R_1 = 1 - T_1$$

(7)

For normally incident light, $n = n_o = 1$ (where n is the refractive index). However, when the filter is tilted, the propagated wave is split into two plane-polarized components, one with the electric vector in the plane of incidence, known as p-polarized, and one with the electric vector normal to the plane of incidence, known as s-polarized. The refractive index of the incident light is therefore modified as follows:

$$n = \frac{n_o}{\cos \theta_o} \text{ (p-polarization)}$$

(8)

$$n = n_o \cos \theta_o \text{ (s-polarization)}$$

(9)

60

T_2 and R_2 are related to the real and imaginary components of E and H (i.e., E_1, E_2 and H_1, H_2 respectively) determined from equation 5.

$$T_2 = \frac{4n_s n}{(E_1 + H_1)^2 + (E_2 + H_2)^2} \tag{10}$$

$$R_2 = \frac{(E_1 - H_1)^2 + (E_2 - H_2)^2}{(E_1 + H_1)^2 + (E_2 + H_2)^2} \tag{11}$$

The total transmittance through the film and substrate can be determined by summing up the infinite series of the combined reflectance and transmittance terms (see Fig.1) i.e., $T_1 T_2$, $T_1 T_2 R_1 R_2$, $T_1 T_2 (R_1 R_2)^2$, $T_1 T_2 (R_1 R_2)^3$, etc, which results in the following expression:

$$T(\lambda, x, \eta_l, \eta_s, \theta_o) = \frac{T_1 T_2}{1 - R_1 R_2} * 100 \tag{12}$$

where η_l and η_s are the complex refractive indices of layer l, and the substrate (s) respectively. For tilted filters, the average transmittance due to the p- and s-polarized components of the incident light is determined.

2.2 Nonlinear Optimization of Filter Layers

The determination of the RMSQ from a calculated filter transmittance spectrum (T) with m wavelength channels starts with the scaling of the spectrum into a regression vector (R) using an appropriate gain factor (G).

$$R = \frac{G(2T - 100)}{m} \tag{13}$$

Using a calibration set of optical spectra (S) representative of real samples, the vector of concentration ($\hat{y}$) values of all the samples is predicted as follows

$$\hat{y} = S * R^T + off \tag{14}$$

where off is the offset. The RMSQ is determined by comparing the concentration of N calibration samples estimated from the regression vector, to known concentration (y) of the same samples.

$$MSQ = \sqrt{\frac{\sum_{i=1}^{N} (y_i - \hat{y}_i)^2}{\sum_{i=1}^{N} y_i^2}} \tag{15}$$

Once the filter profile resulting in an optimal RMSQ is determined, the performance of the MOE in predicting future samples can be gauged by calculating the standard error in sample prediction (SEP) from a separate set of validation samples as shown in equation 16.

61

$$SEP = \sqrt{\frac{VMSQ * \sum_{i=1}^{P} y_i^2}{P}} \tag{16}$$

where VMSQ is the root mean squared error of prediction for P prediction samples. The nonlinear correlation between the layer thicknesses of an optical filter coating and the RMSQ can be visualized as a search for the best (lowest) value of RMSQ on a complex n-dimensional response surface (where there are n-1 layers to be optimized (Figure 2)). The filter design algorithm used is based on the Quasi-Newton method of nonlinear optimization (11,12). The algorithm is initialized by a specified number of layers (n) with either random or pre-determined thicknesses (z), which represent a single point on the response surface. At each iteration (k) of the optimization process, curvature (gradient) information is built up to formulate a quadratic model problem of the form,

$$\min_{x} \frac{1}{2} z^T H z + c^T z + b \tag{17}$$

where the Hessian matrix H, is a positive definite symmetric matrix (crucial in maintaining a constant descent down the slope of the search surface), c is a constant vector, and b is a constant. The optimization converges to a solution (corresponding to the lowest value of the RMSQ), when the partial derivatives of z go to zero i.e.,

$$\nabla f(z^*) = Hz^* + c = 0 \tag{18}$$

The optimal solution point, z^*, can be written as

$$z^* = -H^{-1}c \tag{19}$$

At the starting point, H can be set up to any positive definite matrix (e.g. the identity matrix, I). The observed behavior of f(z) and $\nabla f(z)$ is then used to build up curvature information to make an approximation of H using the updating formula developed by Broyden (13), Fletcher (14), Goldfarb (15), and Shanno (16), also known as the BFGS formula. The formula is given by

$$H_{k+1} = H_k + \frac{q_k q_k^T}{q_k^T s_k} - \frac{H_k^T s_k^T s_k H_k}{s_k^T H_k s_k} \tag{20}$$

where

$s_k = z_{k+1} - z_k$
$q_k = \nabla f(z_{k+1}) - \nabla f(z_k)$

The gradient information is provided by pertubing each of the design variables (i.e. layer thicknesses) in turn and calculating the rate of change in the RMSQ. At each major iteration k, a line search is determined in a direction in which the solution is estimated to lie, and is determined by

$$d = -H_k^{-1} \cdot \nabla f(z_k) \tag{21}$$

During optimization, layers thicknesses that fall below a specified threshold value are not acceptable, keeping in mind that extremely thin layers may not be conveniently deposited during the fabrication process. Therefore, in the event that a layer falls below this threshold value during optimization, the algorithm activates a termination flag after which the layer(s) are deleted and the optimization re-started.

Other termination flags are activated to re-start the process whenever the optimization is stalled or the number of maximum iterations is reached.

The starting point of the optimization routine is important since it can have big bearing on the final results. The descent towards an optimal value of the RMSQ proceeds on the response surface through several possible pathways, depending on the starting point and the best search direction (Figure 2). The choice of an appropriate starting point usually entails a fairly quick descent to the best minimum on the response surface. There are currently two variants to this filter design algorithm, both of which are based on the mode of initialization. The first one initializes the optimization process with a specified number of layers with random thicknesses. For different random starts, the search direction proceeds to different local minima on the response surface hence the possibility of different solutions to the optimization problem. Starting with a specified number of layers, all of which have the same thickness, the second variant to the design algorithm creates a partial design by crudely matching a Principal Components Regression (PCR) vector. This is done by minimizing the sum of squared difference between the p-factor PCR regression vector (v) and the calculated regression vector (R). With this partial design as the starting point (hopefully representing a convenient position on the response surface), the final filter design is then synthesized. A flowchart describing the design algorithm is shown in Figure 3.
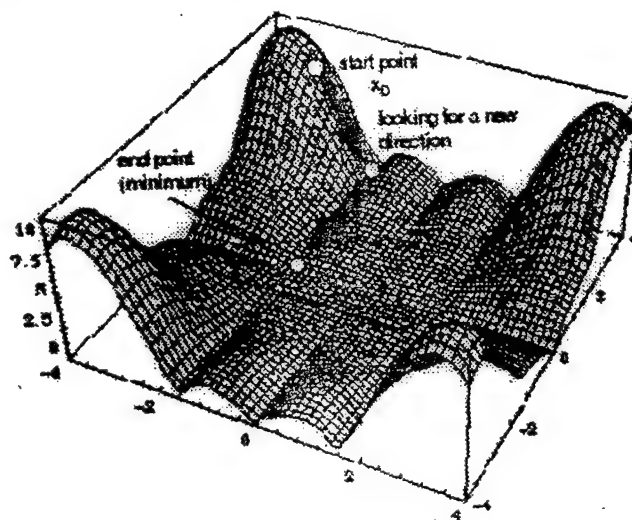
Figure 2: Three-dimensional response surface showing the nonlinear correlation of a two-layer interference coating (in the X-Y axis), with the standard error in sample prediction (Z axis). The search for an optimal solution (minimum value of the prediction error) starts a x_o.

3. EXPERIMENTAL

The porphyrin mixtures used for the MOE design were prepared from four porphyrins obtained from Porphyrin Products Inc. (Logan, UT), Uroporphyrin I Dihydrochloride (Uro), Sn (IV) Uroporphyrin I Dichloride (Sn-U), Cu (II) Uroporphyrin I (Cu-U), and Ni (II) Uroporphyrin I (Ni-U). Stock solutions in $1M$ NH_3 solution of Uro at $106\mu M$, Sn-U at $57.4\mu M$, Cu-U at $62.6\mu M$, and Ni-U at $56.1\mu M$ were prepared. Random numbers were generated and applied in diluting the stock solutions to ensure that the relative concentration of the four porphyrins varied independently. The random numbers were also chosen to ensure that the transmittance spectra of the diluted mixtures were between 30 % and 70 %. In this manner, 40 quaternary porphyrin solutions were prepared in which the concentrations of the four porphyrins varied independently. Cu-U was selected as the analyte while Uro, Ni-U, and Sn-U were treated as uncorrelated interferents whose concentrations varied randomly. The transmittance spectra (Figure 4) were acquired

between 400 nm and 650 nm on a Hewlett-Packard UV-VIS diode array spectrometer (Model 8543). An instrument prototype for the implementation of multivariate optical computing using a single MOE, has already been described (7). The transmittance spectra were convolved with the characteristics of the bandpass filters, lamp source, and detectors in the prototype field instrument to give an accurate representation of the detected response as a function of wavelength (Figure 5). The corrected spectra were used for MOE design and multivariate analysis. The MOE design algorithm was written in MATLAB (Mathworks Inc. Natick, MA). The PCR routine used for multivariate calibration is part of the PLS_Toolbox (Eigenvector Research Inc., Manson WA).

4. RESULTS AND DISCUSSION

The conventional approach to the multivariate analysis of optical spectra requires the use of bilinear regression techniques for the correlation of the spectral wavelengths to concentration (or any other property of interest). In particular, PCR is routinely used to define a regression vector or pattern, which correlates the wavelength channels to the concentration of the species of interest, but is orthogonal to interferences (4). The initial step in PCR analysis involves the reduction in the dimensions of a n x m matrix of optical
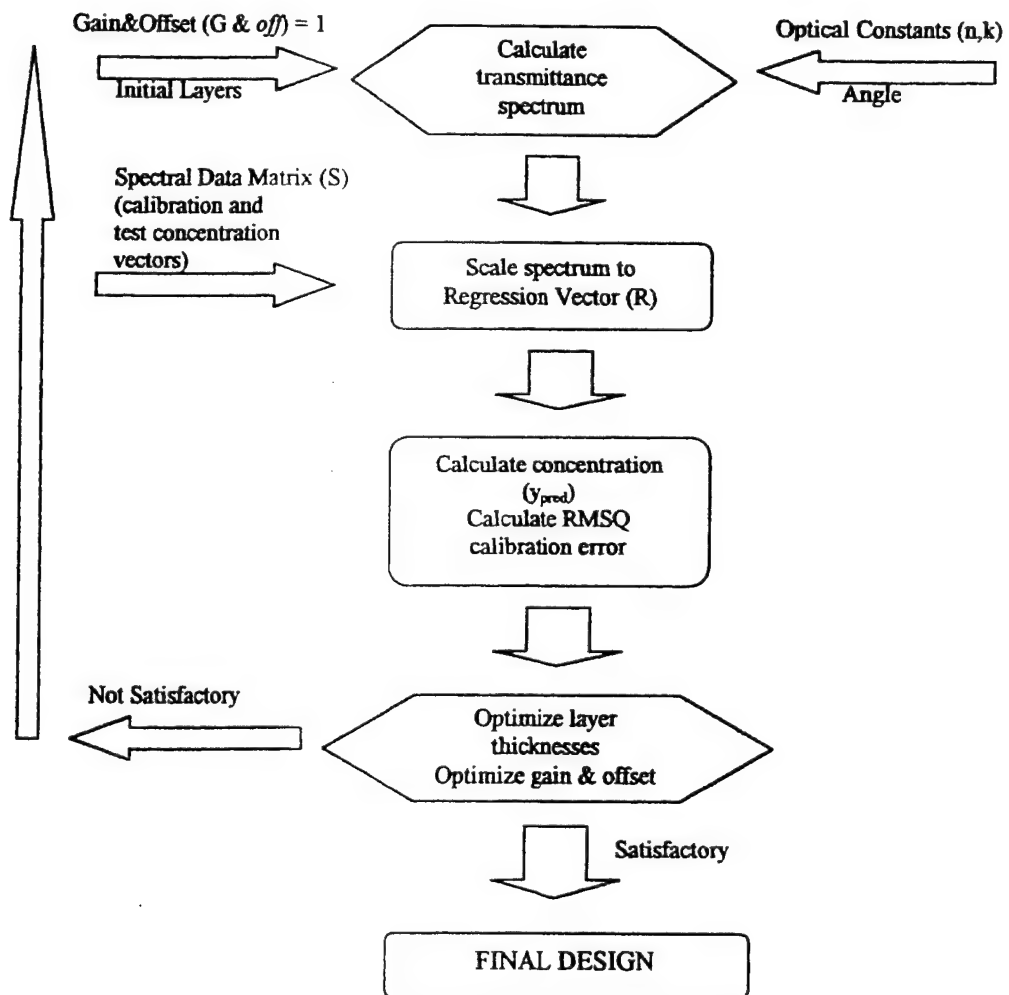
spectra, S (where n is the number of spectra, and m is the number of wavelength channels or variables), into another matrix X with fewer variables (known as principal components) all of which are not only uncorrelated to each, but also describe the data as accurately as the original measurement variables. The dimensions of X are n x p, where p is the number of principal components (or factors) that describe the data set completely without including noise, and is typically less than 10 for optical spectra with 200 or more wavelength channels. The second step in PCR, entails the least-squares correlation of X to a vector of concentration values y for each of the calibration samples as shown in Equation 22.

$$(22)$$

$$R = (X^T X)^{-1} X^T y$$
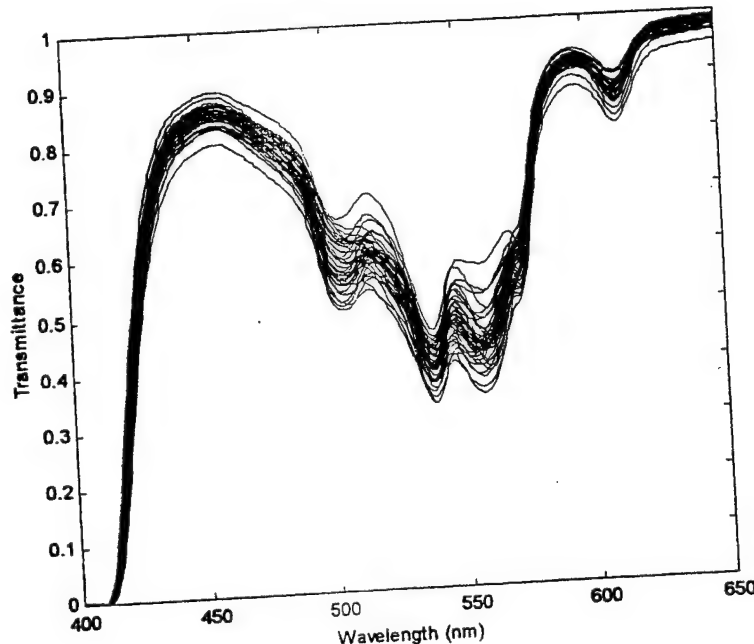
Figure 4. Transmittance spectra of 40 quaternary mixtures of Uroporphyrin (freebase), Copper Uroporphyrin, Tin Uroporphyrin, and Nickel Uroporphyrin.
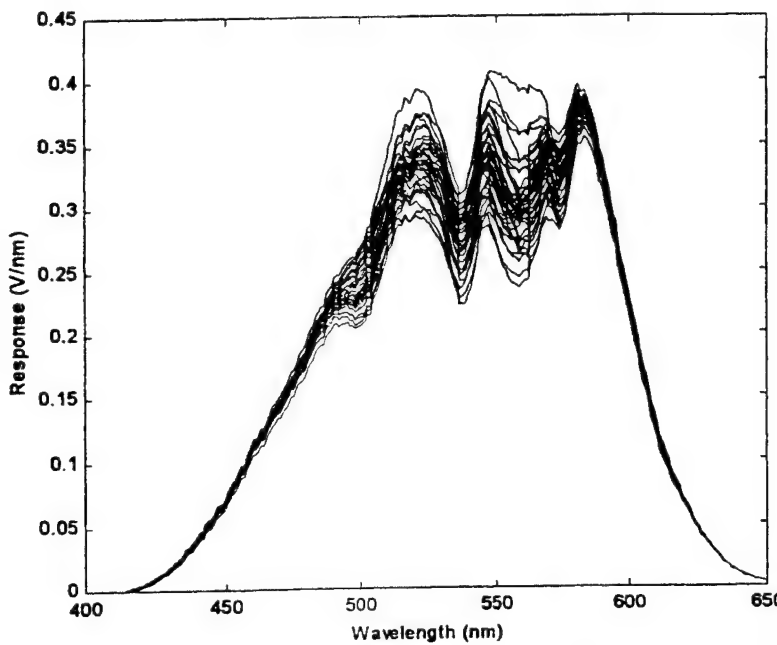
Figure 5. Porphyrin response profiles corrected for filter bandpass, source radiance, and detector sensitivity

The regression vector (R) can then be used to determine the concentration of an unknown compound (y_{un}) from its spectrum (x) as shown in Equation 23.

$$y_{un} = x*R^T \tag{23}$$

A PCR model for the determination of Cu-U was constructed from 20 of the quaternary porphyrin mixtures, corresponding to a 20 x 251 data matrix. Since there are no optical analogs for the kinds of spectral pre-processing used in multivariate calibration, none was carried out on the data set prior to the model construction. The model, which required 4 factors, was validated with the remaining porphyrin mixtures (20) yielding an SEP of 0.31 μM.

Using the same 4-factor PCR regression vector above, the filter design algorithm was initialized by a set of 60 random layer thicknesses. A partial match of the regression vector was made in which the starting layer thicknesses were modified at each iteration to minimize the sum of squared difference between the PCR vector and the calculated regression vector. It is envisaged that the filter layers that define the best match obtained from this minimization process would also define a convenient spot on the response surface from which a search for the "best" minimum (representing the optimal layer thicknesses) is initiated. With this in mind, a final filter design consisting of 34 layers that corresponds to an SEP of 0.29μM (see equations 13-16) was created. The filter spectrum is shown in Figure 6. Thus, the calculated MOE vector is a slight improvement on the PCR regression vector in terms of predictive ability. A gain factor of −32.09, was used to scale the calculated regression vector into the filter spectrum (Equation 13). Table 1 shows alternating layers of the high index material (Nb_2O_5), and the low index material (SiO_2), which make up the filter design. A comparison of the regression vector that yields this filter design, with the PCR regression vector is shown in Figure 7.
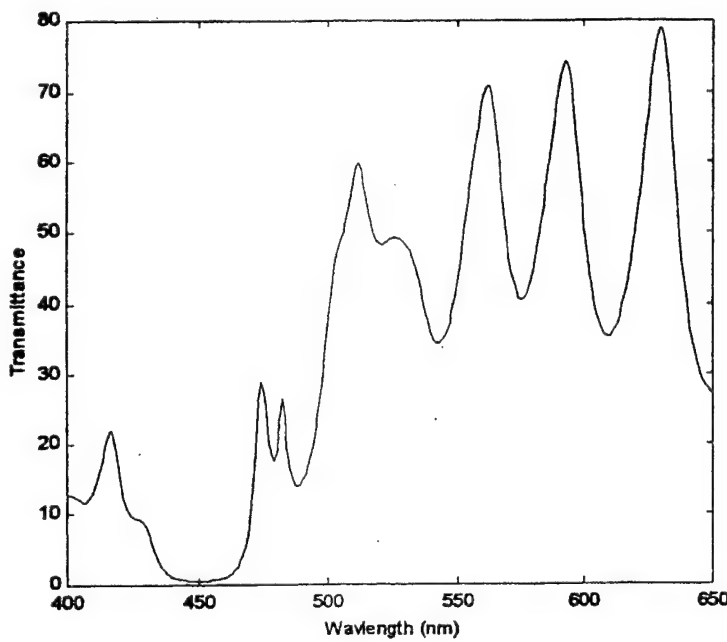
Figure 6. Transmittance spectrum of an MOE element for the determination of copper porphyrin in a quaternary mixture
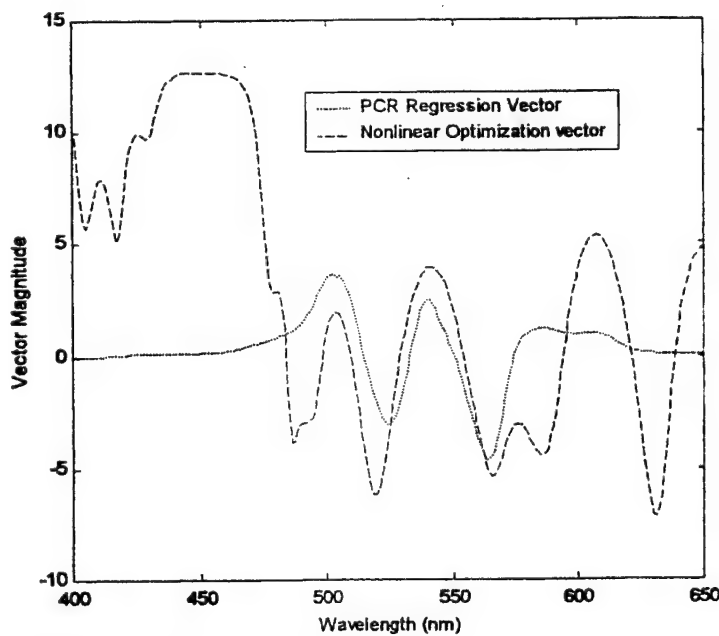
Figure 7. Comparison of PCR regression vector to the regression vector scaled from the MOE transmittance spectrum

Table 1. MOE design for the determination of copper porphyrin in quaternary porphyrin mixture.

Layer	Material	Thickness (nm)	Layer	Material	Thickness (nm)
1	Nb_2O_5	100.95	18	SiO_2	59.84
2	SiO_2	43.2	19	Nb_2O_5	190.81
3	Nb_2O_5	75.32	20	SiO_2	44.53
4	SiO_2	72.66	21	Nb_2O_5	75.82
5	Nb_2O_5	140.66	22	SiO_2	13.66
6	SiO_2	93.78	23	Nb_2O_5	67.92
7	Nb_2O_5	158.18	24	SiO_2	47.21
8	SiO_2	73.07	25	Nb_2O_5	99.1
9	Nb_2O_5	160.45	26	SiO_2	30.35
10	SiO_2	65.66	27	Nb_2O_5	36.65
11	Nb_2O_5	73.69	28	SiO_2	34.61
12	SiO_2	12.05	29	Nb_2O_5	115.19
13	Nb_2O_5	74.52	30	SiO_2	97.09
14	SiO_2	50.2	31	Nb_2O_5	163.76
15	Nb_2O_5	89.35	32	SiO_2	25.06
16	SiO_2	21.35	33	Nb_2O_5	38.55
17	Nb_2O_5	85.51	34	SiO_2	70.98

5. CONCLUSION

A fairly straightforward algorithm for the design of filter elements used for optical computing has been described and successfully demonstrated. The algorithm synthesizes a MOE with the best predictive ability for a chemical species of interest. Unlike design methods that are dependent on matching a fixed profile, this algorithm provides multiple pathways through which various MOE designs are obtained all of which are still subject to maintaining a low RMSQ. Because of this, the algorithm also provides a means by which a particular filter design can be modified continuously during the fabrication process to correct for errors generated from the manufacturing process without seriously compromising the predictive ability of the MOE. The means by which this is implemented is the subject of future work.

ACKNOWLEDGEMENTS

REFERENCES

1. J.F. Aust, K.S. Booksh, M.L. Myrick, "Novel In-Situ Probe for Monitoring Polymer Curing," *Appl.Spectrosc.* **50**, pp 382-387, 1996.
2. E.V. Thomas, and D.M. Haaland, "Comparison of Multivariate Calibration Methods for Quantitative Spectral Analysis," *Anal.Chem.* **62**, pp 1091-1099, 1990.
3. M.M.A. Ruyken, J.A. Visser, and A.K. Smilde, "Identification of Plastics among Non-plastics in Mixed Wastes by Remote Sensing Near-Infrared Spectroscopy. 2. Multivariate Rank Analysis for Rapid Classification," *Anal.Chem.* **67**, pp 2170-2179, 1995.

4. H. Martens, and T. Naes, *Multivariate Calibration*, John Wiley and Sons, New York, 1989.
5. M.P. Nelson, J.F. Aust, J.A. Dobrowolski, P.G. Verly, and M.L. Myrick, "Multivariate Optical Computation for Predictive Spectroscopy," *Anal.Chem.* **70**, pp 73-82, 1998.
6. M.P. Nelson, J.F. Aust, J.A. Dobrowolski, P.G. Verly, and M.L. Myrick, "Multivariate Optical Computation for Predictive Spectroscopy," *Proc.SPIE-Int.Soc.Opt.Eng (Three Dimensional and Multudimensional Microscopy: Image Acquisition and Processing)*. **3261**, pp 232-243, 1998.
7. M.L. Myrick, O. Soyemi, J. Karunamuni, D. Eastwood, H. Li, L. Zhang, and P. Gemperline, "A Single-Element All-Optical Approach to Chemometric Prediction," *Fres.J.Anal.Chem.* (submitted 2000).
8. B.T. Sullivan, and J.A. Dobrowolski, "Deposition of Metal/Dielectric Multilayer Filters," *Appl.Opt.* **32**, pp 2351-2360, 1993
9. A.V. Tikhonravov, "Optical Coating Synthesis using Optimal Conditions," *Vestn.Mosk.Univ., Ser.3: Fiz., Astron.* **23**, pp 91-93,1982.
10. H.M. Liddell, *Computer-Aided Techniques for the Design of Multilayer Filters*, Adam Hilger Ltd., Bristol, UK, 1981.
11. J.E Dennis Jr,., R.B. Schnabel,. *Numerical Methods for Unconstrained Optimization and Nonlinear Equations*, Prentice-Hall, Inc., Englewood Cliffs, NJ, 1983.
12. T.F. Coleman, M. Branch, A. Grace, *MATLAB Optimization Toolbox: User's Guide*, Mathworks Inc., Natick, MA, 1999.
13. C.G. Broyden, "The Convergence of a Class of Double-rank Minimization Algorithms," *J.Inst.Math.Applic.* **6**, pp 76-90, 1970.
14. R. Fletcher, "A New Approach to Variable Metric Algorithms," *Computer Journal.* **13**, pp 317-322, 1970.
15. D. Goldfarb, "A Family of Variable Metric Updates Derived by Variational Means," *Mathematics of Computing.* **24**, pp 23-26, 1970.
16. D.F. Shanno, "Conditioning of Quasi-Newton Methods for Function Minimization," *Mathematics of Computing.* **24**, pp 647-656, 1970.

10.6 Simple Optical Computing Device for Chemical Analysis

A SIMPLE OPTICAL COMPUTING DEVICE FOR CHEMICAL ANALYSIS

Olusola O. Soyemi[a], Lixia Zhang[a], DeLyle Eastwood[a], Hong Li[a] Paul J. Gemperline[b], Michael L. Myrick[a*]

[a]Dept. of Chem. and Biochem., University of South Carolina, Columbia SC 29208
[b]Dept. of Chemistry, East Carolina University, Greenville, NC 27858

ABSTRACT

Multivariate Optical Computing (MOC) devices have the potential of greatly simplifying as well as reducing the cost of applying the mathematics of multivariate regression to problems of chemical analysis in the real world. These devices utilize special optical interference coatings known as multivariate optical elements (MOEs) that are encoded with pre-determined spectroscopic patterns to selectively quantify a chemical species of interest in the presence of other interfering species. A T-format prototype of the first optical computing device is presented utilizing a multilayer MOE consisting of alternating layers of two metal oxide films (Nb_2O_5 and SiO_2) on a BK-7 glass substrate. The device was tested by using it to quantify copper uroporphyrin in a quaternary mixture consisting of uroporphyrin (freebase), tin uroporphyrin, nickel uroporphyrin, and copper uroporphyrin. A standard error of prediction (SEP) of $0.86\mu M$ was obtained for copper uroporphyrin.

Keywords: optical computing, thin films, chemometrics, spectroscopy, interference coatings

1. INTRODUCTION

Multivariate calibration is an established tool in chemometrics for the correlation of a physical or chemical property of interest to information spanning multiple wavelength channels in optical spectroscopy[1-3]. The conventional application of this tool in chemical analysis entails first the acquisition of optical spectra in the appropriate wavelength region (typically from the ultraviolet to the mid-infrared). Next, chemometric tools are used to extract a spectral pattern (the regression vector) which is correlated to the property of interest but orthogonal to interferences[4]. Prediction of the property in an unknown sample is then carried out by determining the magnitude of the spectral pattern in the optical spectrum of the sample. More specifically, the magnitude is calculated by taking the inner product of the regression vector and the optical spectrum of the unknown sample. A major drawback in the widespread use of multivariate calibration, especially for field applications, is its dependence on expensive and bulky laboratory-type equipment for data acquisition and analysis.

A recent publication from our laboratory[5] addressed the feasibility of using optical computing in predictive spectroscopy to simplify and harden the apparatus necessary for chemical prediction from a theoretical standpoint. The first reports of a related hypothetical optical approach to multivariate chemical measurement were those of Bialkowski[6]. The use of a single MOE in a beamsplitter configuration has also been described for the same purpose[7], a permutation most similar to that proposed by Ryabenko and Kasparov[8]. The all-optical approach proposed by our laboratory differs from previous work by centering around the production of one or more optical interference coatings whose transmission spectra incorporate features of a spectral regression vector. Such interference filters based on multivariate spectroscopy will be referred to henceforth as multivariate optical elements (MOEs). MOEs have never been demonstrated as a tool for actual chemical measurement, however.

---

* Correspondence: Email: myrick@psc.sc.edu; Telephone: 803-777-6018; Fax: 803-777-9521.

17

This report describes the first prototype of a simple optical computing device using a MOE. A quaternary porphyrin mixture consisting of uroporphyrin (freebase), copper uroporphyrin, nickel uroporphyrin, and zinc uroporphyrin, was selected to design a MOE that would test the concept of all-optical prediction. The experiments reported below consist of several elements. First, the optical properties of all the pertinent components of a simple T-format spectroscopic system (Figure 1) were evaluated. Second, spectra of a series of binary dye mixtures were recorded and converted to a spectral radiance scale for chemometric interpretation. Third, a theoretical design for a multivariate optical element (MOE) suitable to this measurement was generated. Fourth, the MOE was fabricated in-house. Finally, the MOE was installed in our T-format instrument and measurements of calibration and validation samples were performed.

2. EXPERIMENTAL SECTION

Demonstration of the MOC technique was carried out on a compact T-format instrument (Figure 1), which was constructed using Linos Photonics (Milford, MA) optical components.

A 6V/6W tungsten filament lamp (Linos Photonics) with 1x1.2mm active filament area was used as a light source for the test instrument. The spectral radiance of the lamp was measured in W /sr-cm^2-nm with a CCD spectrometer system consisting of a Chromex 250IS spectrometer with a 300gr/mm grating blazed at 500 nm and a Princeton Instruments 1100 X 300 pixel CCD camera, model TE/CCD-1100-PE. The input optics on the spectrometer system were duplicates of the Figure 1 system. For these measurements, the operating voltage for the lamp was fixed at 5.76 V. The wavelength range of the camera/spectrometer system was calibrated with a standard mercury pen lamp and a standard neon lamp. The spectral radiance of the lamp under these conditions was calibrated against an OL series 455 integrating sphere calibration standard lamp (Optronic Laboratories Inc.) operated under standard conditions.

The two Si photodiode active detectors were type BPW21 (Linos Photonics) with a sensitive area of 2.7 mm^2, spectral range 320-880 nm and radiant sensitivity at the peak wavelength (550 nm) of 3.8 V/mW. The relative spectral sensitivity of the detector wavelength was estimated from a Linos Photonics data sheet giving values measured at 25 degrees C and 12 V DC supply voltage.

A bandpass filter set was used to isolate the spectral region between 400 nm and 650 nm in which the visible absorbances of the two dyes are found. The bandpass set consisted of two 3 mm thick Schott glass filters (Duryea, PA) BG-39 and GG400.

The porphyrin mixtures used for the MOE design were prepared from four porphyrins obtained from Porphyrin Products Inc. (Logan, UT), Uroporphyrin I Dihydrochloride (Uro), Sn (IV) Uroporphyrin I Dichloride (Sn-P), Cu (II) Uroporphyrin I (Cu-P), and Ni (II) Uroporphyrin I (Ni-P). Stock solutions in 1M NH_3 solution of Uro at 106µM, Sn-P at 57.4µM, Cu-P at 62.6µM, and Ni-P at 56.1µM were prepared. Random numbers were generated and applied in diluting the stock solutions to ensure that the relative concentration of the four porphyrins varied independently. The random numbers were also chosen to ensure that the transmittance spectra of the diluted mixtures were between 30 % and 70 %. In this manner, 40 quaternary porphyrin solutions were prepared in which the concentrations of the four porphyrins varied independently. Cu-P was selected as the analyte while Uro, Ni-P, and Sn-P were treated as uncorrelated interferents whose concentrations varied randomly. Optical spectra of the mixtures were recorded on a Hewlett-Packard UV-VIS diode array spectrometer (Model 8543) from 400 nm to 650 nm (Figure 2). The samples were measured in a 1-cm fused-silica cell (Starna Cells Inc., Atascadero, CA).

Following data collection and radiometric corrections for lamp intensity, detector response and bandpass, design of MOE coatings using an iterative spectral-matching synthesis was performed. For this purpose, a nonlinear least squares algorithm was written in-house in the MATLAB programming environment was used[9].

The MOE was manufactured via reactive magnetron sputtering (RMS)[10]. Our sputtering system (Model CV 5.1) was custom-manufactured by Corona Vacuum Coaters of Vancouver, B.C. The system operates at

room temperature and utilizes a 40 kHz mid-frequency RF supply to power four water-cooled planar magnetrons positioned in pairs around a drum that rotates about a horizontal axis. The coating chamber is 22 inches in diameter and 20 inches deep, contains 4 inch x 10 inch magnetron targets, two containing niobium (99.95 % pure, high index) and two containing silicon (99.9999 % pure, low index). Each magnetron target is powered at approximately 0.7 kW, although the power is varied during deposition as one method of controlling deposition rate. The RMS process was used to deposit alternating layers of niobium pentoxide (Nb_2O_5) and silicon dioxide (SiO_2) films by reaction with oxygen in the gas mixture. MOE designs require accurate knowledge of the optical constants of the coating materials. Experimental measurements of the real and imaginary refractive indices of Nb_2O_5 and SiO_2 deposited in our chamber were determined by variable angle spectroscopic ellipsometry.

The MOE tested here was fabricated on a 1-inch BK-7 glass substrate. Layer deposition was optically monitored online with a 1200 line/mm grating monochromator (Model 9030, Sciencetec, London ON) blazed at 250 nm. Light detection was achieved using a photomultiplier tube (Model H5784-03, Hamamatsu, Japan). Visible light was obtained from a tungsten filament lamp (Gilway Technical Lamps, Waltham, MA). After MOE design was completed, the interference effects on transmission for each layer were computed at all accessible monitoring wavelengths. The system can currently monitor wavelengths between 420 nm and 600 nm with approximately 1 nm resolution, and thus about 180 different "monitor curves" were produced for each layer. From the 180 possible curves, the optimum wavelength for monitoring and controlling the deposition of each layer was selected based on a set of criteria developed as a result of experience in our laboratory. Process control of the deposition process was performed with in-house software written in the LabVIEW 5.1 programming environment that operated in concert with the system-control software provided by Corona Vacuum Coaters. The two software packages used the selected monitor curves to deposit each filter layer as accurately as possible.

After the production of the MOE as described above, it was installed in the T-format instrument shown in Figure 1. 20 new samples of the porphyrin mixtures were prepared using the random number generation described above. The difference between the signal due to light transmission through the sample followed by transmission through the optical filter (aligned at approximately 45 degrees), and light transmission through the sample followed by reflection from the surface of the optical filter, were measured for each sample. Ten of these measurements were used for calibrating the instrument (determining the optimum gain factor for the two detectors), while the remaining nineteen samples were used to validate the calibration model.

3. RESULTS AND DISCUSSION

Single MOEs can be designed for chemometric prediction by using them in a beamsplitter arrangement as shown in Figure 1[7]. Consider the optical transmission spectrum of an MOE to be $T(\lambda) = 0.5 + L(\lambda)$, where $L(\lambda)$ is a spectral pattern that can also be represented in vector form as $\vec{L}$. Assuming negligible absorbance in the MOE, the difference between the intensity of light transmitted through the MOE $\left(\vec{T} \bullet \vec{S}\right)$ and light reflected from it $\left(\vec{R} \bullet \vec{S}\right)$ is proportional to the scalar product of the vector $\vec{L}$ with the sample spectrum vector, $\vec{S}$

$$\left(\vec{T} - \vec{R}\right) \bullet \vec{S} = \left(\left(0.5 + \vec{L}\right) - \left(0.5 - \vec{L}\right)\right) \bullet \vec{S} = \vec{L} \bullet \vec{S} \tag{1}$$

To achieve this, the spectrum of the 45-degree filter must be designed such that an optimal multivariate regression vector can be derived from it that results in the best possible standard error of sample prediction.

a. Selection of the Spectral Window and Spectral Mode

Although MOC should function in many linear types of spectroscopy, the most convenient and most basic multivariate measurement to set up is spectral absorbance. MOC should also function in any spectral range where good optical elements can be produced. However, in our laboratory our experimental system lends itself most conveniently to measurements in the visible spectroscopic region. This is because our MOE-

fabrication system is presently process-controlled using an optical monitor between 420 nm and 600 nm. We elected to make measurements of mixtures of visible-absorbing dyes in the spectral window between approximately 420 nm and 600 nm.

Absorbance is nominally linear in concentration within the limits over which Beer's Law holds. A radiometric measurement, however, is more directly related to transmittance of the sample than absorbance, and transmittance is logarithmically related to concentration. Nevertheless, a number of studies correlating single-beam and radiometric measurements to chemical properties using linear chemometric models have been performed with some success[11-12]. In the limit of low absorbances, transmittance varies linearly with concentration; even for high absorbances, transmittance can be considered piecewise linear with concentration. Also, it has been shown that linear multivariate calibration methods like PCR and PLS (Partial Least Squares Regression), can satisfactorily model nonlinear responses by the inclusion of extra factors or latent variables in the calibration model[13]. In the following discussion, the raw data from which an MOE is designed will be analyzed both in transmittance and absorbance mode for comparison purposes to evaluate how the nonlinearity of transmittance with concentration affects the resulting prediction error.

b. Radiometric Correction of Spectral Data

Since measurement by an MOE-based instrument is inherently radiometric in nature, a number of factors not normally considered in absorption measurements must be quantitatively evaluated. A realistic representation of the MOC instrument detector signal mist therefore include a convolution of the following radiometric quatities:

(a) The spectral radiance of the source: A tungsten filament lamp was selected to serve as a light source for the measurement. These lamps are approximately black-body-type emitters, with a spectral radiance maximum in the near-infrared. The spectral radiance of our tungsten filament lamp after passing through a 1 mm pinhole was determined. The spectral radiance profile then was corrected for the solid angle

$(=\dfrac{3}{4}\dfrac{r^2}{f^2}$ steradians, where r and f are the radius and focal length of the focusing lens in the calibration

system), and the pinhole area $(=\pi r_p^2 \text{ mm}^2$, where r_p is the radius of the pinhole).

(b) Transmittance of the bandpass selection filters: In ordinary chemometric applications, out-of-band light can be eliminated by simply ignoring it. That is, light from the sample that is not in the range over which the chemometrics is performed does not have to be sampled. In the MOC measurement, however, band selection filters are used to obtain this result. In order to ensure that light from outside the wavelength range of our targeted response window (400-650 nm) is not transmitted through the MOE onto the detector

(c) The spectral sensitivity of the detector: Si photodiode detectors were selected for the dual channel measurement system (Figure 1). A plot of the detector sensitivity versus wavelength was estimated from manufacturer-provided graph. The sensitivity reaches a maximum at about 550 nm and tapers off in the short-wavelength near infrared region.

Figure 3 shows the sample transmittance spectra corrected for the radiometric quantities described above, and they represent the expected detector spectral response for each sample

c. MOE Design

Once these factors are known, the design of an MOE must be conducted via iterative thin-film synthesis subject to suitable starting, optimization and stopping criteria. A method of MOE design known as Spectral Vector Relaxation (SVR) has been developed in our laboratory with the aid of Prof. Paul Gemperline of East Carolina University. The basis of SVR is that many vectors satisfy the criteria for good regression vectors in addition to the ones that are found by PCR. SVR simply selects the vector that is simplest to fabricate.

If n is the number of layers in the coating, optimization using the SVR algorithm can be visualized in an n+2 dimensional space. The additional two dimensions in the space are scaling (G) and offset (*off*) factors relating the spectral vector to the dependent variable in the sample. The figure of merit in this optimization is the SEP for prediction of the dependent variable using the design of the coating at each iteration. The

steps to calculating the SEP at the end of each iteration is as follows; first, the current optical transmission spectrum ($T(\lambda)$) spanning m wavelength channels is scaled to a regression vector as in equation 4 below:

$$L(\lambda) = \frac{2G[T(\lambda) - 0.5]}{m} \tag{2}$$

Next, an estimate of the concentration of sample i ($\hat{y}_i$), is determined the scalar product of its spectrum ($\vec{x}_i$) with the regression vector ($\vec{L}$);

$$\hat{y}_i = \vec{x}_i \vec{L}^t + off \tag{3}$$

where t represents the vector transpose. By substituting equation 4 into equation 5, the SEP for N validation samples is calculated thus:

$$SEP = \sqrt{\frac{\sum_{i=1}^{N}\left\{\left\{\vec{x}_i\left[\frac{2G(\vec{T} - 0.5)}{m}\right]^t + off\right\} - y_i\right\}^2}{N}} \tag{4}$$

During optimization, layers thicknesses that fall below a specified threshold value are deleted because extremely thin layers are difficult to deposit accurately in our current apparatus. Because the final MOE design that results from SVR can have less than, or equal to, the starting number, this novel algorithm creates designs with smaller overall coating thicknesses than those created with needle optimization. In practice, we have found that this can often be achieved without sacrificing predictive ability.

The starting point of the optimization routine is important since the SVR algorithm can converge to a non-global optimum. The choice of an appropriate starting point usually produces a rapid descent to the global optimum for a given upper-bound level of complexity.

There are currently two variants of the SVR MOE design algorithm that differ in their modes of initialization. The first one initializes the optimization process with a specified number of layers with random thicknesses, which are then modified to give the best MOE design. Starting with a random number of layers or layers with fixed thicknesses, the second variant to the design algorithm creates a partial design by crudely matching the PCR regression vector using standard spectral matching. With this partial design as the starting point, the MOE spectrum is then further refined. The SVR method of MOE synthesis does not add new layers, but instead deletes layers that fall below a specified minimum permissible thickness during iteration.

The SVR design algorithm was used to produce an MOE consisting of 28-layers with a total thickness of 3.08 μM. This design was selected for fabrication as described in the following sections. The spectrum of the MOE is shown in Figure 4.

d. MOE Fabrication

The multilayer thin film coating as synthesized by the filter design algorithm consists of alternating layers of Nb_2O_5 and SiO_2 deposited on a glass substrate (Corning BK-7). These materials have well-defined refractive indices, and are suitable for use between the near UV and the long-wavelength mid-infrared spectral regions. Only one set of targets, either of elemental niobium or elemental silicon, is operated at a given time during deposition, producing films of exclusively one or the other material.

During the RMS process[10], argon atoms are ionized and entrained in a magnetic field. The argon ions strike the elemental targets and eject atoms from the targets by momentum transfer. Oxide films form on the

substrate as a result of the reaction of the metal atoms and oxygen in the chamber gas. This reaction occurs exclusively on the substrate under the conditions of deposition. The placement of the substrate on a 14-inch diameter octagon-shaped rotating drum ensures a uniform coating as the drum sweeps through the deposition zone.

Process Control. The layer thicknesses of the coating materials must be controlled very precisely during deposition to ensure that the MOE spectrum accurately matches the design. The progress of the MOE fabrication is optically monitored by keeping track of the evolving filter spectrum as each layer is deposited. This is done with monitor curves, which are single-wavelength transmittance spectra of the evolving MOE spectrum for individual layers (i.e. transmittance versus layer thickness). In an ideal situation, experimentally measured monitor curves are compared with calculated values to determine the end-point of layer deposition. The facilities that are currently available to us for process monitoring do not allow us to directly measure the true transmittance as the layers are coated, but instead only the power transmitted through the coating. The relationship between the observed monitor values and the predicted monitor curves is found by normalizing the experimental monitor curves to the theoretical curves at turning points in their transmission as a function of layer thickness. Layer deposition is terminated when normalized values of the transmittance match the value expected for the target thickness as closely as possible. In our experience, the fairly complex normalization routines we have built into our LabVIEW process control engine only work well when the monitor curve wavelengths are selected very carefully.

After the selection of appropriate monitor curves, the software program generates a recipe file which contains the chamber operating conditions for the initial deposition of all the individual layers. Since these conditions are based purely on the approximate deposition rate of the materials, they are only accurate to within about 5%. Consequently, the system is designed to automatically deposit only 80% of each layer initially to avoid over-depositing the layer before the process control algorithm comes into play. The parameters entered into the recipe file include the Ar and O_2 flow rates (controlled by mass flow controllers), pre-determined monitor wavelengths for each layer, the number of deposition cycles required for approximately 80% deposition of each layer, the magnetron power, pre-deposition sputtering time (to clean the targets of contaminants) and the detector gain. After each layer is 80% deposited, new commands are entered into the recipe file by our process control engine to make adjustments to the process parameters until the layer deposition is complete. These updates to the recipe file are fully automated.

Deposition rates are rarely constant due to slight fluctuations in power as well as the values of the optical constants (i.e. layer absorption coefficients and refractive indices as functions of wavelength) of the two materials at room temperature over a period of time. Also certain layers are more sensitive to errors than others due to a lack of adequate monitor curves at the available wavelengths. These factors combine to introduce minor errors in the MOE spectrum. In spite of this, we have been able to routinely produce filter elements with better than 95% accuracy. Figure 4 shows a comparison of the measured MOE spectrum at 45 degrees to the design (theoretical) spectrum. Much of the error between the two curves is an offset due to polarization in the spectrometer that recorded the measurement. Even so, there is a reasonably good fit between the two spectra.

e. Installation and Tuning of the MOE in the Measurement System: The optical spectra of the original samples from which the MOE was designed were recorded on a UV-Vis diode array spectrometer. However, the deposition of the coating is controlled with a different spectrometer. If these two spectrometers are not exactly calibrated in wavelength with one another, the result will approximately be a fixed wavelength offset between the actual MOE spectrum at the desired angle of incidence and the designed MOE spectrum at the same angle. Provided that this error is small, it can be corrected by slightly tuning the angle of the MOE in the measurement system. That is, instead of using the MOE at exactly 45 degrees, the optimum angle might be slightly more or less than 45 degrees, depending on the wavelength calibrations of the two spectrometers. The best spectrometer for making this determination is clearly the one on which the original samples were measured. For this reason, a device to adjust the filter angle prior to sample measurements was built. This device consists of a micrometer-driven adjustment for the MOE angle. When the MOE was installed in the optical block shown in Figure 1, the optical block was transferred to the original spectrometer and adjusted with the micrometer-driven tool to match the

wavelength axis with the design as closely as possible. After adjustment, the MOE was locked in place and transferred back to the optical system for measurements.

f. Analysis of Quaternary Dye Mixture: In order to gauge the results of the MOC measurements (using the apparatus in Figure 1 fitted with the fabricated MOE) against conventional multivariate calibration, conventional PCR regression analysis was carried out on the same dataset used for MOE design. A PCR calibration of the Cu-U concentration (requiring 5 factors) was initially carried out with detector response profiles that are obtained by the convolution of the measured transmittance spectra with the radiometric quantities described above. This produced a SEP of 0.31 μM in Cu-U. The SEP produced from the SVR MOE design was 0.60 μM. This fairly large difference between this value and the PCR value is because the SVR algorithm is constrained to produces an MOE regression vector that is easiest fabricate (within the limitations imposed by the sputtering system). Other MOE designs are possible that compare more favorably with the PCR calibration vector, but these are not necessarily the easy to make. Planned upgrades to the hardware would allow us greater latitude in using better MOE designs.

The theoretical SEP for our 26-layer SVR MOE is based on spectra obtained on a conventional spectrometer. To evaluate the way in which a real MOE will operate, we should consider the source of the SEP. If, for instance, 0.26 μM is an SEP attributable to model errors (as is probably the case here), then a real MOE-based device could produce an actual SEP no better than this value. In other words, if model errors are responsible for the SEP, then the theoretical (model) SEP is a lower-bound for the real SEP. Errors in the production of the MOE or errors in the calculations preceding the model could negatively impact the result, but probably not improve it. On the other hand, if the SEP is not limited by model error but by signal to noise in the original measurements on conventional instruments, an MOE could conceivably improve the result. As described in reference 5, MOEs are far less sensitive to detector noise contributions and low light levels than are conventional spectrometry systems. In general, UV-Vis spectroscopy and modeling is not limited by noise but by model errors. Thus, we should anticipate that our actual MOE will not miraculously reduce the expected SEP.

Determination of Copper Uroporphyrin with the MOC approach. The difference (in millivolts) in detector signals between detectors viewing MOE-reflected vs. MOE-transmitted light that first passed through validation samples was measured for 20 samples. These samples were different from those samples that were used for MOE design, but were designed with a similar spread of concentration values. 10 of these samples were used to evaluate the relative responsivities of the two detection arms of the measurement system. To understand this why this is necessary, consider that the two detectors shown in Figure 1 are physically different devices and thus can have slightly different relative responses. Since the MOC measurement is given by the difference in the two detector responses, a correction factor (K) is necessary to give them the same overall gain. With an incorrect value of K, correlation between the detector differences and the Cu-P concentration is seriously degraded. Figure 5 shows the optimum correlation obtained between the detector differences and BB concentration by giving K=1.18 in the MOC equation:

$$C = 1.97 \ (T-KR) + 46.59 \tag{5}$$

where C is Cu-P concentration in μM, and T and R are the detector outputs in millivolts.

The calibration model was tested by using the linear regression model in equation 1 to predict the concentrations of the remaining 10 samples. Figure 6 shows a plot of the predicted Cu-P concentrations versus the actual Cu-P concentrations using this model. The SEP was determined to be 0.86 μM.

A number of factors exist to explain the disparity between the estimated linear SEP (0.86 μM) for MOC in this example and the expected SEP of 0.60 μM. First, we were unable to calibrate the detectors because of instrumental limitations. Instead, data from the manufacturers specifications were relied upon in determining detector spectral response. This information is of a general nature and better results are expected when all the individual optoelectronic components used in assembling the MOC measurement system are fully calibrated.

Second, fabrication errors resulting in the mismatch between the measured MOE spectrum and the theoretical spectrum can play an important role in the final results. An accurate reproduction of the MOE coating layers as specified by the design is necessary to achieve a value of the SEP that is comparable with that predicted for the design. The current process control system for the fabrication of MOEs does not provide the most effective means of monitoring the deposition process to produce layers with accurate thicknesses. Fortunately, many of the shortcomings of our current process control system can be rectified. These improvements will be the subject of future reports.

Third, normalization of the data was not performed. The acquisition of the test data in our laboratory was performed over the course of two 2-hour sessions, so slight drift in the detectors probably contributes to our error. Normalization is an aspect of multivariate optical computation that will be the subject of a future report.

Fourth, the lamp whose calibration we show in Figure 3c burned out early in our testing. Although a new lamp of the same type was installed and operated at the same voltage, there is no guarantee that the color temperature of the new lamp matched that of the old. This is an interesting problem that is common to many spectrometry systems using lamps, and one that is ultimately addressable with MOC technology: a spectral vector for color temperature can be produced that will enable lamps to be controlled for color temperature. This problem is one that we are currently beginning to address, and will also be the subject of a future report.

CONCLUSIONS

The use of a simple optical computing device has been demonstrated with the successful design and testing of an MOE for the analysis of a quaternary porphyrin mixture. The results obtained compare quite favorably with conventional PCR regression in spite of the non-idealities in sample measurement using the current prototype instrument, as well as those stemming from MOE manufacture. Measurements will be extended to the determination of chemical species in more complex systems with a greater number of interferents.

There exist several areas of theory that still need to be explored in order to gain a better understanding of MOC. For example, no theory has been developed covering the susceptibility of this technology to manufacturing errors. Also, the application of chemometrics to radiometric data has not been fully developed, so that there is currently no way to quantitatively predict the errors accumulates from nonlinearities in radiometry. All these areas are subjects of further study.

In general, we think it is important to keep in mind the following truth about multivariate optical computing: It is not a panacea. It is subject to all the same problems to which conventional multivariate spectroscopy is prone. In the case of weak signals or noisy detectors, it can hypothetically produce better SEPs than conventional spectroscopy; but it is no less sensitive to model errors than conventional measurement techniques. Instead, MOC trades one set of problems for another. At the cost of a complex design and manufacturing process and the loss of some experimental flexibility, one gains a far simpler instrument with dramatically lower cost and maintenance. In our laboratory, for example, we estimate that the cost of producing the 28-layer MOE used here is much less than $100 per element when 50 or more are made. In some instances, multivariate optical computation is a tool that could make complex spectroscopic measurements accessible to a mass market.
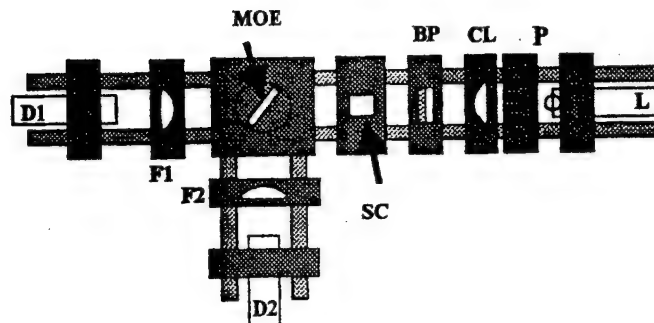
Figure 1. Schematic of the prototype of a multivariate optical computing device for the measurement of Cu-P in a quaternary porphyrin mixture. MOE=multivariate optical element, SC=quartz sample cell, OB=optical block, BP=bandpass filter set consisting of two 3 mm schott glasses, CL=achromatic collimating lens, L=Tungsten halogen lamp, P=pinhole, D1/D2= Si photodiode detectors for light radiation transmitted through and reflected from the MOE, F1/F2=focusing lens.
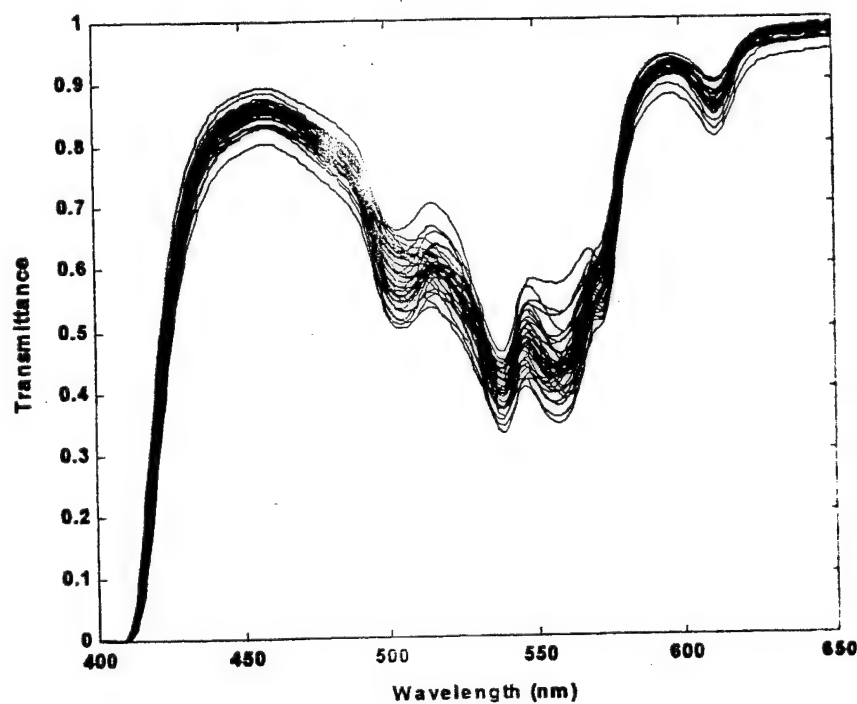
Figure 2. Optical transmittance spectra of 40 quaternary mixtures of Uro, Cu-P, Sn-P, and N_1-P
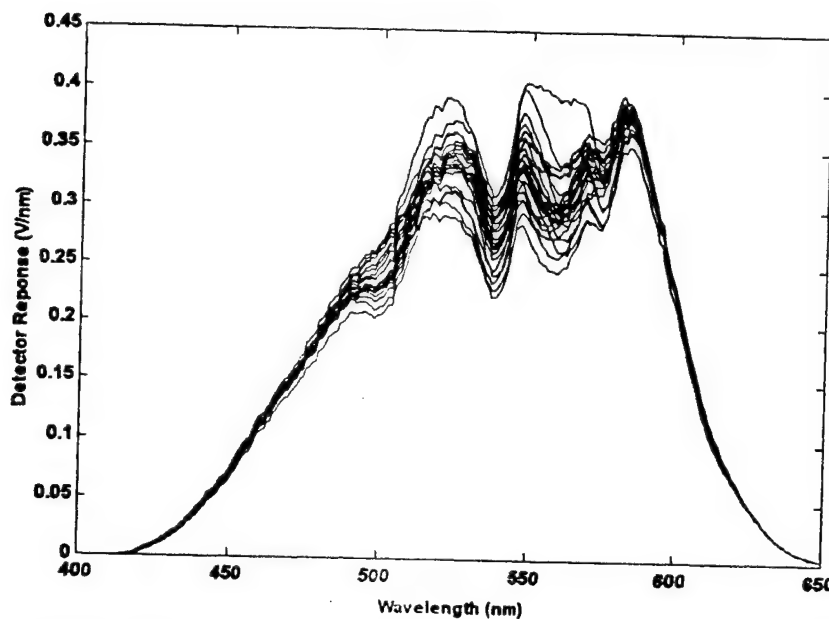
Figure 3. Detector response profiles for the quaternary porphyrin mixture produced from a convolution of the spectra shown in Figure 3, with the source radiance, detector sensitivity, and the filter bandpass.
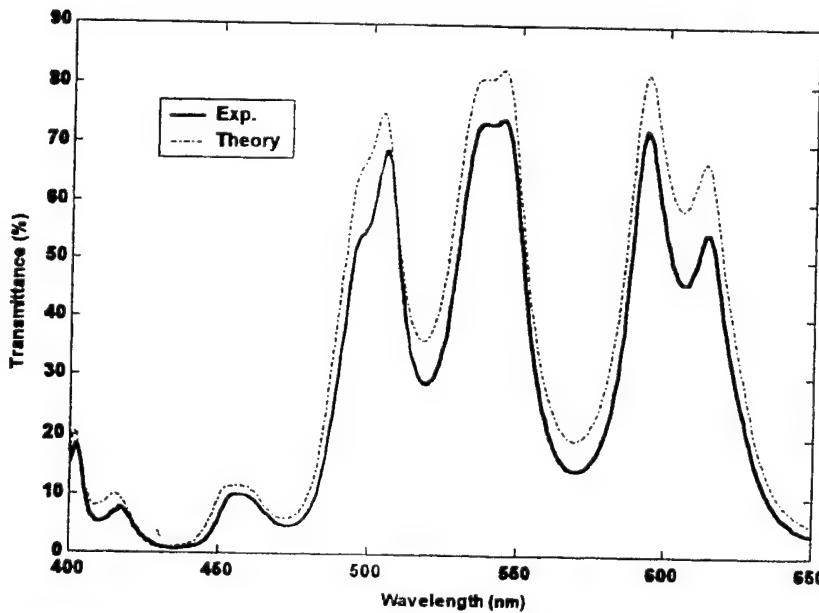
Figure 5. A comparison of the designed MOE spectrum (dashed line) consisting of 28 alternating layers of Nb_2O_5 and SiO_2, to the spectrum of the fabricated MOE (solid line).
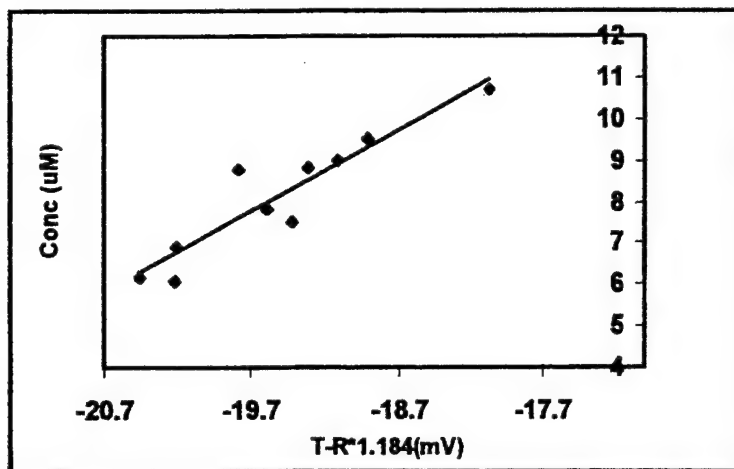
Figure 5. Correlation of Cu-P concentration (μM) the detector measurements (mV).
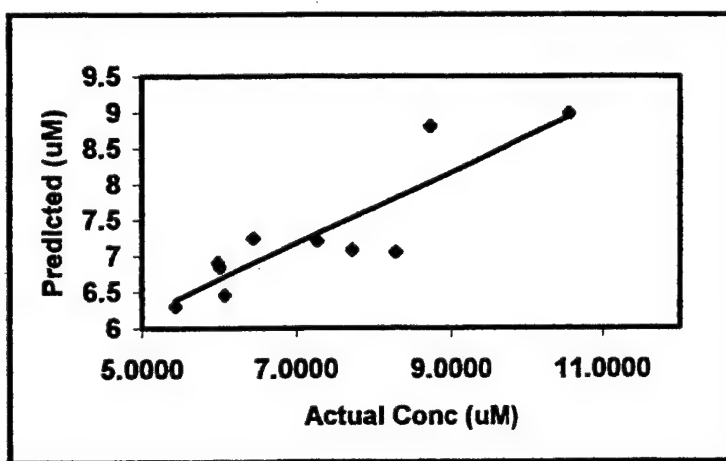
Figure 6. Plot of predicted Cu-P concentration (μM) to the actual Cu-P concentration (μM).

ACKNOWLEDGEMENT

81

REFERENCES

1. J.F. Aust, K.S. Booksh, M.L. Myrick, "Novel In-Situ Probe for Monitoring Polymer Curing," *Appl.Spectrosc.* **50**, pp 382-387, 1996.
2. E.V. Thomas, and D.M. Haaland, "Comparison of Multivariate Calibration Methods for Quantitative Spectral Analysis," *Anal.Chem.* **62**, pp 1091-1099, 1990.
3. M.M.A. Ruyken, J.A. Visser, and A.K. Smilde, "Identification of Plastics among Non-plastics in Mixed Wastes by Remote Sensing Near-Infrared Spectroscopy. 2. Multivariate Rank Analysis for Rapid Classification," *Anal.Chem.* **67**, pp 2170-2179, 1995.
4. H. Martens, and T. Naes, *Multivariate Calibration*, John Wiley and Sons, New York, 1989.
5. M.P. Nelson, J.F. Aust, J.A. Dobrowolski, P.G. Verly, and M.L. Myrick, "Multivariate Optical Computation for Predictive Spectroscopy," *Proc.SPIE-Int.Soc.Opt.Eng (Three Dimensional and Multudimensional Microscopy: Image Acquisition and Processing).* **3261**, pp 232-243, 1998.
6. S.E. Bialkowski. " A Scheme for Species Discrimination and Quantitative Estimation Using Coherent Linear Optical Signal Processing" *Anal.Chem.* **58**., pp 2561-2563, 1986.
7. M.L. Myrick, O. Soyemi, J. Karunamuni, D. Eastwood, H. Li, L. Zhang, and P. Gemperline, "A Single-Element All-Optical Approach to Chemometric Prediction," *Vibrational Spectroscopy.* (submitted 2000).
8. A. Ryabenko, and V. Kasparov. *Pattern Recognition in Image Analysis*, **1**. pp 347-354, 1991.
9. O. Soyemi, P.J. Gemperline, L. Zhang, D. Eastwood, H. Li, and M.L. Myrick. " A Nonlinear Optimization Algorithm for Multivariate Optical Element Design", *Anal.Chem* (submitted 2000).
10. J.L. Vossen, and W. Kern. *Thin Film Processes II; Academic Press*: San Diego, 1991; Chapter 4.
11. Q. Ding, G.W. Small, and M.A. Arnold. "Evaluation of Data Pre-Treatment and Model Building for the Determination of Glucose in Near-Infrared Single Beam Spectra." *Appl.Spectrosc.* **53** pp 402-414, 1999.
12. K.H. Hazen, M.A. Arnold, and G.W. Small. "Measurement of Glucose and other Analytes in Undiluted Human Serum with Near Infrared Transmission Spectroscopy" *Anal.Chim.Acta.* **371**. pp 255- 267, 1998.
13. P.J. Gemperline, J.R. Long, and V.G. Gregoriou. "Nonlinear Multivariate Calibration Using Principal Components Regression ans Artificial Neural Networks." *Anal.Chem.* **63**. pp 2313-2323, 1991.

10.7 INTERFERENCE FILTER REFINEMENT FOR ARTIFICIAL NOSE FLUORESCENCE SENSING

Interference filter refinement for artificial nose fluorescence sensing

Jeevananda Karunamuni, MEMBER SPIE
Katherine E. Stitzer
DeLyle Eastwood, MEMBER SPIE
University of South Carolina
Department of Chemistry
Columbia, South Carolina

Keith J. Albert, MEMBER SPIE
David R. Walt
Tufts University
The Max Tishler Laboratory for Organic
    Chemistry
Department of Chemistry
Medford, Massachusetts 02155

Steven B. Brown
Lawrence Livermore National Laboratory
P.O. Box 808, L-171
Livermore, California

Michael L. Myrick, MEMBER SPIE
University of South Carolina
Department of Chemistry
Columbia, South Carolina
E-mail: myrick@psc.sc.edu

Abstract. Optical interference coatings are used in filter-based *T*-format fluorimeters to make beamsplitters, bandpasses, and bandblocking filters that separate excitation and emission signals. Commercially available filters usually perform well in these applications, but better performance may be possible if the system of optical filters is tailored to the specific analysis. We provide a general method for designing optical filters for the optical train of a specific fluorescence sensor system simultaneously using two light-emitting diode (LED) excitation sources (blue and green) and two different fluorescent indicators. We approach the problem of designing the optics of the system by first constructing a hypothetical target spectrum for each filter using the optical spectrum of the excitation source, and the excitation and emission spectra of the fluorescence sensors. Structural designs for Nb_2O_5/SiO_2 multilayer interference filters are then synthesized. An iterative evaluation procedure is then used to improve the performance of the system for minimal leakage of the excitation sources onto our detector array. We also provide experimental results for the construction of these filters using reactive magnetron sputtering. © *2001 Society of Photo-Optical Instrumentation Engineers.*
[DOI: 10.1117/1.1367255]

1 Introduction

One common type of optical instrument is the filter-based *T*-format (an epi-illumination geometry) fluorimeter. The purpose of such an instrument is to either directly measure an analyte's fluorescence intensity, or to interrogate a fluorescence transducer that is sensitive to an analyte concentration or an environmental condition, e.g., temperature. A basic *T*-format instrument has three arms: the excitation, detection, and sensor arms. It normally uses a beamsplitter of some type to separate the beam paths of the excitation and detection arms of the instrument, while combining them into a single optical train on the sensor arm. Optical filters are incorporated into these instruments because they reduce costs, have higher throughput efficiencies, and are smaller and thus more portable than other wavelength selection devices. Commercially available optical filters make the job of constructing a basic *T*-format system simple: once the excitation and emission wavelengths are defined for the sensor arm, and the excitation source and detector are selected, adequate filters for the application are often available from various companies that manufacture multilayer interference filters. A number of companies produce optical filters specifically for *T*-format instruments, among which are Omega Optical, Inc., Chroma, Inc., and Corion, Inc.

The recent introduction of fiber optic-based sensors for the measurement of various analytes using arrays of different fluorescence transducers[1-11] has complicated the design of these systems. For example, recent work by Walt et al.[6-11] focuses on previously developed "artificial nose" technology to detect low-level nitroaromatic vapors that may be present on the soil surface above buried land mines. This work employs an array of multiple transducer types for vapor detection by computational analysis.[6-11] Many of the available fluorescence-based transducers have different optimal excitation and emission wavelengths. One possible approach to instrument design for these array-based sensors is, in effect, to design a separate *T*-format system for each transducer. The basic concepts governing the design of such instruments is well known.[12,13] Another approach is to design more complex optics that permit a single instrument to excite and detect fluorescence of multiple transducers and/or analytes.

The complex combinations of excitation and emission spectra possible for these arrays has prompted us to investigate systematic means for filter selection or synthesis in systems combining fluorescence sensors with very different spectroscopies. It is often possible to retain the simple layout of a filter-based *T*-format instrument even when multiple excitation and emission bandpasses are needed. The purpose of the present report is to illustrate an integrated method for designing a complete system of optics for a sensor array, considering the details of light sources and the spectroscopies of more than one transducer type. In the following discussion, we consider a recent sensor package for 2,4,6-trinitrotoluene (TNT) vapor detection that resulted
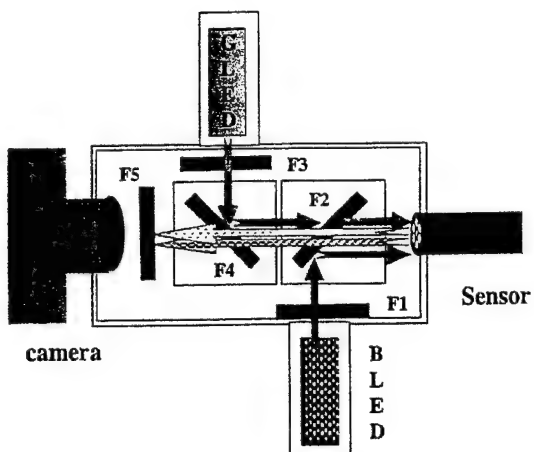
Fig. 1 Schematic layout of the filter-based fluorimeter described in the text. F1-F5 are optical interference filters. The sensor is an array-type sensor containing two different optical transducers, Polymer #58 (MIT) and Nile Red-coated microspheres (Tufts). The camera is a charge-coupled device (CCD) Epoch, Inc.(CA) Pixel™ CCD camera 192×165 pixels with off chip binning. F1 and F2 are a bandpass and a beamsplitter, respectively, to excite Polymer #58 with a blue light-emitting diode (BLED). F3 and F4 are a bandpass and beamsplitter, respectively, to excite Nile Red with a green LED (GLED). F5 is a filter to select the emission wavelengths of both fluorophores.

Fig. 2 58X is the excitation spectrum of Polymer #58, detected at the peak emission wavelength. 58M is the emission spectrum of Polymer #58, excited at the peak excitation wavelength. NRX is the excitation spectrum of Nile Red on silica beads, detected at the emission maximum. NRM is the emission spectrum of Nile Red on silica beads, excited at the excitation maximum. The left-hand intensity axis is for Nile Red curves, while the right-hand axis is for Polymer #58 curves.

from a collaboration between Tufts University, Lawrence Livermore National Laboratory, and the University of South Carolina, as an example of a more complicated sensor package. A schematic diagram of the sensor optical train is shown in Fig. 1. We show how the spectroscopy of the components of the system can be combined to form an initial target for the spectra of the necessary filters, how such filters can be designed with the aid of a computerized synthesis program, and how the iteration of the resulting initial designs can be refined. After this, we compare the spectra for real filters made in our laboratory to the targets that they were intended to approximate.

2 Experimental

Excitation and emission spectra for the Nile Red porous silica microsensors and Polymer #58 were acquired using a single-core optical fiber and a double-monochromator fluorescence system as described previously.[14] The Nile Red microbead sensors were electrostatically fixed to the distal tip of a 750-μm single-core optical fiber and placed onto the double monochromator system. For Polymer #58, a 1-mg/mL stock solution in toluene was used to dip and spin-coat the polymer onto the distal tip of the single-core optical fiber before positioning it onto the system. The excitation spectrum for each sensor type was recorded at the emission maximum and vice versa for the emission spectrum. A photomultiplier tube (PMT) detector was employed for detection.

Optical filters were designed using TFCalc™ software (Software Spectra, Inc.) based on target excitation and emission profiles for sensory materials provided by MIT and Tufts (see Fig. 2). The spectra of the blue and green LED excitation sources (Nichia, Inc.) used in the instrument are shown in Fig. 3. These curves were obtained from

a calibrated fluorimeter constructed in-house based on a double-monochromator (SPEX, Inc.). The values of parameters obtained for a refined filter design from the TFCalc™ software form the basis for our experiment. Software provides the physical thickness as well as the optical thickness of each layer of a multilayer system of a filter design.

Reactive magnetron sputtering (RMS) is used in our laboratory to construct the interference filters. RMS is a room-temperature process for depositing thin films of simple compounds, beginning with elemental targets amenable to sputtering. Our system (Model CVC 5.1) was custom manufactured by Corona Vacuum Coaters of Vancouver, B.C., and uses a 40-kHz mid-frequency RF supply to power four water-cooled planar magnetrons positioned in pairs around a rotating drum with a horizontal axis. The 22-in.-diam, 20-in.-deep chamber of our system contains
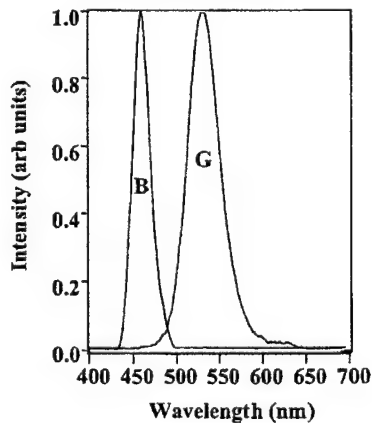
Fig. 3 Emission intensity of blue (B) and green (G) light-emitting diode sources used in the system shown in Fig. 1. Intensities are scaled to be relative to the maximum of each curve.

85

two 4×10 in. magnetrons with niobium (high index) targets and two with silicon (low index) targets.

In RMS, argon ions are ionized and entrained in a magnetic field, after which they collide with the surface of a target. In our system, the targets are 99.95% purity niobium and 99.9999% purity silicon. If the chamber atmosphere is free of oxygen, films of the pure materials are deposited. When O_2 is added to the gas mixture, the deposited film can be continuously oxidized as it forms. RMS is a relatively slow deposition process, but it yields very high quality films with low porosity and near-bulk optical constants that are nearly invariant with increasing deposition time. The surface roughness of these films is exceptionally low, and the deposition rate is extremely stable compared to evaporative sources. Unlike evaporative sources, the rate of deposition is almost linearly dependent on the power supplied to the magnetrons.

The substrates used to fabricate our filters were 1-in.-diam BK-7 glass optical flats (Esco Products, Inc.). These substrates were mounted on a 14-in.-diam rotating drum shaped like an octagonal prism. The substrate size is very small compared to the area of the magnetron sources and the rotational motion of the substrate drum enables the production of very uniform thin films.

Deposition rates for niobia and silica via RMS are given in nanometers per kilowatt-toggle, where the unit "toggle" represents a single sweep of the substrate through the deposition zone. The deposition rate for Nb_2O_5 (4.62 nm per kW-toggle) and SiO_2 (10.45 nm per kWtoggle) was measured for the instrument prior to manufacture of the multilayer films, providing an estimated deposition time for each layer of the film. Baseline oxygen and argon flows were set to optimal values for each material. In the case of Nb_2O_5, the O_2 flow was set 3.4 to standard cubic centimeters per minute (SCCM) and the argon flow was set to 2 SCCM. For production of SiO_2, the O_2 flow was set to 3.5 SCCM and Ar flow was set to 2 SCCM. Initial power input for the targets was set to 0.7 kW for both targets. The total gas pressure in the system was approximately 7 millitorr during sputtering.

3 Results and Discussion

3.1 Overview

The optical sensing system described in Fig. 1 operates by measuring the change in fluorescence intensity of two fluorescence sensors. The first of these transducers is a dispersion of Nile Red dye on porous silica microspheres. The fluorescence excitation and emission spectra shown in Fig. 2 for this sensor are for Nile Red dye on OH-terminated silica surfaces. The second transducer is a fluorescent polymer (Polymer #58) prepared by the group of T. Swager at MIT, similar to materials previously reported.[15–17] Both of these sensors exhibit fluorescence quenching or enhancement when they are in the presence of vapors to which they are sensitive, although details of the mechanisms are incomplete.

Nile Red is a common dye for which T-format systems have long been developed. Omega Optical, Inc. (http://www.omegafilters.com), for example, offers a filter set (XF35) that would serve to effectively measure the fluores-

cence of Nile Red alone. Another Omega Optical filter set (XF18) could be used for Polymer #58 alone.

However, from the standpoint of the optical system design in Fig. 1, simultaneous excitation and detection of the signals from these two sensors are somewhat challenging. This is because they require two different excitation bands, two different emission bands, and one of the emission bands is interposed between the two excitation bands.

3.2 Initial Design

The blue light source in Fig. 1 is used to excite the Polymer #58 sensor, while the green source is used to excite the Nile Red sensor. The initial design of the optical filters for the instrument described in Fig. 1 is only intended to list the desired bandpasses and bandblocks for each filter. For example, F1 in Fig. 1 is the "blue bandpass," and is intended to select the useful portion of the emission of the blue light-emitting diode source, while blocking any wavelengths that are not important to excitation of Polymer #58. In wavelength regions where the blue source has no intensity, the transmission and blocking of filter F1 does not matter. F2 is more complicated because it is active at every wavelength: this is the "blue beamsplitter" that reflects the blue excitation toward the sensor array, while allowing all other wavelengths to pass through. The reflection of the blue excitation should be very high, since this filter is the first line of defense to prevent blue scattered light from reaching the detector ("camera" in Fig. 1). The wavelengths at which the sensors emit should have the highest possible transmission, since returning luminescence from the sensors must pass through six filter interfaces before it can be detected. The wavelengths at which the green light source emits should also be represented by high transmission in F2, because any loss will reduce the excitation of the Nile Red sensors.

F4 as shown in Fig. 1 is the "green beamsplitter." It is intended to pass the emission bands of both sensors as well as possible while reflecting the green excitation wavelengths as completely as possible. This last requirement is because, like F2 for short wavelengths, F4 is the first line of defense preventing backscattered green excitation light from returning to the detector. F3 is the "green bandpass," and selects the useful part of the illumination from the green light-emitting diode, while blocking wavelengths at which the two sensors emit light.

F5 is the most complex of all the five filters, because it is the final defense of the detector from backscattered excitation from both LED sources, and must simultaneously exhibit high transparency to the emission from both sensor types.

From the preceding considerations, it is apparent that a reasonable first guess of the optimal properties of our filters is as shown in Fig. 4.

3.3 Initial Synthesis

Synthesis, in the context of this report, refers to the theoretical design of a multilayer filter with a given spectrum. The determination of the spectral characteristics of a given multiplayer layer is straightforward, while the determination of the structure of a multiplayer filter that fits a specific spectrum is far from straightforward. Only an approxima-
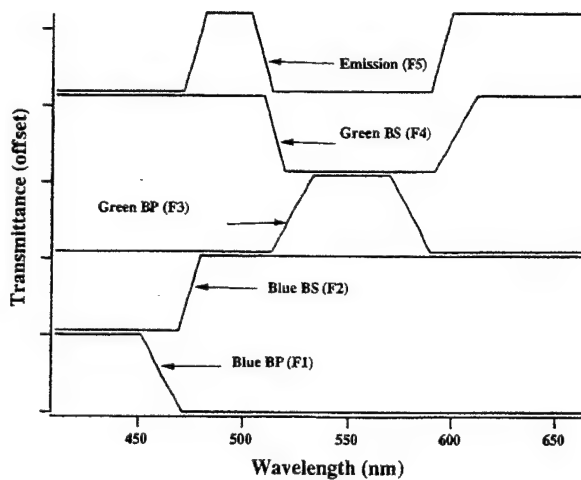
Fig. 4 Initial targets for the spectra of F1 to F5. Curves are offset for clarity; each begins at zero and rises to a maximum of 100% transmittance.


Fig. 5 Initial fits to the target spectra for F3, F4, and F5 obtained by filter synthesis. Curves are offset for clarity, with the center curve offset by 100% and the upper curve by 200%.

tion of a given spectrum is generally possible within the limits of what can be achieved with current multilayer deposition technologies.

We can make a few general points about the relationship between spectral characteristics and film structure that governs whether a given spectrum will be achievable. One equation that describes this relationship from a theoretical standpoint was provided by Sossi[18] and Verly and Dobrowolski[19]:

$$\ln\left(\frac{n(x)}{n_0}\right) = \frac{i}{\pi} \int_{-\infty}^{\infty} \frac{\hat{Q}(\sigma)}{\sigma} \exp(-i2\pi\sigma x) d\sigma, \qquad (1)$$

where $\sigma = 1/\lambda$, n_0 is the refractive index of the surrounding media, λ is the wavelength, $n(x)$ is the refractive index profile of the multilayer, x is twice the optical thickness:

$$x = 2 \int_0^z n(u) du, \qquad (2)$$

z is the physical thickness, and $\hat{Q}(\sigma)$ is a spectral function that is empirically related to the transmittance of the multilayer film stack. The origin for x and z is in the center of the film. From a fabrication standpoint, achieving the continuous variation of refractive index implied by Eq. (1) is difficult to achieve. Also, there is a maximum practical thickness for a multiplayer filter beyond which the films will delaminate from the substrate, this thickness being somewhere near 10 to 25 μm.

The relationship in Eq. (1) is a Fourier transform relationship between the transform pair $\ln[n(x)/n_0]$ and $\hat{Q}(\sigma)/\sigma$. This equation implies that sharp variations in the transmission spectrum of a film require a thick multilayer. However, as Refs. 19 and 20 make clear, $\hat{Q}(\sigma)$ is a function that changes rapidly when transmittance is small. This means that a sharp feature at low transmittance requires a thicker film than the same feature at low transmission. The dependence on the wavenumber σ in Eq. (1) means that a

sharp feature at long wavelengths requires a thicker film than the same feature at a shorter wavelength. As a general rule of thumb, sharp features and low transmittances are difficult to achieve, and a combination of sharp features and low transmittance is especially difficult.

From the standpoint of ease of manufacture, our initial spectral targets present some obvious problems. All call for ''zero'' transmittance, and there are sharp edges at zero transmittance for all. To find spectra and structures for real filters that will fit our purposes, we take these targets and attempt to synthesize best-fit spectra for filters with reasonable thicknesses.

A requirement of low transmittance in some spectral regions places constraints on the maximum transmittance that we can expect in the bandpasses of our filter set. It is relatively easy to achieve high compared to low transmittances. Our best performance is likely to result by only requiring low transmittances where they are truly necessary. Thus, we can focus our efforts primarily on the problem of blocking the backscattering of the light sources to the detector. This strategy is also reasonable from the standpoint of improving the signal-to-background ratio for the optical system, which is more amenable to improvement by reducing the background toward zero than by increasing the signal level toward 100%. When we turn our attention to source-blocking subsets of our original five-filter problem we can identify two workable subsets, namely the F1-F2-F5 and the F3-F4-F5 filter subsets. These have critical low transmission specifications in the blue and green spectral regions, respectively. For simplicity, we restrict our further discussion only to the F3-F4-F5 set, since the F1-F2-F5 filter set is treated analogously.

Using TFCalc™, a commercially available thin-film design program, we obtain the initial spectral set shown in Fig. 5 for the F3-F4-F5 filter set. Since TFCalc™ requires a tolerance value for each wavelength, a larger tolerance, e.g., 25%, is permitted for high-transmission wavelengths than for low, e.g., 0%. This is consistent with our prior arguments that the low transmission regions will be simultaneously more difficult to achieve and more important to improving the signal to background ratio of the optical system.

87

Since our best-fit spectra cannot be the same as our targets in Fig. 4, they will not perform as well as the targets: they will not transmit as much of the fluorescence signal back to the detector, and, more importantly, they will permit some light from the excitation sources to leak back to the detector. For this reason, we will employ an iterative solving procedure to refine the result of our initial "synthesis" of the filters. In this procedure, we: 1. isolate the regions of the spectra that are most offensive: 2. identify the filter(s) that are supposed to clean up this spectral region: 3. modify one or more of the filter spectra accordingly: and 4. resynthesize the filter(s).

3.4 Performance Evaluation

We need to define a metric to determine in which regions of the spectra the filters are performing poorly. Since our arguments regarding the quality of the optical system revolve more around leakage of the excitation sources into the detector than on total signal levels, we define our metric with this in mind. The leakage of the green light source into the detector, for example, should be prevented by the F3-F4-F5 combination of filters. Because proper internal baffling should prevent off-axis scattering into the detector, we neglect scattering produced by light that passes through F4, strikes the opposing wall of the optical block, and then scatters into the detector past F5. Our major contributor to background from the excitation sources will be from on-axis light from the source that passes through F3, reflects from F4, backscatters from the sensor, passes through F4, and then passes through F5 to reach the detector. The backscatter from the sensor may have a wavelength dependence, but this is unknown and omitted. For both filter sets, the excitation light must also pass through the beamsplitter of the other set before reaching the camera. The beamsplitter of the other set is not designed to block this radiation, and therefore it is also omitted from the calculation of performance. Our performance factor is derived from the product of the spectrum of the light source, $G(\lambda)$, with the transmittance of the optical train for scattered light. This latter factor is itself a product of other terms, so our performance factor can be written in the form:

$$\gamma(\lambda) = G(\lambda) T_{F3}(\lambda) R_{F4}(\lambda) T_{F4}(\lambda) T_{F5}(\lambda), \tag{3}$$

where γ is the performance factor as a function of wavelength, T_{Fn} is the transmittance (on a scale of 0 to 1) of filter F_n, and R_{Fn} is the reflectance of the filter. Reflectance and transmittance of an all-dielectric filter sum almost exactly to unity, and therefore we can calculate γ for our green filter subset by curve $\gamma_{Initial}$ in Fig. 6. In general we could also include detector spectral responsivity in this equation. In this particular case, the CCD camera spectral responsivity varies only slightly across the spectrum of the fluorophores, so we have not included it.

3.5 Iteration

The initial estimation of leakage in Fig. 6 shows that most of the leakage for this filter subset would come from the 530 to 560-nm region. This region should be transmitted by F3, and therefore no change to F3 is required. F4 and F5 are both supposed to be high reflectors in this wavelength range, and we iterate the filters by tightening the constraints
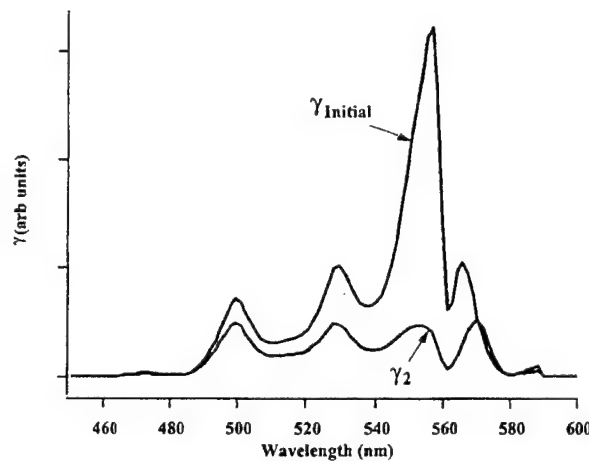
Fig. 6 Performance factor plots for green backscatter in the optical system. The upper curve, labeled $\gamma_{initial}$, is for the filters in Fig. 5. The lower curve is the result after improving F3 and F4.

on F4 and F5 in this wavelength region while relaxing them further in their high-transmission windows. When we resynthesize the filters, the leakage calculated from Eq. (3) using the revised filters becomes the curve shown as γ_2 in Fig. 6. The structure of one of these filters, F5, is shown in Table 1.

3.6 Construction

Once an appropriate set of filters has been defined and their structures known, they must be fabricated. Using manual control of the deposition, we deposited the 19-layer struc-

Table 1 Films thicknesses in nanometers for filter F5. Layers are numbered from the substrate outward. Optical thickness is calculated at 550 nm.

Layer no.	Material	Physical thickness	Optical thickness
1	Nb_2O_5	191.74	3.2302
2	SiO_2	85.87	0.9087
3	Nb_2O_5	50.75	0.8551
4	SiO_2	80.94	0.8565
5	Nb_2O_5	48.68	0.8201
6	SiO_2	78.15	0.827
7	Nb_2O_5	108.99	1.8361
8	SiO_2	79.06	0.8366
9	Nb_2O_5	50.89	0.8574
10	SiO_2	86.69	0.9173
11	Nb_2O_5	52.1	0.8778
12	SiO_2	88.41	0.9356
13	Nb_2O_5	53.01	0.8931
14	SiO_2	89.57	0.9478
15	Nb_2O_5	205.4	3.4603
16	SiO_2	85.13	0.9009
17	Nb_2O_5	50.68	0.8538
18	SiO_2	82.84	0.8766
19	Nb_2O_5	51.13	0.8614

88
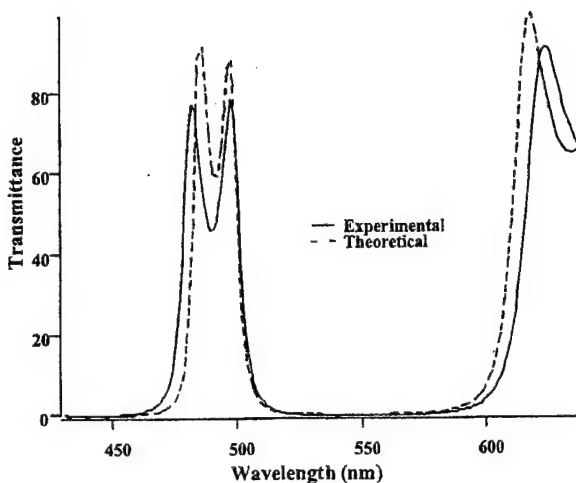
Fig. 7 Theoretical filter spectrum for F5, and an experimental result for a typical deposition run.

ture described in Table 1 and generated a filter with the spectrum shown in Fig. 7. Although similar to one another, the theoretical and experimental spectra are not identical. This is because, after 19 layers of deposition, the spectra are sharper in the wavelength domain than the resolution of

the spectrometer we use for monitoring. Improved spectral fits could be expected from monitoring through "witness samples" that are changed after every ten layers or so. Even with this level of precision the results are adequate for our system design.

3.7 Instrument Performance

The Fig. 1 instrument can be used as an artificial nose through measurement of the spatially distributed response of the fluorophores to analytes. Operation of the instrument is accomplished by exciting the fluorophores and recording the changes in intensity of their fluorescence as a function of exposure to various vapors. The Nile Red sensors, for example, respond differently depending on the environment in which the Nile Red dye is deposited. Thus, different substrates for the Nile Red produce different relative responses. Polymer #58 has its own relative set of responses to analytes. Interpretation of the data produced by the instrument is based on pattern recognition and measurement.

The performance of the instrument with explosives vapors is the subject of another manuscript.[21] The performance with different fragrances is the subject of yet another manuscript.[22] In both studies we were able to show that pattern recognition based on the sensor responses could selectively identify and even quantify (within limits) vapor-
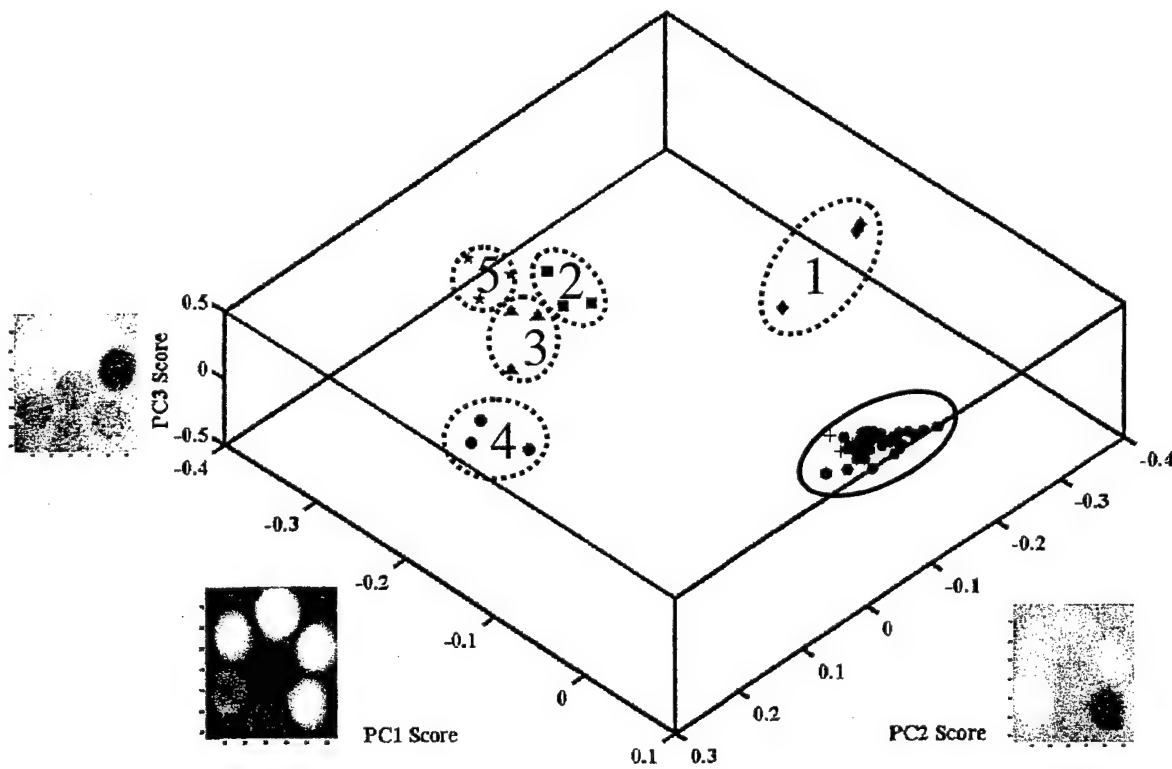
Fig. 8 System performance. The responses of a sensor set to five samples of perfumes from the same manufacturer. The large number of samples that cluster together and which are surrounded by a solid line are measurements of air, a clean cotton pad, and the nitrile gloves used by the scientist performing the experiment. The clusters of three points with dashed circles around them are labeled 1 through 5 for the fragrance they represent. The three axes are the magnitudes of three major spatial patterns in the camera images of the sensor set following exposure to the fragrances. Details on the fragrances, sensors, and data analysis are given in Ref. 22.

89

phase analytes. An example is shown in Fig. 8, taken from Ref. 22. In this figure, the responses of a sensor set to samples of perfumes are recorded, as well as the responses to blank samples of different types. The axes for this plot are magnitudes of spatial patterns measured in the system response of the "artificial nose" array. Reference 22 contains more complete information about this result.

4 Conclusions

A systematic procedure can be followed for designing thin-film multilayer interference filters for complex optical systems such as those that may be required by arrays of fluorescence sensors. The method we describe here is a very user-intensive procedure, involving off-line synthesis of filters after evaluating performance based on an empirical factor.

It is likely, however, that the basis for this technique can be incorporated into an automated process that works alone or in concert with a thin-film design program such as TF-Calc™. The matrix mathematics by which the transmission spectra of multilayer stacks are calculated are straightforward, so an automatic synthesis of several filters that work in concert in a set is reasonable, within limits. Input to such a system could consist of a listing of the required zero-transmission regions for each filter, plus a definition akin to Eq. (3) by which the quality of the stack can be judged.

References

1. K. S. Bronk, K. L. Michael, P. Pantano, and D. R. Walt, "Combined imaging and chemical sensing using a single optical imaging Fiber," *Anal. Chem.* **67**, 2750–2757 (1995).
2. K. L. Michael, L. C. Taylor, S. L. Schultz, and D. R. Walt, "Randomly ordered addressable high-density optical sensor arrays," *Anal. Chem.* **70**, 1242–1248 (1998).
3. D. R. Walt, "Fiber-optic imaging sensors," *Acc. Chem. Res.* **31**, 267–278 (1998).
4. K. L. Michael, J. A. Ferguson, B. G. Healey, S. L. Schultz, L. C. Taylor, P. Pantano, and D. R. Walt, "Fabrication of micro- and nanostructures using optical imaging fibers and their use as chemical sensors," *Proc. Electrochem. Soc.* **97**(5), Microstructures and Microfabricated Systems, 152-158 (1997).
5. J. A. Ferguson, B. G. Healey, K. S. Bronk, S. M. Barnard, and D. R. Walt, "Simultaneous monitoring of pH, CO_2 and O_2 using an optical imaging fiber," *Anal. Chim. Acta* **340**, 123–131 (1997).
6. T. A. Dickinson, J. White, J. S. Kauer, and D. R. Walt, "A chemical-detecting system based on a cross-reactive optical sensor array," *Nature (London)* **382**, 697–700 (1996).
7. J. White, J. S. Kauer, T. A. Dickinson, and D. R. Walt, "Rapid analyte recognition in a device based on optical sensors and the olfactory system," *Anal. Chem.* **68**, 2191–2202 (1996).
8. D. R. Walt, T. Dickinson, J. White, J. Kauer, S. Johnson, H. Engelhardt, J. Sutter, and P. Jurs, "Optical sensor array for odor recognition," *Biosens. Biotechnol.* **13**, 697–699 (1998).
9. K. J. Albert, T. A. Dickinson, D. R. Walt, J. White, and J. S. Kauer, "Designing optical sensor arrays with enhanced sensitivity for explosives detection," *Proc. SPIE* **3392**, 426–431 (1998).
10. K. J. Albert, M. L. Myrick, S. B. Brown, F. P. Milanovich, and D. R. Walt, "High-speed fluoresence detection of explosives vapor," *Proc. SPIE* **3710**, 308–314 (1999).
11. Private Communication.
12. M. L. Myrick, S. M. Angel, and R. A. Desiderio, "Comparison of Some Fiber-Optic Configurations for Measurement of Luminescence and Raman Scattering," *Appl. Opt.* **29**, 1333–1344 (1990).
13. F. P. Milanovich, P. F. Daley, S. M. Klainer, and L. Eccles, "Remote Detection of Organochlorides with a Fiber Optic Based Sensor. 2. A Dedicated Portable Fluorimeter," *Anal. Instrum.* **15**, 347–358 (1986).
14. C. Munkholm, F. P. Milanovich, and D. R. Walt, "A fiber-optic sensor for CO_2 measurement," *Talanta* **35**, 109–112 (1998).
15. J.-S. Yang and T. M. Swager, "Porous shape persistent fluorescent polymer films: An approach to TNT sensory materials," *J. Am. Chem. Soc.* **120**, 5321–5322 (1998).
16. J.-S. Yang and T. M. Swager, "Fluorescent porous polymer films as TNT chemosensors: Electronic and structural effects," *J. Am. Chem. Soc.* **120**, 11864–11873 (1998).
17. T. M. Swager, "The molecular wire approach to sensory signal amplification," *Acc. Chem. Res.* **31**, 201–207 (1998).
18. L. Sossi, "A method for the synthesis of multilayer dielectric interference coatings," *Eesti NSV Tead. Akad. Toim., Fuus., Mat.* **23**, 229–237 (1974).
19. P. G. Verly and J. A. Dobrowolski, "Iterative correction process for optical thin-film synthesis with the Fourier-transform method," *Appl. Opt.* **29**, 3672–3684 (1990).
20. J. A. Dobrowolski and D. G. Lowe, "Optical thin film synthesis program based on the use of Fourier transforms," *Appl. Opt.* **17**, 3039–3050 (1978).
21. K. J. Albert, M. L. Myrick, S. B. Brown, D. L. James, F. P. Milanovich, and D. R. Walt, "Portable sniffer for 2,4-Dinitrotoluene detection," *Environ. Sci. Technol.* (in press, 2001).
22. M. L. Myrick, K. J. Albert, S. B. Brown, D. L. James, F. P. Milanovich, and D. R. Walt, "Discrimination of fragrances from the same manufacturer using a cross-reactive optical 'Artificial Nose'," *Analyst* (submitted, 2001).

Jeevananda Karunamuni received his PhD in physics from LSU in 1998. He conducted postdoctoral research at the University of South Carolina from 1998 to 2000, and is employed in the thin-film coating industry.

Katharine E. Stitzer received her BS in chemistry and mathematics from Francis Marion University in 1998. She is presently a graduate student with Prof. Hans-Conrad zur Loye at the University of South Carolina. Her research interests include crystal growth, structure determination, and magnetic characterization of new rhodium containing oxides related to the 2H perovskite structure.

DeLyle Eastwood received her PhD in physical chemistry from the Universtiy of Chicago in 1964. She conducted postdoctural research in spectroscopy at Harvard from 1964 to 1966, at Washington from 1966 to 1969, and at Northeastern from 1970 to 1971. She has held research positions at Lockheed-Martin, the U.S. Coast Guard and U.S. Army Corps of Engineers, Brookhaven National Lab, UNLV and AFIT. She is currently with the Department of Agriculture. Her research interests are in several areas of applied spectroscopy and chemical sensors.

90

Keith J. Albert attended Colby College where he did a one year exchange program at UCC in Cork, Ireland. He received his BS in 1996 and is presently a graduate student at Tufts University with Prof. David R. Walt. His research interests include optical sensors, explosives vapor detection with microsensor array platforms, and instrumental designs for field use.

David R. Walt is Robinson Professor of Chemistry at Tufts University. Professor Walt's research is in the area of fiber-optic chemical sensors. He has received numerous national and international awards and honors recognizing his work. He was elected a fellow of the American Association for the Advancement of Science in 2000. Dr. Walt has published over 140 papers, holds over thirty patents, and has given hundreds of invited scientific presentations.

Steven B. Brown received his AS in mechanical engineering from Green River Community College and has been at Lawrence Livermore National Laboratory since 1968. He has been involved with photonic related research since the early 1970s and optical detection of chemical compounds and biological agents for the past 20 years.

Michael L. Myrick received his BS in chemistry from North Carolina State University in 1985 and PhD in physical chemistry from New Mexico State University in 1988. He conducted postdoctoral research at Lawrence Livermore National Laboratory. He was named an NSF Graduate Fellow (1986-88), and an Army Research Office Young Investigator (1992-1995). He is currently an associate professor in the Department of Chemistry and Biochemistry at the University of South Carolina.

91

10.8 A Single-Element All-Optical Approach to Chemometric Prediction

A single-element all-optical approach to chemometric prediction

M.L. Myrick[a,*], O. Soyemi[a], J. Karunamuni[a], D. Eastwood[a], H. Li[a],
L. Zhang[a], A.E. Greer[a], P. Gemperline[b,1]

[a]Department of Chemistry and Biochemistry, University of South Carolina, Columbia, SC 29208, USA
[b]Department of Chemistry and Biochemistry, East Carolina University, Greenville, NC 27858, USA

Abstract

A single-element approach to multivariate optical computing is described. Data for mixtures of Crystal Violet and Bismarck Brown dyes are analyzed as an example application. Radiometric information is combined with transmission spectra of the samples to obtain representative system responses for the samples. Direct synthesis of a multivariate optical element (MOE) is compared to a novel new approach for synthesizing simpler MOEs. The results show that less complex spectral vectors can be designed that perform adequately in this example. Experimental results for fabrication of an MOE are shown. © 2002 Published by Elsevier Science B.V.

Keywords: Multivariate; Chemometrics; Optical computing; Thin films; Spectroscopy

1. Introduction

Multivariate spectroscopy is a powerful tool for analytical determinations of the chemical and physical characteristics of a wide range of sample types. In one common approach for applying multivariate modeling to chemical problems, a spectral pattern that correlates with a dependent variable is found. In subsequent measurements of unknown samples, predictions of the dependent variable are made by computing the magnitude of this spectral pattern in the optical spectrum of the unknown.

After collecting spectra of solutions containing various amounts of the component of interest and interferent(s), principal component analysis (PCA) is used to decompose this set of independent variables into a set of principal components (PCs). These PCs are linear combinations of the original variables and can be thought of as a new set of orthogonal axes in the space defined by the original spectra and their detector channels. The primary axis, PC1, is the vector which describes the greatest variability in the data, while each successive PC describes smaller variability. Principal component regression (PCR) is then used to relate the dependent variable (concentration of a component of interest) to the independent variables (the coordinates of each spectrum on the PCs). A regression vector is determined in this way which correlates with the dependent variable. A calibration curve can then be created by taking the direct product of each spectrum and the regression vector.

A recent report from this laboratory [1,2] describes an all-optical interference-filter-based approach to the last step in this procedure, the magnitude calculation

* Corresponding author. Tel: +1-803-777-9521;
fax: +1-803-777-9521.
E-mail addresses: myrick@mail.chem.sc.edu (M.L. Myrick),
gemperlinep@mail.ecu.edu (P. Gemperline).
[1] Fax: +1-252-328-6767.
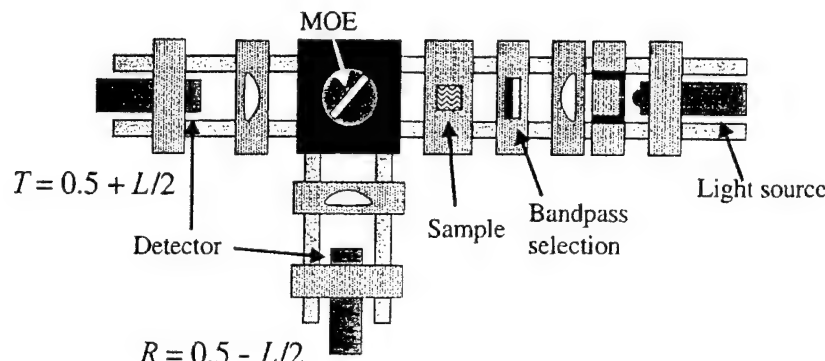
Fig. 1. Schematic diagram of a simple single-element system for the prediction of chemical properties based on the transmission spectroscopy of samples in cuvettes. In this design, MOE is the multivariate optical element, the bandpass selection filters are simple colored glass filters that roughly limit the spectral window, the detectors are matched, T and R stand for transmittance and reflectance on the scale of zero to one, and L is the scaled regression vector of the MOE.

given by the product of a regression vector with the spectrum of an unknown sample. The idea of using incoherent linear optical signal processing (OSP) for computation of an analytical parameter in a sample mixture was described as early as 1986 by Bialkowski [3]. An alternative to digital signal processing, linear OSP allows for the calculation of the product of two vectors by passing light with an intensity representing one vector (here, the spectrum of the unknown sample) through a filter with a transmittance representing a second vector (the regression vector). Our approach centers around the production of one or more optical interference coatings (MOEs) whose transmission spectra incorporate features of the spectral regression vector. The MOE consists of a substrate, such as glass, on which are deposited a series of thin film layers with differing optical properties. The thicknesses of the layers are designed so that the spectrum of the MOE matches a predetermined spectral profile that incorporates features of the regression vector. The design is such that there is a linear relationship between the component of interest and the transmittance through the experimental apparatus containing the MOE.

The original report makes use of a two-filter all-optical design, in which the spectral pattern is divided into positive and negative "lobes", each of which is transferred to a separate filter design. This approach, although workable in some cases, suffers from a fundamental problem. When multiple reflections are neglected, the Fourier spectrum of a target spectrum is directly related to the refractive index profile of a coating designed to match that target [4]. The process of separating the positive and negative portions of a regression vector from which two filters are designed introduces an unavoidable discontinuity in the target transmission profile at the points where the regression vector crosses zero. The result is two filters that each contain discontinuities in the slopes of their transmittance spectra at the points where the transmittance reaches zero. These discontinuities introduce very high Fourier frequencies in the filter spectrum, necessitating thick filters.

The present work describes a design alternative that resolves some of these problems. The concept behind this approach is shown in Fig. 1. In the new concept, a target spectrum is generated such that a single filter, operating as a beamsplitter, can function effectively in the same role as two filters in the original report. Further, the single-filter design relaxes some of the constraints present in the two filter design.

2. Experimental

A Hewlett-Packard UV–VIS diode array spectrophotometer Model 8543 was used to collect transmission and absorption data on binary dye mixtures for this study. A compact prototype field instrument (Fig. 1) was designed and constructed for this project to show proof of concept using Linos Photonics (Milford, MA) optical components. The characteristics of bandpass filters, lamps and detectors in the

113 prototype instrument were used to convert transmit-
114 tance spectra of calibration samples into detector
115 spectral responses.
116   A 6 V/6 W tungsten filament lamp with 1 mm × 1.2
117 mm active filament area was used as a light source in
118 the Fig. 1 instrument. The spectral radiance of the
119 lamp was measured in watts per (steradian × cm^2 ×
120 nm) with a CCD spectrometer system (consisting of a
121 Chromex 250IS spectrometer with 300 gr/mm grating
122 and a Princeton Instruments 1100 × 300 pixel CCD
123 camera, model TE/CCD-1100-PE). The input optics
124 on the spectrometer system were duplicates of the
125 Fig. 1 system. For these measurements, the operating
126 voltage for the lamp was fixed at 5.76 V. The wave-
127 length range of the CCD camera/spectrometer system
128 was calibrated with a standard mercury penray lamp
129 and a standard neon lamp. The spectral radiance of the
130 lamp under these conditions was calibrated against a
131 OL series 455 integrating sphere calibration standard
132 lamp (Optronic Laboratories, Inc.) operated under
133 standard conditions.
134   The two Si photodiode active detectors were type
135 BPW21 with a sensitive area of 2.7 mm × 2.7 mm,
136 spectral range 320–820 nm and radiant sensitivity at
137 the peak wavelength (550 nm) of 3.8 V/mW. The
138 relative signal intensity (detector response) versus
139 wavelength was estimated from a Linos Photonics
140 data sheet with values measured at 25 °C and 12 V dc
141 supply voltage.
142   The filter band pass set, used to isolate the spectral
143 region between 400 and 650 nm, consisted of two
144 3 mm thick Schott glass filters (Duryea, PA) BG-39
145 and GG400.
146   The binary dye mixtures used for initial testing of
147 our MOC filter design were prepared from two water-
148 soluble dyes obtained from Aldrich, Bismarck Brown
149 Y (BB) (maximum 457 nm, dye content 50%) and
150 Crystal Violet (CV) (maximum 590 nm, ACS reagent
151 dye content 95%). Stock solutions in distilled water of
152 BB at 6.72E−5 M and CV at 1.64E−5 M were pre-
153 pared. Then random numbers were generated and
154 applied to the concentrations of the dyes with dilution
155 to determine that the relative concentrations of the two
156 dyes were varied independently. In the dilution pro-
157 cess transmission values were kept between 10 and
158 90% in the mixtures. In this manner 40 binary dye
159 solutions were prepared and their transmittance spec-
160 tra were measured. After the samples were made and

161 measured, PCA was performed to show that the data
162 were linear with respect to component concentration.
163 Twenty-five of these spectra were used to generate a
164 regression vector and 15 were kept as a test set.
165   TFCalc^{TM}, a commercial software product from
166 Software Spectra, Inc. (Portland, OR) was used to
167 synthesize multilayer thin film designs to match a
168 spectral target. An in-house thin-film design program
169 written in the MATLAB programming environment
170 was used to design "relaxed" multilayer structures for
171 chemical prediction.

3. Results and discussion   172

173   Fig. 1 shows the experimental set-up for imple-
174 menting the single-filter design in a simple transmis-
175 sion measurement. In this system, a spatial filter and
176 collimating lens is used to restrict the angular disper-
177 sion of light reaching a single filter. A single optical
178 element is used in a beamsplitter arrangement, with
179 part of the light passing through the sample being
180 reflected and part being transmitted. A similar con-
181 figuration was reported by Ryabenko [5]. The spec-
182 trum of the 45° optical element is designed to be
183 precisely $T(\lambda) = 0.5 \pm L(\lambda)$, where T is the filter
184 transmittance and L is proportional to the loading
185 of a spectral vector obtained via principal components
186 regression of a chemical system, or some related
187 mathematical procedure. In the event that the absor-
188 bance of the optical element can be neglected (a
189 reasonable assumption for most oxide materials in
190 the visible and short-wavelength near-infrared), the
191 reflectance is adequately represented by $R(\lambda) =$
192 $0.5 \pm L(\lambda)$. The difference between these values is
193 proportional to the spectral regression vector, while
194 the sum of the two is independent of the spectral
195 vector. In the original report [2], normalization of the
196 signal was not possible exactly. The independence of
197 $(T(\lambda) + R(\lambda))$ with respect to an arbitrary spectral
198 vector allows true signal normalization to be per-
199 formed.

3.1. Radiometric corrections   200

201   The optical computation of chemometric predic-
202 tions is inherently radiometric in nature rather than
203 ratiometric. Absorbance is non-linearly related to the

204   intensity of light passing through a sample and is
205   difficult to represent exactly. Sample transmittance
206   is directly related to radiometric quantities in our
207   measurement scheme. Unfortunately, while Beer's
208   law relates absorbance linearly to concentration, sam-
209   ple transmittance is not as simply related. In conse-
210   quence, the number of principal components required
211   to describe a radiometric data set is greater than the
212   number of independent species [6].

213   Fig. 2 shows the absorption spectra for two dyes,
214   Bismarck Brown and Crystal Violet, in the region
215   between 400 and 600 nm. Fig. 3 shows transmission
216   spectra for a series of 40 mixtures of these dyes,
217   mixtures in which the concentrations of the two dyes
218   are varied independently of one another based upon a
219   random number generation. Bismarck Brown was
220   arbitrarily selected as the analyte, while Crystal Violet
221   was treated as a random interferent. These 40 mixtures
222   provide a starting point for development of a suitable
223   regression vector for Bismarck Brown that could be
224   incorporated into a single-element multivariate optical
225   element (MOE).

226   Before calculation of a regression vector, the trans-
227   mission spectra are converted into system units by
228   measuring the spectral radiance of the light source to
229   be used for illumination of the sample, the transmit-
230   tance of a spectral bandpass filter set, and the spectral
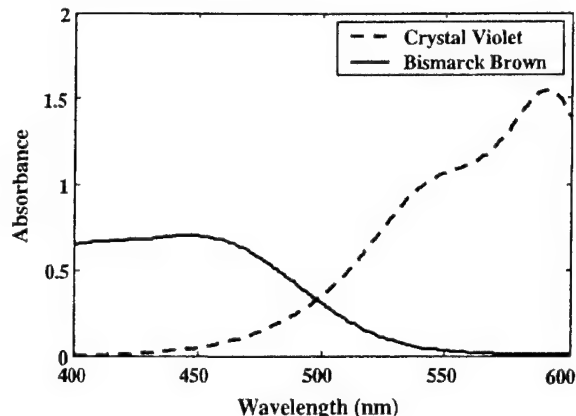
Fig. 2. Absorption spectra for solutions of two pure dyes Bismarck Brown and Crystal Violet, used in this report.

sensitivity of the detector selected for the measure-   231
ment. The product of these factors with the sample   232
transmittance spectra gives the system-corrected spec- 233
tra shown in Fig. 4.   234

3.2. A direct principal components regression approach

235
236

Principal component regression was used to derive   237
a linear relationship between the concentration of   238
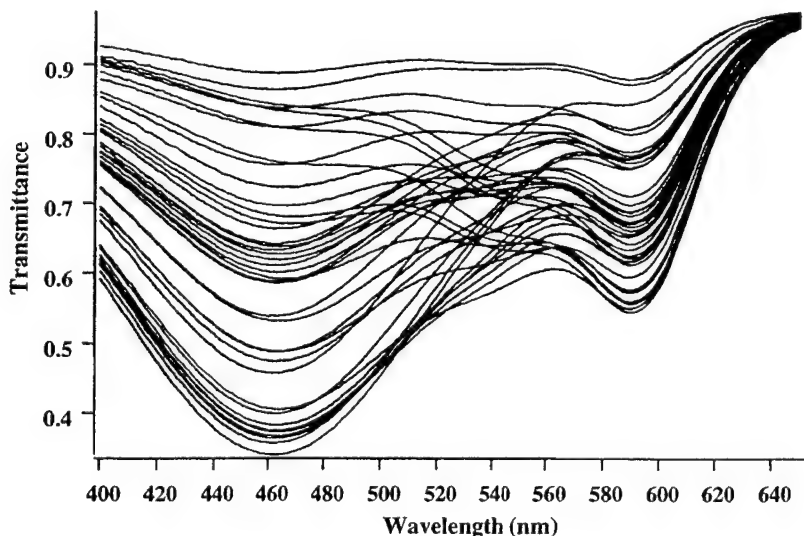
Fig. 3. Transmission spectra for 40 mixtures of Bismarck Brown and Crystal Violet using random concentrations of both dyes. The maximum concentration of each was limited so that absorbances of the two dyes individually would not be more than 0.3.
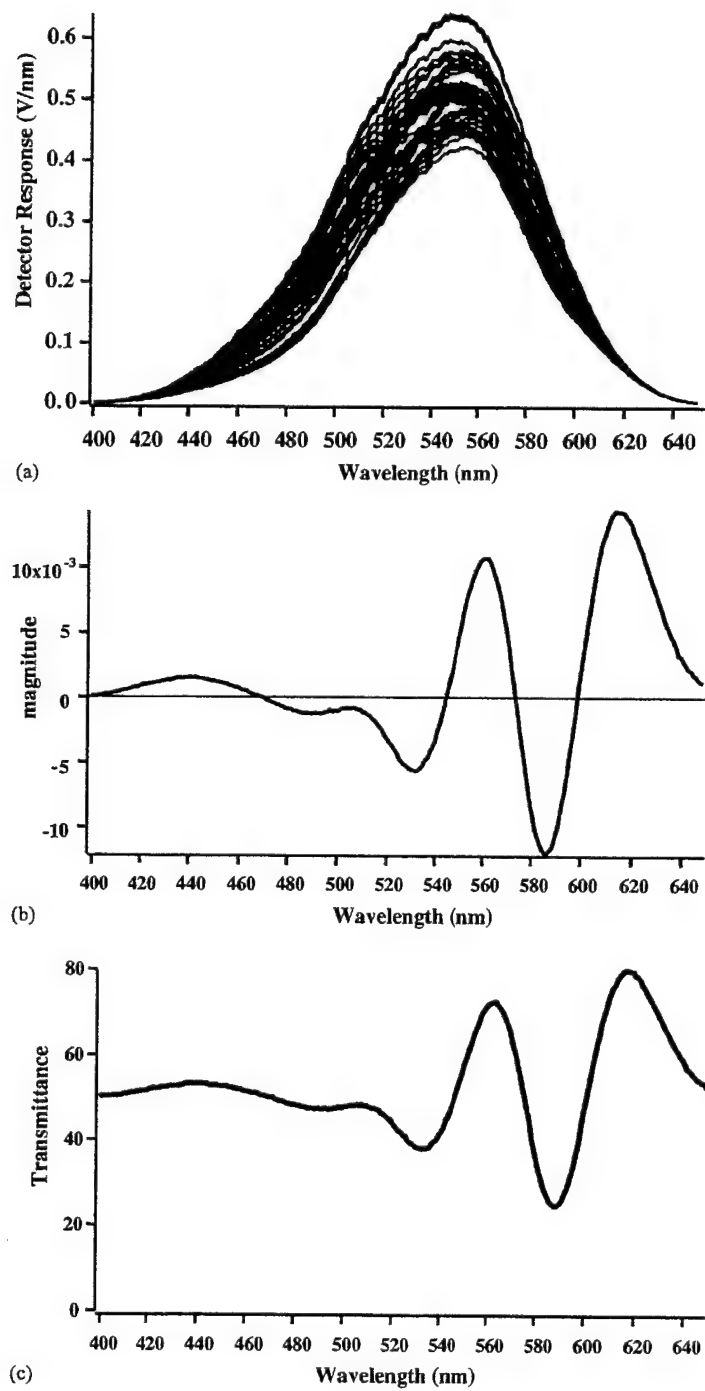
Fig. 4. Sample spectra used for analysis and target spectra derived from them: (a) sample spectra. These data are based on the transmission spectra in Fig. 3, corrected for the instrument response function, taking into account the spectral radiance of the tungsten light source, the spectral sensitivity of the silicon detectors, and the transmission spectra of the bandpass filter set described in the experimental section. (b) Regression vector for the calibration shown in part a. The vector has been scaled to unit length. (c) Target transmission spectrum for a single-element, 45° angle-of-incidence MOE coating based on the regression vector in (b).
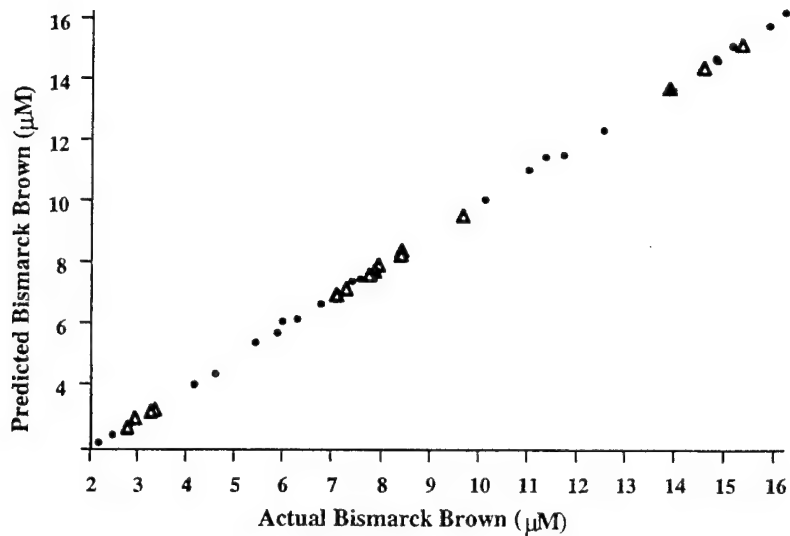
Fig. 5. Calibration based on Fig. 4 data. Filled Circles, Calibration set; Open Triangles, Validation set. SEP = 0.3 µM for the validation set.

239 Bismarck Brown and the coordinates of the sample
240 spectra on each of four principal component axes. The
241 results of this four-factor PCR of the data in Fig. 4 is
242 shown in Fig. 5. In this figure, triangles represent
243 validation samples, while black dots represent cali-
244 bration samples. The standard error of prediction
245 (SEP) for this calibration is 0.3 µM. The regression
246 vector that produces this calibration is shown in Fig. 6,
247 normalized to unit length. This vector can be used to

248 design a MOE by appropriate scaling as in Fig. 7,
249 which shows a target transmission spectrum for an
250 MOE based on the Fig. 6 vector. As this figure shows,
251 all the points at which the vector has a magnitude of
252 zero correspond to transmittances of 50%. The scaling
253 of the vector into the MOE is somewhat arbitrary,
254 limited only by a need to end with realistic transmit-
255 tance values. For example, too large a scaling factor
256 from Fig. 6 to Fig. 7 would result in target transmit-
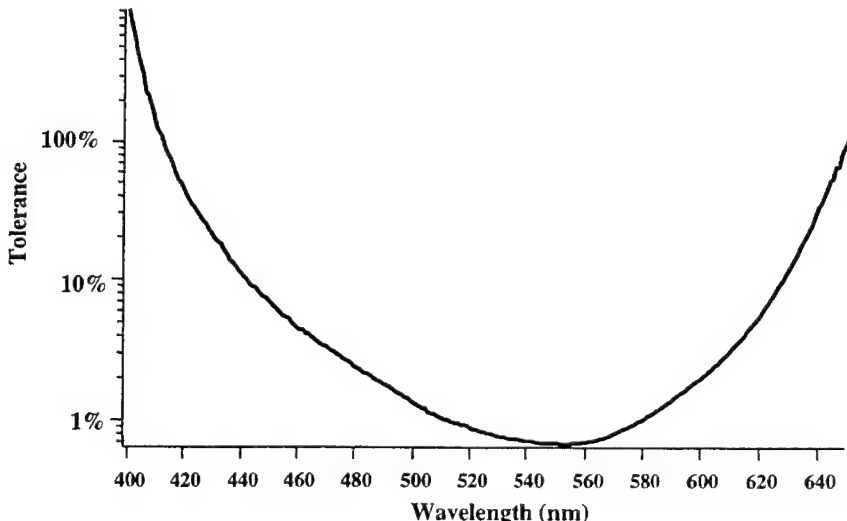
Fig. 6. Spectral tolerances for the design and fabrication of an MOE for this data set and calibration. Values are inversely proportional to the spectral variances, and directly proportional to the SEP.
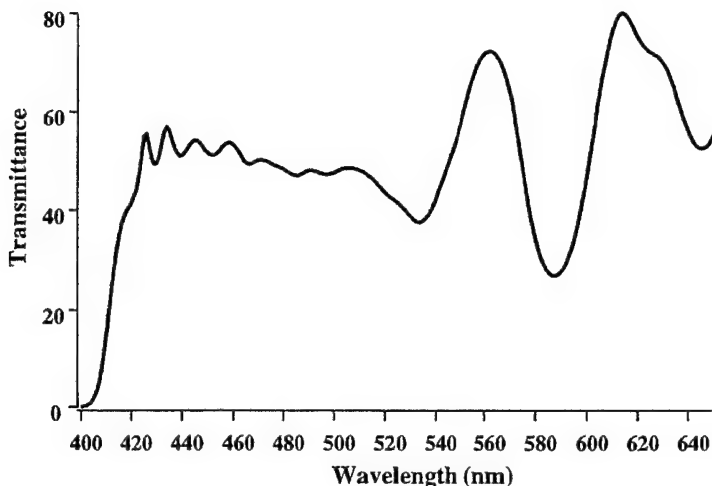
Fig. 7. Direct synthesis solution using the tolerances in Fig. 8 and the target spectrum in Fig. 7.

tances above 100% or below 0%. The practical limits are about 96 and 0%, since each MOE has two interfaces (one with the MOE coating and one without), and the uncoated interface will reduce the total transmitted light intensity.

As a general rule, it is impossible to exactly reproduce the target spectrum. How closely the design much match the target is determined by the SEP of the calibration. A small SEP corresponds to very small tolerance for deviations from the target. Large SEPs correspond to larger tolerances. Fig. 8 shows the tolerance distribution for this data set and calibration.

Derivation of the quantitative relationship between SEP, spectral variance and tolerance is described elsewhere [7]. The general trend is that tolerances are inversely related to spectral variance in the data set, increasing to large values at the edges of the spectral bandpass where intensity (and therefore variance) decreases toward zero. The tolerance calculation provides a means of defining the "effective bandpass". The effective bandpass can be defined as the wavelength window within which manipulation of the light intensities can introduce relative error equal to or greater than the standard error of prediction for our
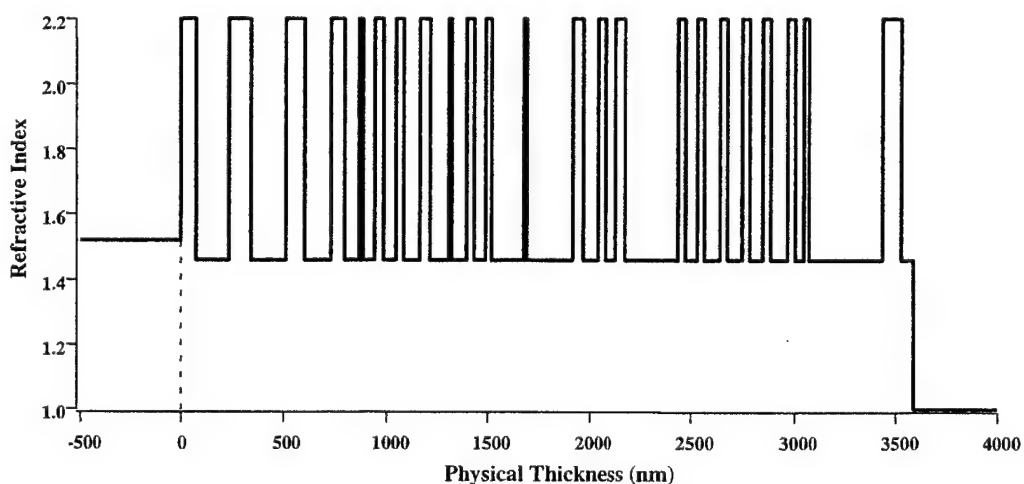
Fig. 8. Refractive index profile of the MOE design in Fig. 7.

ARTICLE IN PRESS

8

M.L. Myrick et al./Vibrational Spectroscopy 857 (2002) 1–9
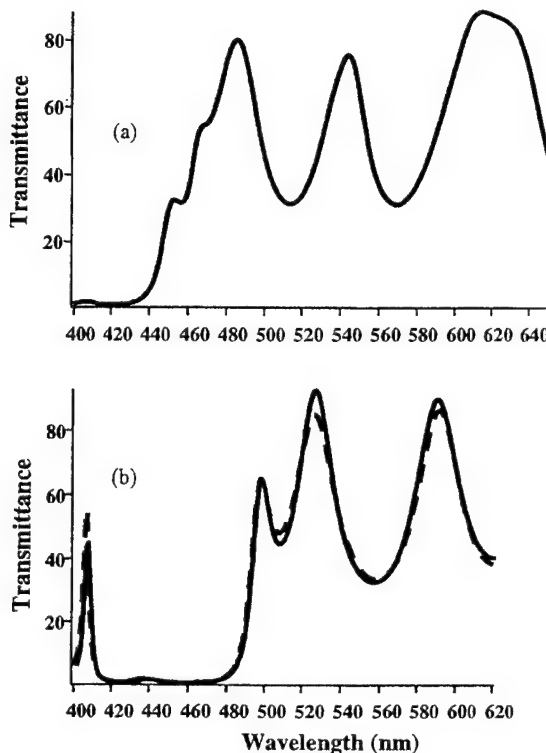
Fig. 9. (a) MOE spectrum at 45° angle-of-incidence based on vector relaxation from a partial direct solution as described in the text. This solution can be construed as the best solution at this level of complexity in the MOE. (b) MOE in (a) at normal incidence. Dashed line, theoretical; Solid line, experimental.

281 data model. Conversely, outside the effective band-
282 pass, the variability of the signal from sample to
283 sample is too small to matter within the range of
284 the SEP. In our example the effective bandpass for
285 the Fig. 4 data is between 423 and 624 nm, since in the
286 regions 400–423 and 624–650 there is negligible
287 variability among sample spectra in relation to the
288 concentration of Bismarck Brown.
289 Using these tolerances, a suitable design for a MOE
290 can be developed as shown in Fig. 9a, which gives the
291 spectrum at 45° angle-of-incidence of the resulting
292 MOE structure. The structure of this MOE is shown in
293 Fig. 10 as a plot of refractive index versus physical
294 thickness, assuming layer materials of SiO_2 and
295 Nb_2O_5 with refractive indices determined by ellipso-
296 metry in our laboratory. This design required approxi-
297 mately 24 h of computer iteration using the
298 commercial software TFCalc^{TM}. Qualitatively, a close

299 solution to the target was obtained quickly, with
300 approximately >90% of the iterations used to gain
301 the last few percentage points of spectral fit to the
302 target. Further, the solution shown in Fig. 10 includes
303 46 layers of material with a thickness near 4 μm. In
304 our deposition system, this would require about two
305 full days of deposition to achieve.

3.3. A second approach to MOE design: vector 306
relaxation 307

308 Because of the complexity of the direct spectral
309 matching result given above, a new software approach
310 to designing MOEs was developed. In this approach,
311 commercial thin-film design programs like TFCalc^{TM}
312 are used to give a very approximate solution in a short
313 time, using a relatively small number of layers. This
314 result is then used as a starting point for an in-house
315 algorithm that iterates this structure to find a result that
316 can be characterized as "the best solution at this level
317 of complexity". The in-house algorithm is described
318 separately [8], but uses the original data (Fig. 4) to
319 optimize the structure of the MOE coating in a way
320 that minimizes the SEP. Fig. 9a shows the "vector
321 relaxed" result for comparison to Fig. 7. Although the
322 "relaxed" result is very different from the target based
323 on the regression analysis that is given in Fig. 5, Fig. 10
324 shows that the SEP produced by this vector is equally
325 good, 0.3 μM. This relaxed design has the benefit of
326 requiring only 26 layers versus 46 in the direct design,
327 having a total thickness near 2 μm versus 4 μm for the
328 direct design, and requiring significantly less compu-
329 tation time.

3.4. MOE production 330

331 The MOEs designed in this report are all specified
332 to work at 45° angle-of-incidence. Our coating sys-
333 tem, however, operates best when coating substrates at
334 normal incidence. For production purposes, we took
335 the second (smaller, relaxed) structure for the Fig. 9a
336 MOE and recalculated its optical spectrum at normal
337 incidence. A multilayer coating was fabricated to this
338 target, and both the target and experimental result are
339 shown in Fig. 9b.
340 Results from testing of this MOE have been
341 reported elsewhere [9]. Implementation of this type
342 of all-optical approach to multivariate spectroscopy

100

9
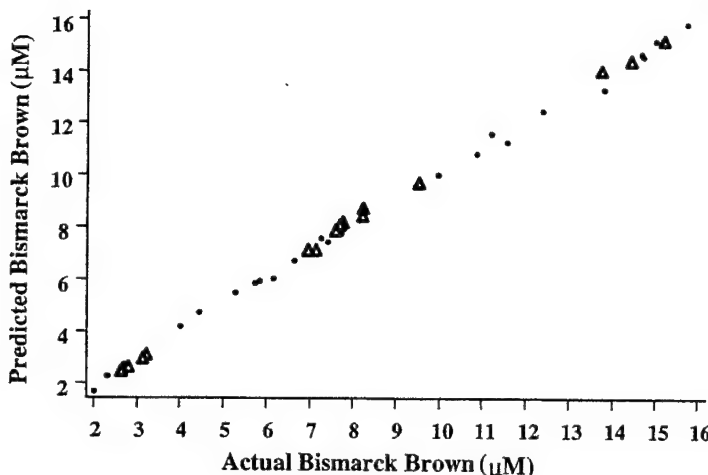
Fig. 10. Concentration of Bismarck Brown predicted with the MOE of Fig. 9 as a function of actual Bismarck Brown concentration. SEP = 0.3 μM.

has many advantages over conventional computational methods, including ease of use and higher S/N ratios. Use of this approach allows the user to determine the concentration of a component of interest without the use of conventional digital signal processing or acquisition of a spectrum. In addition, the need for only one optical element instead of two provides for less difficult and time consuming fabrication of the MOE as well as a simpler apparatus configuration.

References

[1] J.A. Dobrowolski, P.G. Verly, J.F. Aust, M.P. Nelson, M.L. Myrick, in: Proceedings of the SPIE Annual Meeting on Optical Science and Engineering, San Diego, CA, July 1997, p. 232.
[2] M.P. Nelson, J.F. Aust, J.A. Dobrowolski, P.G. Verly, M.L. Myrick, Anal. Chem. 70 (1998) 73.
[3] S. Bialkowski, Anal. Chem. 58 (1986) 2561.
[4] J.A. Dobrowolski, D. Lowe, Appl. Optics 17 (1978) 3039.
[5] A. Ryabenko, V. Kasparov, Pattern Recogn. Image Anal. 1 (1991) 347–354.
[6] E.R. Malinowski, Factor Analysis in Chemistry, 2nd edition, Wiley, New York, 1991.
[7] M.L. Myrick, S. Soyemi, H. Li, L. Zhang, D. Eastwood, Fres. J. Anal. Chem., 2000, in press.
[8] S. Soyemi, H. Li, L. Zhang, D. Eastwood, P. Gemperline, M.L. Myrick, 2000, in preparation.

10.9 A Nonlinear Optimization Algorithm for Multivariate Optical Element Design

A NONLINEAR OPTIMIZATION ALGORITHM FOR MULTIVARIATE OPTICAL ELEMENT DESIGN

Olusola O. Soyemi[a], Paul J. Gemperline[b], Lixia Zhang[a], DeLyle Eastwood[a], Hong Li[a], Michael L. Myrick[a*]

[a]Dept. of Chemistry and Biochemistry, University of South Carolina, Columbia SC 29208
[b]Dept. of Chemistry, East Carolina University, Greenville, NC 27858

ABSTRACT

A new algorithm for the design of optical computing filters for chemical analysis otherwise known as Multivariate Optical Elements (MOEs), is described. The approach is based on the nonlinear optimization of the MOE layer thicknesses to minimize the standard error in sample prediction for the chemical species of interest using a modified version of the Gauss-Newton nonlinear optimization algorithm. The design algorithm can either be initialized by random layer thicknesses or with layer thicknesses that approximate a multivariate principal component regression (PCR) vector for the constituent of interest. The algorithm has been successfully tested by using it to design various MOEs for the determination of Bismarck Brown dye in a binary mixture of Crystal Violet and Bismarck Brown.

Keywords: optical computing, thin films, chemometrics, spectroscopy, multivariate

1. INTRODUCTION

Multivariate calibration is a well-established tool in chemometrics for the correlation of a physical or chemical property of interest to multiple wavelength channels of optical spectra. (1-3) The conventional application of this tool in chemical analysis entails the acquisition of optical spectra in the appropriate wavelength region (typically from the ultraviolet to the mid-infrared). Next, chemometric tools such as principal component regression (PCR) and partial least-squares (PLS) are used to estimate multivariate regression vectors correlated to the property of interest but orthogonal to interferences (4). Prediction of the property in an unknown sample is carried out by taking the inner product of the spectral pattern in the regression vector with the optical spectrum of the unknown compound. A major drawback in the widespread use of multivariate calibration, especially for field applications, is its dependence on expensive and bulky laboratory-type equipment for data acquisition and analysis.

In Multivariate Optical Computing (MOC), spectral patterns are encoded into the transmission spectrum of optical interference filters for the purpose of chemical prediction. Earlier reports by Myrick et al. (5,6), have shown that the prediction step in multivariate calibration can be optically mimicked by passing light of a fixed bandwidth which has interacted with the sample through two optical filters whose combined transmission profiles accurately describes the

---

positive and negative portions of the spectral patterns in a multivariate regression vector. A more recent study (7) has described a new approach to this method of optical computation that uses a single filter for prediction.

A typical interference filter consists of alternating layers of high- and low-refractive index materials with specified thicknesses. Interference coatings with irregular transmittance profiles are fabrication through the process of reactive magnetron sputtering (RMS) (8). As was originally envisaged, the profile of a pre-determined spectral pattern is transferred to the optical coating by a process of iterative synthesis (9). The original filter design technique synthesized a multilayer coating that minimized the sum of squared difference between the desired spectral pattern (e.g., a multivariate regression vector) and the filter's computed spectral pattern. A generic form of the merit function is shown in equation 1, where Z_j^D is the calculated response (e.g. filter transmittance) at wavelength j, Z_j is the target value, Tol_j is the design tolerance, m is the number of discretely sampled wavelengths, and k is a gain factor used to change the relative importance of the mismatched regions (with integer values of 1,2,4 or 16).

$$F = \left(\frac{1}{m} \sum_{j=1}^{m} \frac{\left| Z_j^D - Z_j \right|^k}{Tol_j} \right)^{1/k} \qquad (1)$$

This approach has been used by Heavens and Liddell (10) to create a filter design algorithm that minimizes the following function,

$$F(x) = \sum_{k=1}^{m} \left(R_O(\lambda_k) - R(x, \lambda_k) \right)^2 \qquad (2)$$

where x is the vector of design variables, R_o is the specified reflectance at wavelength λ_k, and R is the computed value of reflectance at λ_k for particular values of x. For multivariate calibration problems, this approach causes problems, however, because complex spectral patterns encoded in regression vectors necessitate filters of high complexity with many layers. Multilayer filters having an excessive thickness tend to have rough surfaces that scatter incident radiation, absorb significant amounts of incident light, and break easily due to increased internal stress.

As a way of overcoming this limitation in filter design, we present the description of two alternative design algorithms that can result in filters having substantially fewer layers. This avoids the problems described above, while in many cases, offers better predictive performance than filters designed to match PCR or PLS regression vectors. Both new methods employ a nonlinear least squares optimization technique to design an optical coating that minimizes the sample prediction error for the chemical species of interest. In other words, instead of creating an optical coating whose spectrum matches a predetermined regression vector, a coating is created whose spectral profile strives to minimize the value of the root mean standard error of calibration, *RMSEC*.

104

2. DESCRIPTION OF FILTER DESIGN ALGORITHM

2.1. Calculation of filter transmittance

A fast and efficient method for calculating filter transmittance is crucial to developing an algorithm for designing optical filters. The matrix method for calculating the transmittance and reflectance of multilayer optical thin films meets these criteria (11), and was incorporated into the design algorithm. This method is easily implemented on a digital computer and has become the mainstay of most filter design algorithms. In this method, each layer of a thin film stack is represented by a 2x2 characteristic matrix (Equation.3), which describes the layer properties at particular wavelengths of incident light and at specified angles of incidence. These properties include layer thickness, refractive index and the absorption coefficient.

$$\mathbf{Y}_l = \begin{matrix} Y_{1,1} + iY_{1,1} & Y_{1,2} + iY_{1,2} \\ Y_{2,1} + iY_{2,1} & Y_{2,2} + iY_{2,2} \end{matrix} = \begin{matrix} \cos\delta & i/\eta\sin\delta \\ i\eta\sin\delta & \cos\delta \end{matrix} \tag{3}$$

$\mathbf{Y}_l$ is the characteristic matrix for the lth layer, η is the complex refractive index $(= n_l{+}ik_l)$, where n_l is the real refractive index and k_l is the absorption coefficient. The phase factor, δ, is given by equation 4,

$$\delta = \frac{2\pi n_l k_l x}{\lambda}\cos\theta_l \tag{4}$$

where λ is the wavelength, x is the layer thickness, and θ_l is the interior angle of propagation in medium l. For normally incident light, $\cos\theta_l = 1$. However, for tilted filters in which the incident angle is oblique,

$$\cos\theta_l = \sqrt{1 - \frac{n_0^2 \sin^2\theta_0}{n_l^2}} \tag{5}$$

where n_0 is the refractive index of the incident medium (air), and θ_0 is the angle of incidence in radians. The characteristic matrix of the entire film stack (**M**) is determined by multiplying the matrices of individually layers, i.e.;

$$\mathbf{M} = \mathbf{Y}_{layer1} \times \mathbf{Y}_{layer2} \times \cdots \times \mathbf{Y}_{layerl} \tag{6}$$

Layer 1 is the layer that is closest to the substrate. Light transmitted through the film layers consists of an electric vector component, $\bar{E}$, and a magnetic vector component, $\vec{H}$. The characteristic matrix relates the electric and magnetic fields at individual layer boundaries in the following manner:

$$\begin{bmatrix} \bar{E} \\ \bar{H} \end{bmatrix} = \mathbf{M} \times \begin{bmatrix} 1 \\ n_S + ik_S \end{bmatrix} \tag{7}$$

where n_s and k_s are the refractive index and absorption coefficient of the substrate respectively. The propagation of light through a single thin film coating is illustrated in Figure 1. As is shown in the diagram, there are multiple reflections of the incident light at the air/film and substrate/air interfaces. The transmittance and reflectance at the air/film interface, is given by equations 8 and 9.

$$\bar{T}_1 = \frac{4 n_s n}{(n + n_s)^2} \tag{8}$$

$$\bar{R}_1 = 1 - \bar{T}_1 \tag{9}$$

For normally incident light, $n = n_0 = 1$, where n is the refractive index; however. when the filter is tilted, the propagated wave is split into two plane-polarized components, one with the electric vector in the plane of incidence, known as p-polarized, and one with the electric vector normal to the plane of incidence, known as s-polarized. The refractive index of the incident light is therefore modified as follows:

$$n = \frac{n_o}{\cos\theta_o} \text{(p-polarization)} \tag{10}$$

$$n = n_o \cos\theta_o \text{ (s-polarization)} \tag{11}$$

$\bar{T}_2$ and $\bar{R}_2$ are related to the real and imaginary components of $\bar{E}$ and $\bar{H}$ (i.e. $\bar{E}_1$, $\bar{E}_2$ and $\bar{H}_1$, $\bar{H}_2$ respectively) determined from equation 7.

$$\bar{T}_2 = \frac{4 n_s n}{(\bar{E}_1 + \bar{H}_1)^2 + (\bar{E}_2 + \bar{H}_2)^2} \tag{12}$$

$$\bar{R}_2 = \frac{(\bar{E}_1 - \bar{H}_1)^2 + (\bar{E}_2 - \bar{H}_2)^2}{(\bar{E}_1 + \bar{H}_1)^2 + (\bar{E}_2 + \bar{H}_2)^2} \tag{13}$$

The total transmittance through the film and substrate can be determined by summing up the infinite series of the combined reflectance and transmittance terms (see Figure 1) i.e.. $\bar{T}_1 \bar{T}_2$, $\bar{T}_1 \bar{T}_2 \bar{R}_1 \bar{R}_2$, $\bar{T}_1 \bar{T}_2 (\bar{R}_1 \bar{R}_2)^2$, $\bar{T}_1 \bar{T}_2 (\bar{R}_1 \bar{R}_2)^3$, etc, which results in the following expression:

$$T(\lambda, x, \eta_l, \eta_s, \theta_o) = \frac{\bar{T}_1 \bar{T}_2}{1 - \bar{R}_1 \bar{R}_2} * 100 \qquad (14)$$

where η_l and η_s are the complex refractive indices of layer l, and the substrate, s, respectively. For tilted filters, the average transmittance due to the p- and s-polarized components of the incident light is determined.

2.2. Titled filter application for optical prediction

In the optical computing approach to predicting sample properties or composition, a radiation source, filter, and detector is used to replace the traditional multiwavelength absorption or emission spectrometer. The combined spectral response of the filter instrument matches the spectral pattern of the desired shape of a multivariate regression factor from a PCR or PLS calibration. The signal produced at the detector is a product of the intensity of the incident beam as a function of wavelength, $\bar{I}$, the transmission spectrum of the filter, $\bar{T}$, and the sensitivity of the detector, $\bar{Q}$, as a function of wavelength. By directing the multiwavelength light through the sample and then onto a single detector, a summation operation is effectively performed, giving a detector response proportional to the summed intensity of detected photons. One complication with this approach lies in the fact that multivariate regression vectors have negative and positive lobes, whereas, optical transmission spectra are nonnegative. In earlier reports, a solution to this problem was proposed by fabricating two filters, one representing the positive lobes of the multivariate regression vector, and the other representing the negative lobes of the multivariate regression vector **(5, 6)**. The light from the two filters was then directed to two separate detectors. The resulting two signals were then subtracted by means of a simple difference amplifier circuit.

With the new filter optimization procedure described below, it is possible to envision an alternative instrument configuration that utilizes a single tilted filter instead of two discrete filters, thereby reducing the complexity and cost of the device (see Figure 2). By using a filter tilted at an angle 45° to the plane of the incident beam, the incident beam is split into a reflected beam, $\bar{R}$, and a transmitted beam, $\bar{T}$, that are then directed to two different detectors. Assuming no light is absorbed by the filter, the transmitted radiation and reflected radiation from a filter tilted at 45° are related to one another by equation 15,

$$\bar{R} = 1 - \bar{T} \qquad (15)$$

A difference amplifier is then used to subtract the two signals, thereby achieving an output given by equation 16:

$$V_O = G \times \bar{I} \times \bar{T} \times \bar{Q} \bullet \bar{S} - G \times \bar{I} \times \bar{R} \times \bar{Q} \bullet \bar{S} \qquad (16)$$

where V_o is output voltage, G are amplifier gain constants, and $\bar{S}$ is the sample spectrum vector. Substituting equation 15 into equation 16 and simplifying gives the overall instrument response function:

$$V_{out} = G \times \bar{I} \times \bar{Q} \times \left[2\bar{T} - 1\right] \bullet \bar{S} + V_{offset} = G \times \bar{L} \bullet \bar{S} + V_{offset} \qquad (17)$$

where $\bar{L}$ represents the spectral pattern produced by the tilted filter instrument.

2.3 Nonlinear Optimization of Filter Layers

The optimization of filter parameters is carried out in a manner that minimizes the root mean standard error of calibration ($RMSEC$) using a simulated filter transmission spectrum, $\bar{T}$, at m discrete wavelength channels. In order to design the thickness of layers of a MOC filter on a digital computer, the tilted filter response function described in equation 17 is simulated. Using a set of digitized calibration spectra representative of real samples, the vector of concentration values, y_i, of the calibration samples is predicted according to equation 18.

$$\hat{y}_i = V_{out} = G \times \bar{L} \bullet \bar{S}_i + V_{offset} \qquad (18)$$

From the estimated concentration values of the calibration set, $\hat{y}_i$, $RMSEC$ is calculated according to equation 19.

$$RMSEC = \sqrt{\frac{\sum_{i=1}^{n}(y_i - \hat{y}_i)^2}{m}} \qquad (19)$$

The objective function optimized is simply the root mean squared error of calibration. The amplifier gain, offset, and thicknesses of the $N\text{-}2$ layers of the filter are the parameters adjusted during the optimization process. The minimum $RMSEC$ of the optical filter approach can be visualized as a search on a complex N-dimensional response surface. The filter design algorithm created for this purpose is based on the quasi-Newton method of nonlinear optimization (12,13).

Two variants of the filter optimization program were developed, differing from each other only in how the optimization starting point is initialized. In the both approaches, the filter design algorithm is initialized by specifying the number of layers, $N\text{-}2$, with predetermined thicknesses, z_i, representing a single point on the response surface. At each iteration of the optimization process, curvature (gradient) information is built up to formulate a quadratic model problem of the form,

$$\min_{x} \frac{1}{2} z^T H z + c^T z + b \qquad (20)$$

where $\mathbf{z}$ is the vector of N optimization parameters, the Hessian matrix, $\mathbf{H}$, is a positive definite symmetric matrix (crucial in maintaining a constant descent down the slope of the search surface), $\mathbf{c}$ is a constant vector, and b is a constant. The optimization converges to a solution corresponding to the lowest value of the *RMSEC* when the partial derivatives of $\mathbf{z}$ go to zero. i.e.,

$$\nabla f(\mathbf{z}^*) = \mathbf{H}\mathbf{z}^* + \mathbf{c} = 0 \tag{21}$$

The optimal solution point, $\mathbf{z}^*$, can be written as

$$\mathbf{z}^* = -\mathbf{H}^{-1}\mathbf{c} \tag{22}$$

At the starting point, $\mathbf{H}$ can be set up to any positive definite matrix (e.g. the identity matrix, $\mathbf{I}$). The observed behavior of $f(\mathbf{z})$ and $\nabla f(\mathbf{z})$ is then used to build up curvature information to make an approximation of $\mathbf{H}$ using the updating formula developed by Broyden (**14**), Fletcher (**15**), Goldfarb (**16**), and Shanno (**17**), also known as the BFGS formula. The formula is given by

$$\mathbf{H}_{k+1} = \mathbf{H}_k + \frac{\mathbf{q}_k \mathbf{q}_k^T}{\mathbf{q}_k^T \mathbf{s}_k} - \frac{\mathbf{H}_k^T \mathbf{s}_k^T \mathbf{s}_k \mathbf{H}_k}{\mathbf{s}_k^T \mathbf{H}_k \mathbf{s}_k} \tag{23}$$

where

$$\mathbf{s}_k = \mathbf{z}_{k+1} - \mathbf{z}_k$$
$$\mathbf{q}_k = \nabla f(\mathbf{z}_{k+1}) - \nabla f(\mathbf{z}_k)$$

The gradient information is provided by perturbing each of the design variables (i.e. layer thicknesses) in turn and calculating the rate of change in the *RMSEC*. At each major iteration k, a line search is determined in a direction in which the solution is estimated to lie, and is determined by

$$\mathbf{d} = -\mathbf{H}_k^{-1} \cdot f(\mathbf{z}_k) \tag{24}$$

During optimization, layers thicknesses that fall below a specified threshold value (ca. 0.5 nm) are not acceptable, keeping in mind that extremely thin layers do not contribute appreciably to the transmission curve of the filter and may not be conveniently deposited during the fabrication process. Therefore, in the event that a layer falls below this threshold value during optimization, the optimization processes is stopped, the offending layer is deleted, and the optimization re-started at the previous design point with one fewer layers. Other flags are activated to re-start the process whenever the optimization is stalled or the number of maximum iterations is reached.

The starting point of the optimization routine is important since it can have a significant bearing on the final results. The descent towards an optimal value of *RMSEC* proceeds on the response surface through several possible pathways, depending on the starting point and the search direction. The choice of an appropriate starting point usually entails a fairly quick descent to a local minimum on the response surface. There are currently two variants to the filter design algorithm, both of which are based on different modes of initialization. In the first approach, one initializes the optimization process with a specified number of layers having random thicknesses uniformly distributed in the range from 1 to 100 nm. For different random starts, the search

frequently proceeds to different local minima on the response surface, hence, different solutions. In this manner, many different solutions having useful predictive properties are found. In this approach, one typically starts with a large number of layers that will give a filter having a thickness near the upper practical limit. Since the algorithm automatically deletes layers that become negligibly thin during the optimization process, this approach is observed to produce filters having different numbers of layers, and thus regression vectors of differing levels of parsimony.

In the second method of filter initialization, the optimization process starts with a specified number of layers having random thicknesses as before. Using the tilted filter model, a filter is designed using equations 25 and 26 (**10**) to match the filter's combined transmission and reflectance spectrum to an N-factor principal component regression (PCR) vector at m digitized wavelengths,

$$\bar{R}_{PCR} \cong \bar{L} = \left[2\bar{T} - 1 \right] \tag{25}$$

$$F(x) = \sum_{i=1}^{m} (R_{i,PCR} - L_i)^2 \tag{26}$$

where $\bar{R}_{PCR}$ is the regression vector, $\bar{T}$ is the filter's transmission spectrum, and $\bar{L}$ is the filter's combined transmission and reflection spectrum described in equation 17. The results of the PCR optimization step (e.g., layer thicknesses) are used as the initial starting point in the optimization of *RMSEC*, as described previously.

3. EXPERIMENTAL

Simulated data

Simulated data was used during the development and testing of the filter design algorithms, since this provided ideal mixture spectra having precisely known characteristics. Two simulated pure component UV spectra were generated by summing scaled Gaussian bands to produce the pure component spectra shown in Figure 3. Mixture spectra were generated by adding components of the mixture together to construct a training set and validation set using a 3-level, 2-factor central composite experimental design shown in Table 1. Design points for the validation samples were selected at locations between calibration points in or exercise the calibration model's ability to interpolate. The resulting absorbance spectra were log transformed to produce transmission spectra. Scaled, normally distributed random numbers with a mean of zero and a standard deviation of 0.1%T were added to the resulting transmission spectra to simulate measurement noise. The resulting training and validation set of transmission spectra were used to develop the filter design algorithms.

Experimental data

A set of binary dye mixtures were prepared from two water soluble dyes obtained from Aldrich Chemical Company, Bismarck Brown (BB) (λ_{max}=457 nm, dye content 50 %) and Crystal Violet (CV) (λ_{max}=590 nm, ACS reagent dye content 95 %). Stock solutions in distilled water of BB at 8.23×10^{-5} M and CV at 3.77×10^{-5} M were prepared. Random numbers were generated and applied in diluting the stock solutions to ensure that the relative concentration of the two dyes were varied independently. The random numbers were also chosen to ensure that the transmittance spectra of the diluted mixtures were between 30 % and 70 %. In this manner, 40 binary dye solutions were prepared in which the concentrations of the two dyes varied independently. Bismarck Brown was selected as the analyte because the spectrum of CV overlapped it at all wavelengths. CV was treated as an uncorrelated interferent whose concentration varied randomly. The transmittance spectra (Figure 4) were acquired between 400 nm and 650 nm on a Hewlett-Packard UV-VIS diode array spectrometer (Model 8543). An instrument prototype for the implementation of multivariate optical computing using a single MOE, has already been described (7). The transmittance spectra were convolved with a bandpass filter transmission spectrum, the source lamp emission spectrum, and detector response function of the prototype field instrument to give an accurate representation of the detected response as a function of wavelength (Figure 5). The corrected spectra were used for MOE design and multivariate analysis. PCR and the MOE design algorithm were written in MATLAB (Mathworks Inc. Natick, MA).

4. RESULTS AND DISCUSSION

4.1 Estimation of figures of merit from PCR calibration

The conventional approach to the multivariate analysis of optical spectra requires the use of bilinear regression techniques for the correlation of the spectral wavelengths to concentration (or any other property of interest). In particular, PCR is routinely used to define a regression vector or pattern, which correlates the wavelength channels to the concentration of the species of interest, but is orthogonal to interferences (4). The initial step in PCR analysis involves reduction in the dimension by use of the truncated singular value decomposition (SVD) of an n x m matrix of calibration spectra, **X**, where n is the number of spectra, and m is the number of wavelength channels or variables ,

$$\mathbf{X} = \mathbf{U}_{n \times p} \mathbf{S}_{p \times p} \mathbf{V}_{p \times m}^{T} \tag{27}$$

and p is the number of singular values retained in the truncated SVD. The resulting p factor PCA model is used to estimate a regression vector, **r**, that can be used for prediction, where p, the number or principal components, is selected to give adequate prediction properties to the regression model.

$$\hat{\mathbf{r}}_{PCR} = \mathbf{V}_p \mathbf{S}_p^{-1} \mathbf{U}_p^{T} \mathbf{y} \tag{28}$$

$$\hat{\mathbf{y}} = \mathbf{x} \cdot \mathbf{r}^{T} \tag{29}$$

111

A PCR calibration model was constructed for the simulated optical transmittance spectra in order to provide a baseline level of calibration performance for comparison with the optical regression technique. Examination of *SEC* and *SEP* revealed 3 factors gave an adequate calibration model (see Figure 6) (*SEC* = 0.0163, *SEP* = 0.0096). This error level corresponds to 1.6% and 0.96% error relative to the mean of the calibration set. A slight amount of curvature can be observed in the calibration curve due to the fact that the calibration model was developed using transmission spectra, which is necessitated by the nature of the tilted filter instrument. Here, a linear 3 factor PCR model achieves an acceptable approximation to the non-linear calibration problem. Since the validation points cover a narrower working range than the calibration standards, *SEP* is slightly lower than *SEC*. For comparison, an ideal two-factor PCR model developed from absorbance spectra instead of transmission spectra can be used to establish an approximate lower error bounds of *SEC*=0.0019 and *SEP*=0.0021. The calibration developed using transmission spectra is slightly worse than the calibration model developed using absorption spectra, however, it still possess useful predictive properties.

A four factor PCR calibration model was constructed for the BB-CV training sets of optical transmittance spectra. A plot of the root mean squared error of cross validation vs. number of principal components (Figure 7) shows that four principal components are required for optimum predictive ability. The standard error of calibration (*SEC*) was 0.0907 µM, corresponding to 1.0% error relative to the mean of the calibration set. The four-factor model was validated with the test set of optical spectra, and the standard error of prediction (*SEP*) was estimated to be 0.2583 µM, or 2.8% relative to the mean of the calibration set. A slight amount of curvature was also observed in this calibration curve for the reasons stated above.

4.2 Estimation of the figures of merit for a conventional numerical filter design

In a previous report (**18**), a filter design was synthesized by using the needle optimization technique to match a target transmission spectrum that was arbitrarily scaled from the 4-factor regression vector for the BB-CV data set. Here, the spectral profile of the scaled regression vector is iteratively synthesized by minimizing the merit function, F (see Equation 1), which describes the difference between a calculated spectrum (based on the MOE layer thicknesses in each iteration), and a target spectrum (represented by the spectral profile of the scaled PCR vector). The regression vector was scaled according equation 30, where $\bar{T}$ is the target transmittance spectrum and $\bar{R}$ is the regression vector.

$$\bar{T}(\%) = 50 + 1.85\bar{R} \qquad (30)$$

It is virtually impossible to exactly reproduce the target spectrum over a wide wavelength range, since the distribution of design tolerances (see Equation 1) are not likely to prevent spectral mismatch across all the wavelength channels. At best, a range of tolerances have to be selected that would minimize the deviation from the target for a portion of the spectrum relative to others. It is however possible to define a wavelength range over which the transmittance function of the MOE must be defined. Outside this operational bandpass, all values of transmittance for the MOE are permissible because the variance of the signal strength is so small that it has a

negligible impact on prediction. Determination of the operational bandpass limits has already been examined in a discussion of spectral tolerance for MOE design in reference 7. For the binary dye system, the effective bandpass was determined to be between 423 nm and 624 nm. By solving for $\overline{R}$ in equation 30, the calibration and prediction error from the spectrum resulting from the filter design was determined to be 0.4471 μM and 0.4908 μM respectively.

Clearly, this approach to MOE synthesis degrades the calibration and prediction error of the designed filter. This development has necessitated a paradigm shift in terms of approaching the filter design problem. Instead of approaching the filter design in terms of matching the structure of a regression vector, a filter design that minimizes calibration error is even more desirable, considering that a further degradation in *SEC* is to be expected from likely manufacturing errors that would prevent the accurate deposition of filter layers as specified by a given design.

4.3 Minimization of calibration error with random initialization of filter design algorithm

In the first approach to designing optical computing filters, a filter design is initialized by a specified number of random filter coefficients (i.e. layers thicknesses). Using the simulated calibration spectra, an initial rapid convergence to the mean y-value of the calibration set was observed, followed thereafter by a slow descent to a local minimum value of the sum of squared calibration error. It was observed that different random starts using the same number of starting layers will result in different filter designs. This suggests that the descent towards an optimal value of the sum of squared calibration error proceeds on a complex N-dimensional response surface through several possible pathways, depending on the random starting point and best search direction. For different random starts, the search direction proceeded to different local minima on the response surface, hence the possibility of different solutions to the optimization problem.

Table 2 shows 10 of the best filter designs obtained by systematically designing filters having 1 to 31 initial layers of random thickness and 10 different trials per layer setting. Figure 8 shows the response curves of the 10 selected filters described in Table 2. The overall best filter had 15 layers and gave *SEC* = 0.0070 and *SEP* = 0.0079, corresponding to 0.7% and 0.8% error relative to the mean of the calibration set. It is interesting to note that the performance of this optical filter calibration is better than the best PCR regression vector when transmission spectra are considered, as necessitated by the tilted filter instrument design. While the optical filters designed by non-linear optimization produced calibration curves that were substantially better, they were not as good as the results obtained in the ideal case, e.g., a two-factor PCR calibration with absorbance spectra. As before, a slight amount of curvature can be observed in the calibration curve due to the fact that the calibration model was developed using transmission spectra, and since the validation points cover a narrower working range compared to the calibration standards, *SEP* is slightly lower than *SEC*.

A similar study was conducted for the BB-CV mixtures. Table 3 shows several random initializations for various filter designs based on the binary-dye data, along with the final filter parameters and the corresponding figures of merit (i.e. *SEC* and *SEP*). Figure 9 shows the

response curves of the various filter designs in Table 3. In this case the best overall filter gave better predictions than a 4-factor PCR regression.

4.4 Minimization of calibration error via initialization to PCR regression vector

As described previously, the second approach to designing MOE filters involves an initial step in which filter parameters with random initial values are optimized to give response vectors that fairly approximate a PCR regression vector. The optimized filter parameters obtained by matching the PCR vector are then used to initialize the filter design algorithm that searches for a minimum $RMSEC$. Typically, slow convergence to the shape of the PCR vector was observed, followed by a relatively fast "relaxation" to the final design vector. Table 4 shows 10 of the best filter designs obtained for the simulated data set by systematically designing filters having 1 to 31 initial layers of random thickness and 1 to 3 factors in the initial PCR regression. Figure 10a compares a fitted optical regression vector with the target PCR vector for a two factor PCR calibration model using 22 layers. As can be seen in this figure, the initial filter gives a good approximation to the shape of the PCR regression vector. Figure 10b shows the response curves of the 10 selected filters described in Table 4. As can be seen in Figure 10b, the final shape of the filter regression vectors have diverged significantly from the original PCR shape, such that they now match the general shape of the some of vectors shown in Figure 8. This suggests that the non-linear optimization strategy finds many different local minima that produce regression vectors having similar shapes. The overall best filter for this simulated data sets was initialized from a one factor PCR regression, had 22 layers, and gave $SEC = 0.0095$ and $SEP = 0.0083$, corresponding to 0.95% and 0.83% error relative to the mean of the calibration set. The performance of this optical filter calibration is better than the best PCR regression vector when transmission spectra are considered, however, the best filter performed slightly worse than the best filter obtained using the random initialization method. The main advantage of the PCR initialization approach for this data set was that less computational effort was required, so filters with useful predictive properties can be generated quickly during feasibility studies. As before, a slight amount of curvature can be observed in the calibration curve due to the fact that the calibration model was developed using transmission spectra, and since the validation points cover a narrower working range compared to the calibration standards, SEP is slightly lower than SEC.

For the BB-CV data set, the optimization algorithm was initialized with a 25-layer filter with each layer thickness at 100 nm. The spectral profile of this intermediate design was used to initialize the filter design algorithm that minimizes RMSEC, producing a final design with 19 layers whose spectrum is shown in Figure 11. Even though the calculated vectors turned out to be slightly different from each other, they are both relaxed to give identical final filter designs. This ensures that for a given number of starting random layers, the final design is always reproducible.

The two filter design approaches described above often produced designs that do not resemble the PCR regression vector as shown in Figures 9 and 11. The PCR regression vector can be visualized as a point in p-factor space that describes a linear relationship between the analyte and the measurement variables (i.e. spectral wavelengths), that is orthogonal to interferents. Whereas there is only one such direction for a p-factor PCR calibration model, there are several paths to

114

the various local minima on the multi-dimensional response surface depending on the starting point of the optimization. Because the attainment of a global least squares minimum is difficult under these conditions, there is therefore the possibility of obtaining several solutions to the optimization problem, as is evident from the results obtained.

5. CONCLUSION

A fairly straightforward algorithm for the design of filter elements used for optical computing has been described and successfully demonstrated. The algorithm is used to design MOE filters with the good predictive ability for a chemical species of interest. Unlike design methods that are dependent on matching a fixed profile, this new algorithm provides multiple pathways through which various MOE designs are obtained, all of which strive to achieve a low *SEC*. Because of this, the algorithm also provides a means by which a particular filter design can be modified continuously during the fabrication process to correct for errors generated from the manufacturing process without seriously compromising the predictive ability of the MOE. The means by which this is implemented is the subject of future work.

ACKNOWLEDGEMENTS

REFERENCES

1. J.F. Aust, K.S. Booksh, M.L. Myrick, "Novel In-Situ Probe for Monitoring Polymer Curing," *Appl.Spectrosc.* **50**, pp 382-387, 1996.
2. E.V. Thomas, and D.M. Haaland, "Comparison of Multivariate Calibration Methods for Quantitative Spectral Analysis," *Anal.Chem.* **62**, pp 1091-1099, 1990.
3. M.M.A. Ruyken, J.A. Visser, and A.K. Smilde, "Identification of Plastics among Non-plastics in Mixed Wastes by Remote Sensing Near-Infrared Spectroscopy. 2. Multivariate Rank Analysis for Rapid Classification," *Anal.Chem.* **67**, pp 2170-2179, 1995.
4. H. Martens, and T. Naes, *Multivariate Calibration*, John Wiley and Sons, New York, 1989.
5. M.P. Nelson, J.F. Aust, J.A. Dobrowolski, P.G. Verly, and M.L. Myrick, "Multivariate Optical Computation for Predictive Spectroscopy," *Anal.Chem.* **70**, pp 73-82, 1998.
6. M.P. Nelson, J.F. Aust, J.A. Dobrowolski, P.G. Verly, and M.L. Myrick, "Multivariate Optical Computation for Predictive Spectroscopy," *Proc.SPIE-Int.Soc.Opt.Eng (Three Dimensional and Multudimensional Microscopy: Image Acquisition and Processing).* **3261**, pp 232-243, 1998.
7. M.L. Myrick, O. Soyemi, J. Karunamuni, D. Eastwood, H. Li, L. Zhang, and P. Gemperline, "A Single-Element All-Optical Approach to Chemometric Prediction," *Fres.J.Anal.Chem.* (submitted 2000).

8. B.T. Sullivan, and J.A. Dobrowolski, "Deposition of Metal/Dielectric Multilayer Filters," Appl.Opt. **32**, pp 2351-2360, 1993

9. H.M. Liddell and O.S Heavens, *Optica.Acta.*, **15**, pp 129.

1 0 A.V. Tikhonravov, "Optical Coating Synthesis using Optimal Conditions," *Vestn.Mosk.Univ., Ser.3: Fiz., Astron.* **23**, pp 91-93,1982.

11. H.M. Liddell, *Computer-Aided Techniques for the Design of Multilayer Filters,* Adam Hilger Ltd., Bristol, UK, 1981.

12. J.E Dennis Jr,., R.B. Schnabel,. *Numerical Methods for Unconstrained Optimization and Nonlinear Equations*, Prentice-Hall, Inc., Englewood Cliffs, NJ, 1983.

13. T.F. Coleman, M. Branch, A. Grace, *MATLAB Optimization Toolbox: User's Guide*, Mathworks Inc., Natick, MA, 1999.

14. C.G. Broyden, "The Convergence of a Class of Double-rank Minimization Algorithms," *J.Inst.Math.Applic.* **6**, pp 76-90, 1970.

15. R. Fletcher, "A New Approach to Variable Metric Algorithms," *Computer Journal.* **13**, pp 317-322, 1970.

16. D. Goldfarb, "A Family of Variable Metric Updates Derived by Variational Means," *Mathematics of Computing.* **24**, pp 23-26, 1970.

1 7. D.F. Shanno, "Conditioning of Quasi-Newton Methods for Function Minimization," *Mathematics of Computing.* **24**, pp 647-656, 1970.

18. M.L. Myrick, O. Soyemi, J. Karunamuni, D. Eastwood, H. Li, L. Zhang, and P. Gemperline. A Single-Element All-Optical Approach to Chemometric Prediction. *Vibrational Spectroscopy* (submitted, 2000)

Table captions

1. Relative amounts of components 1 and 2 in simulated calibration and validation spectra.
2. Performance characteristics of 10 best filters for the simulated calibration and validation data set using the random initialization method.
3. Performance characteristics of 5 filters for the BB-CV data set using the random initialization method.
4. Performance characteristics of 10 best filters for the simulated calibration and validation data sets using the PCR initialization method.

Table 1

	Calibration set		Validation set	
Std no.	Comp. 1	Comp 2	Comp. 1	Comp 2
1	0.8	0.8	0.9	0.9
2	1.2	0.8	1.1	0.9
3	0.8	1.2	0.9	1.1
4	1.2	1.2	1.1	1.1
5	1.0	1.0	1.0	1.0
6	1.0	1.0	1.0	1.0
7	1.0	1.0	1.0	1.0
8	1.4	1.0	1.3	1.0
9	0.6	1.0	0.7	1.0
10	1.0	1.4	1.0	1.3
11	1.0	0.6	1.0	0.7

Table 2:

No. initial layers	SEC	SEP	RMS avg	No. final layers
29	0.00950	0.00792	0.00875	27
28	0.00924	0.00802	0.00865	26
19	0.00923	0.00796	0.00862	17
29	0.00841	0.00875	0.00858	29
20	0.00885	0.00822	0.00854	14
30	0.00919	0.00782	0.00853	30
21	0.00909	0.00784	0.00849	21
20	0.00879	0.00794	0.00838	20
25	0.00728	0.00846	0.00789	23
15	0.00699	0.00794	0.00748	15

Table 3:

No. initial layers	SEC (μM)	SEP (μM)	RMS error	No. final layers
15	0.2587	0.4151	0.3459	15
20	0.2546	0.4025	0.3368	20
25	0.251	0.4026	0.3355	19
30	0.2435	0.3782	0.3181	24
35	0.2574	0.4167	0.3463	35

Table 4:

No. factors	No. initial layers	SEC	SEP	RMS error	No. final layers
2	22	0.01164	0.00808	0.01002	16
2	26	0.01143	0.00837	0.01002	22
1	21	0.01134	0.00827	0.00992	15
1	29	0.01134	0.00797	0.00980	25
1	22	0.01103	0.00802	0.00964	18
1	27	0.0108	0.00796	0.00949	27
2	30	0.01051	0.00807	0.00937	26
2	31	0.01051	0.00807	0.00937	26
2	23	0.01036	0.00803	0.00927	19
1	28	0.00952	0.00827	0.00892	22

Figure 1
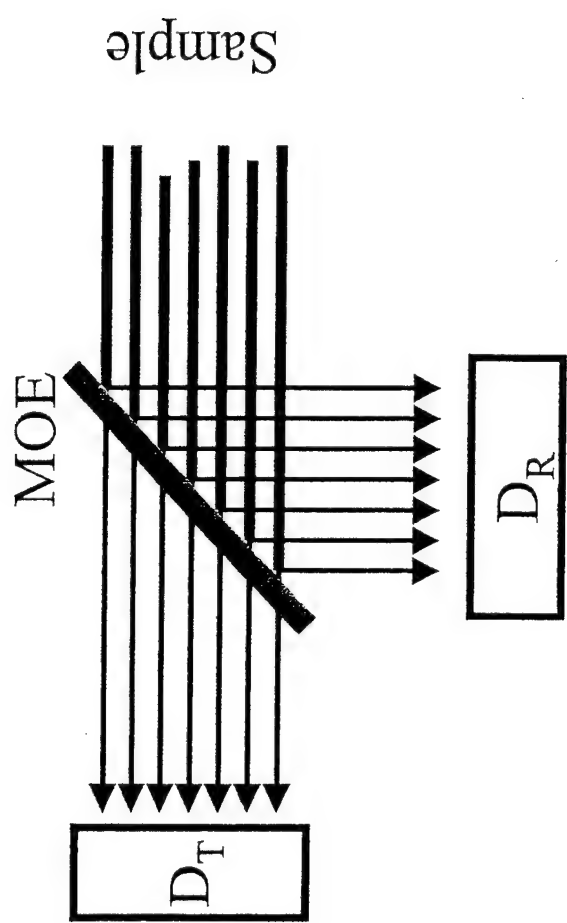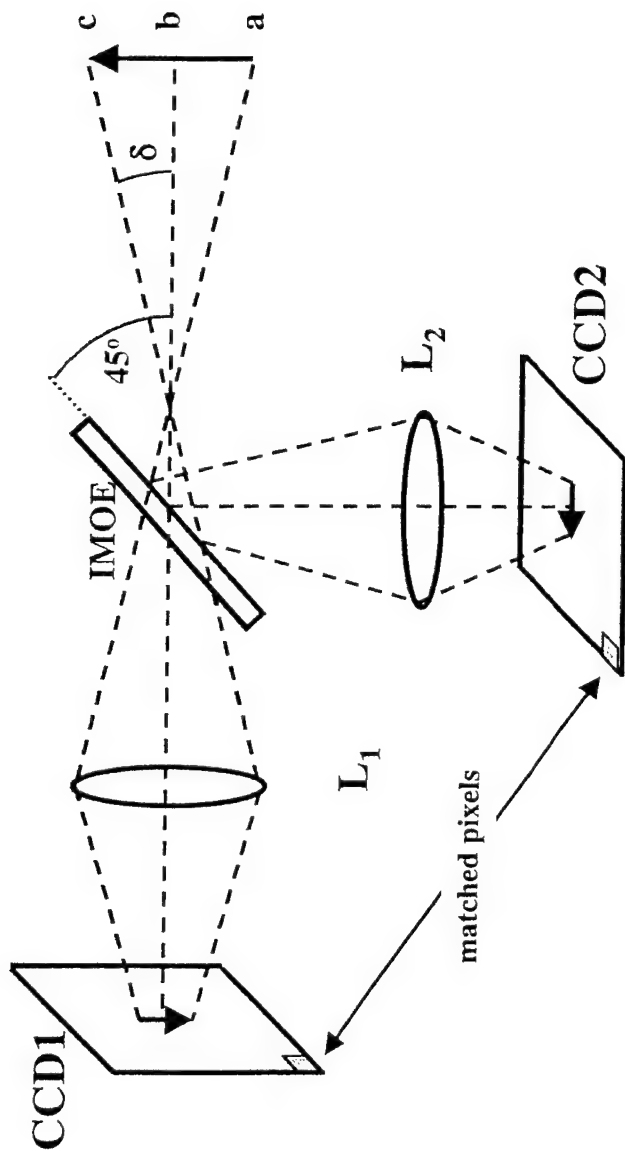
Sample

MOE

D_T

D_R

119

Figure 2

120

Figure 3

121

Figure 4

Figure 5

123
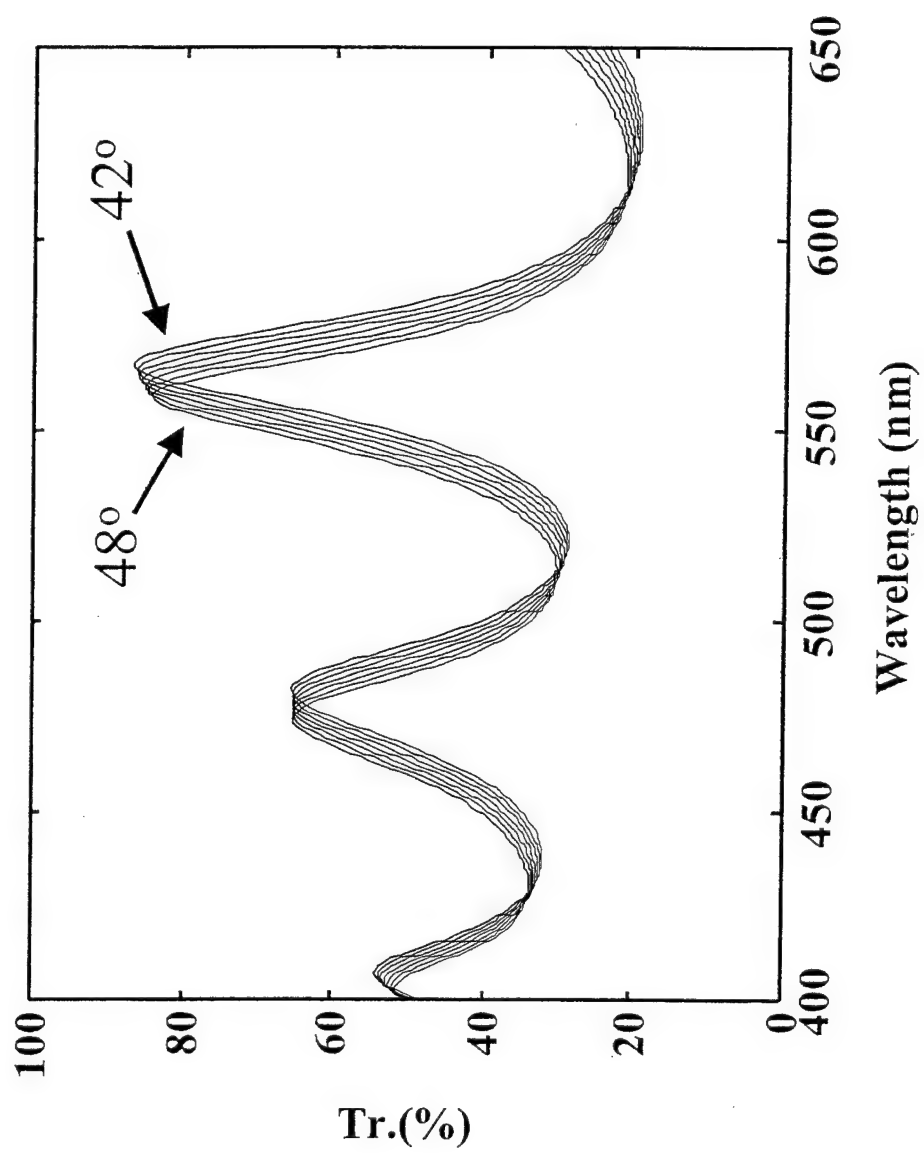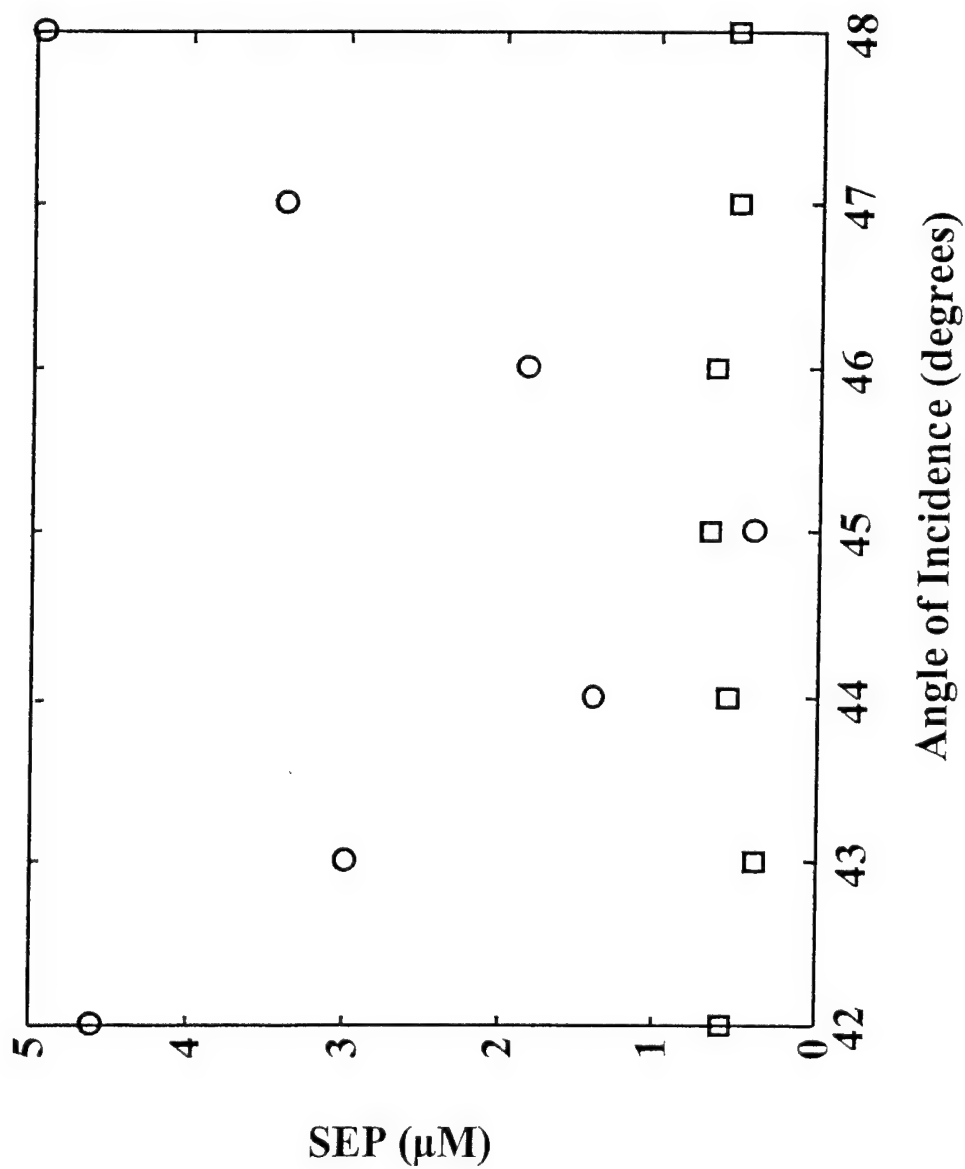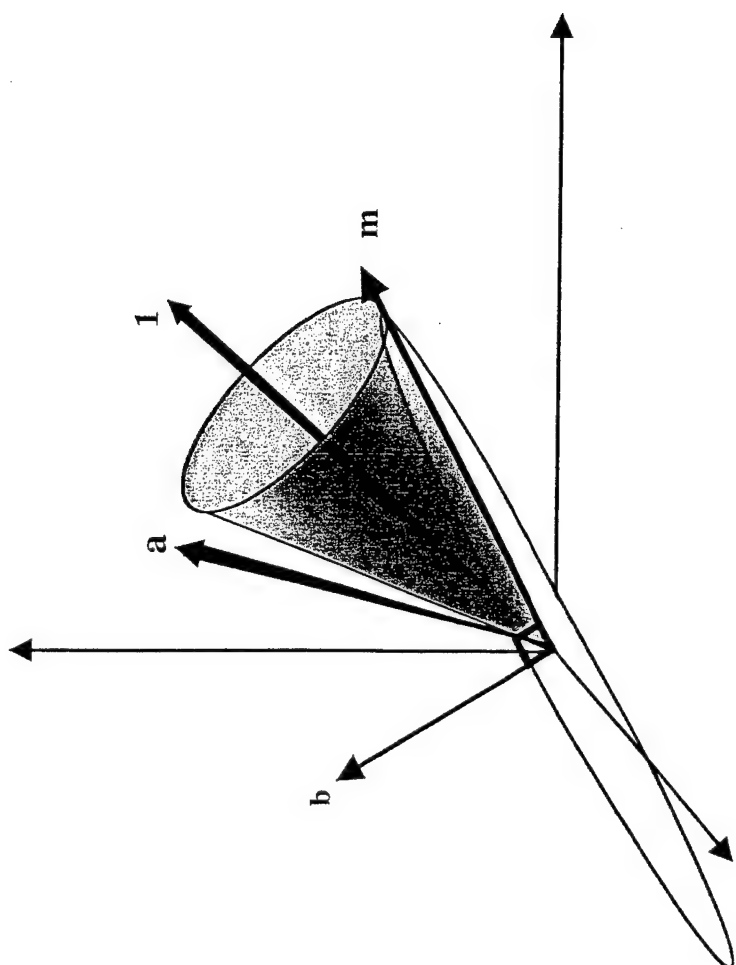
10.10 DESIGN OF ANGLE-TOLERANT MULTIVARIATE OPTICAL ELEMENTS OF CHEMICAL IMAGING

Design of Angle-Tolerant Multivariate Optical Elements for Chemical Imaging

O.O. Soyemi[1], P.J. Gemperline[2], M.L. Myrick[1*].

[1]Department of Chemistry and Biochemistry, University of South Carolina, Columbia, SC 29208.
[2]Department of Chemistry, East Carolina University, Greenville, NC 27858.

Multivariate optical elements (MOEs) are multilayer optical interference coatings with arbitrary spectral profiles that are used in multivariate pattern recognition to perform the task of projecting magnitudes of special basis functions ("regression vectors") out of optical spectra. Because MOEs depend on optical interference effects, their performance is very sensitive to the angle of incidence of incident light. This angle dependence frustrates their simple use in imaging applications. We report a method for the design of angle-insensitive MOEs based on modification of a previously described nonlinear optimization algorithm. This algorithm operates by simulating the effects of deviant angles of incidence prior to optimization, treating the angular deviation as an "interferent" in the measurement. In demonstrating the algorithm, a 13-layer imaging MOE (IMOE, with alternating layers of high index Nb_2O_5 and low index SiO_2) for the determination of Bismarck Brown dye in mixtures of Bismarck Brown and Crystal Violet, was designed and its performance simulated. For angles of incidence that range from 42° to 48°, the IMOE has an average standard error of prediction (SEP) of 0.55μM for Bismarck Brown. This compares to a SEP of 2.8 μM for a MOE designed by a fixed-angle algorithm.

---

[*] Author to whom correspondence should be addressed. Telephone: 803-777-6018. Fax: 803-777-9521. Email: myrick@mail.chem.sc.edu.

INTRODUCTION

Optical spectroscopy coupled with multivariate mathematics is routinely used in analytical chemistry for species quantification and chemical/biomedical imaging. However, the widespread application of this type of analytical spectroscopy has been limited by heavy reliance on bulky and expensive multichannel instruments, as well as the need for fast computing technology to process the vast amounts of multivariate data that are generated (1). In 1986, Bialkowski proposed that optical filters could be designed to aid in this process (2), an idea refined by Ryabenko in 1991 (AA) and our laboratory in 1998 (BB). In each of these studies, the use of an optical interference filter to project a spectral pattern out from collimated multiwavelength light was proposed, a simple form of optical computing. Recent reports of optical regression studies using conventional acousto-optical tunable spectrometer systems show the potential for such multivariate optical computing methods as supplements to, or replacements for, conventional spectrometer systems (Booksh,CC).

Our laboratory recently demonstrated this promise by designing, fabricating and characterizing the performance of an optical interference filter for a chemical measurement (4). These interference filters, which we refer to as multivariate optical elements or MOEs, permit the estimation of chemical properties based on the measurement of a spectral pattern. While conventional spectroscopy is still needed to characterize samples so that a suitable spectral pattern on which to base an analytical measurement can be found, MOEs permit the magnitude of these spectral patterns to be measured without the necessity of recording spectra for unknown samples.

126

A further application for MOEs is as color-separation-type elements in imaging systems. Hypothetically, an MOE can be designed to provide immediate imaging of chemical distributions. For instance, if light from a scene (the "source scene") transmitted through an MOE were imaged and mapped to the red channel of an RGB display, while the reflectance were imaged and mapped to the green and blue channels of the same display, the resulting image should contain an implicit color-coding of the MOE projection of the light source. However, this relatively simple concept is complicated by the angular distribution of light inherent in imaging systems.

In the demonstration of reference 4, a pinhole was used to define an approximate point source of light so that nearly collimated light could be used. MOEs, like other interference filters, have transmission spectra that are strongly angle-dependent. Since the transmission/reflection spectra of the MOE are key to its operation, a change of angle will deleteriously affect the chemical analysis performance of the MOE. Light that is incident on the MOE with an angular distribution will likewise degrade its performance.

In the present report, we describe a means for designing MOEs that are less sensitive to the angular distribution of light from a source scene. In this approach, imaging MOEs (IMOEs) are designed by simulating the effects of an angular distribution of light from the source scene. Iterative design of the IMOE then treats the angular distribution as an "interferent", a factor in the measurement that obscures the desired spectral content of the source scene, similar to the treatment of chemical species whose spectra overlap with and obscure the spectra of a chemical species of interest. The standard error of calibration for the IMOE is used as a figure of merit to be minimized by iterative solving, resulting in an

IMOE that minimizes both the contributions of chemical interferents and angular distribution of light in the source scene.

.

To illustrate this approach to IMOE design, we return to data from reference 4 for the measurement of the dye bismarck brown in a random mixed solution with the dye crystal violet (CV). The concentration of bismarck brown (BB) varied in the samples in the range 0-18 μM. We assume unpolarized light from the source scene and an angle of incidence of 45 $\pm$ 3 degrees. An MOE derived from a fixed-angle design algorithm resulted in a SEP of 2.8 μM when employed in this simulated imaging application. For comparison, a MOE designed by the distributed-angle algorithm resulted in a 0.55 μM SEP.

EXPERIMENTAL

The binary dye (bismarck brown-BB, and crystal violet-CV) data used in this study have previously been described (4). In brief, optical transmission spectra of the dye mixture from 400 nm to 650 nm were convolved with the spectral characteristics of the lamp source, the filter bandpass, and the detector, to provide an estimate of the radiometric response of a prototype measurement system as a function of wavelength. The MOE design algorithm was written in the MATLAB programming language (version 6).

RESULTS AND DISCUSSION

Multivariate Spectroscopy   In brief, conventional multivariate spectroscopy is used in analytical chemistry by finding multiwavelength patterns that correlate with chemical

analyses (e.g., octane ratings) of a set of calibration samples (e.g., gasolines). Once found, new (unknown) samples of the same type (gasolines) are analyzed by determining the magnitude of this pattern in the spectra of the unknowns. The magnitude of the pattern is evaluated by multiplying the intensity of the spectrum at each wavelength by the "loading" of the pattern at the same wavelength, and then summing the result over all wavelengths. This is illustrated symbolically in Equation 1 below:

$$1. \qquad y_i = \sum_{j=1}^{N} l(\lambda_j) \, x_i(\lambda_j)$$

where $l(\lambda_j)$ is the loading of the pattern at wavelength j, $x_i(\lambda_j)$ is the intensity of the spectrum of the ith mixture at wavelength j, y_i is the chemical analysis result, and j is an index that runs over all the N wavelengths of the spectrum.

Prediction of a desired property of an unknown is carried out by determining the magnitude of the spectral pattern in the optical spectrum of the sample. More specifically, the magnitude is calculated by taking the inner product of the regression vector and the optical spectrum of the unknown sample.

MOEs. MOEs make chemical predictions by effecting an optical computation equivalent to equation 1. As Figure 1 illustrates, MOEs are used as optical beamsplitters. They are designed so that their transmittance (on a scale of 0 to 1) at wavelength j can be expressed as:

$$2. \qquad T(\lambda_j) = 0.5 + k\,l(\lambda_j)$$

where k is a proportionality constant that is the same for all wavelengths. In the event that the MOE is free of absorption, the sum of the reflectance and transmittance of the

filter is unity at each wavelength, giving equation 3 for reflectance at the same wavelength.

$$3. \quad R\left(\lambda_j\right) = 0.5 - k l\left(\lambda_j\right)$$

Light coming from a sample at wavelength j with intensity $x_i(\lambda_j)$ is partially reflected by the MOE. If light from the sample at all N wavelengths strikes the MOE, then the total intensity of reflected light for sample i, $R_{t,i}$ is a sum over N as shown in Equation 4.

$$4. \quad R_{t,i} = \sum_{j=1}^{N}\left(0.5 - k l\left(\lambda_j\right)\right) x_i\left(\lambda_j\right) = 0.5 \sum_{j=1}^{N} x_i\left(\lambda_j\right) - k \sum_{j=1}^{N} l\left(\lambda_j\right) x_i\left(\lambda_j\right)$$

The corresponding equation for the total transmitted light is given in equation 5:

$$5. \quad T_{t,i} = 0.5 \sum_{j=1}^{N} x_i\left(\lambda_j\right) + k \sum_{j=1}^{N} l\left(\lambda_j\right) x_i\left(\lambda_j\right)$$

If the magnitude of these two total intensities is measured with a corrected detector, the difference between the two is:

$$6. \quad \left(T_{t,i} - R_{t,i}\right) = 2 k \sum_{j=1}^{N} l\left(\lambda_j\right) x_i\left(\lambda_j\right) = 2 k y_i$$

In other words, the difference between the transmittance and reflectance of an MOE, when detected with a corrected detector, is directly proportional to the chemical (or physical) property for which the regression pattern was developed. In practice, the spectral efficiency of the detector(s) is convoluted with the optical spectra prior to development of a regression pattern so that uncorrected detectors can be used on all N wavelengths in parallel.

IMOE Devices: The proposed schematic for a T-format IMOE-based imaging device is shown in Figure 2A. IMOE imaging is a straightforward extension from the discussion

of fixed-angle MOEs above, treating each set of matched pixels (of which one set is illustrated in the Figure) in the image detectors (CCD1 and CCD2) as matched point detectors.

If the spectral pattern of the MOE is designed with no offset (i.e., as shown in equation 6), then when the analytical result is zero, the transmittance and reflectance of the MOE are equal. When the MOE analytical result is nonzero, the reflectance and transmittance are unequal. Thus, if the transmitted image is mapped to (for example) the red channel while the reflected image is mapped to the green and blue channels of an RGB display, all channels should have the same intensity where the analytical result is zero. If an offset is included, then an offset to either the red or green/blue channels is necessary. The image displayed will therefore appear in pure grayscale where the analytical result is zero, presuming the display to be balanced appropriately. Where the analytical result is nonzero, either the red or green/blue channels will dominate. The degree to which one or the other dominates would be determined by the analytical result. Thus, the displayed image would appear as a grayscale image with an implicit colorcode that reveals the spatial distribution of the analytical result in its intensity and color. A complete MOC digital image is obtained without the benefit of the extensive investment in calculation time typical of conventional chemical imaging techniques (1).

Unfortunately, as comparison of Figures 1 and 2 shows, normal MOEs are designed for fixed angles of incidence – usually 45 degrees. IMOEs are required to function accurately at all angles around the centerline of the optical system up to the extremes defined by the field of view of the system. As Figure 2 illustrates, the IMOE is stationed forward of the lenses of the cameras to restrict the angles of incidence to a minimum

131

range. In the event of short working distances, a front lens would be necessary to accomplish this.

Design of Angle-Insensitive IMOEs: The design algorithm for MOEs in which radiation emanating from the sample is incident on the MOE at one angle has already been described (17). We refer to the algorithm as "spectral vector relaxation", or SVR, since it begins with a specific MOE spectrum and adjusts it to best fit the calibrated spectral data. The SVR design algorithm uses the quasi-Newton nonlinear optimization technique (18) to calculate an N-layer MOE whose spectrum \results in low analysis error for the chemical species of interest. The objective function (f(x)) to be minimized is the root mean squared error of calibration (RMSEC), and it is given by:

$$7. \qquad f(x) = RMSEC = \sqrt{\sum_{i=1}^{s} \frac{(y_i - \hat{y}_i)^2}{s}}$$

where s is the number of calibration samples, and y_i and $\hat{y}_i$ are the known and estimated concentrations for the ith sample respectively. At each iteration of the optimization process, the layer thicknesses (plus a scale and offset value) are adjusted to give a spectral vector from which $\hat{y}_i$ and subsequently f(x) are calculated. The RMSEC is typically calculated from a spectral vector that is evaluated at an angle of incidence of 45°. By replacing the RMSEC with an objective function that describes the mean RMSEC (i.e. $\overline{RMSEC}$) evaluated from several spectral vectors representing various angles of incidence, it is possible to design an MOE whose performance is relatively insensitive to spectral shifts that result from these angles of incidence. For each value (δ)

132

of the angle of incidence relative to 45 degrees, the concentration estimate for the ith sample ($\hat{y}_{i,\delta}$) is evaluated as:

$$8. \qquad \hat{y}_{i,\delta} = \mathbf{x}_i \, {G}\big/{m} \, [2T(l)_\delta - 1] + \text{off}$$

where $T(\lambda)_\delta$ is the transmittance of the MOE as a function of the wavelength, λ, and the angle of incidence δ, and m is the number of digitized wavelengths in the spectrum. $\overline{RMSEC}$ is determined for all values of δ.

Performance Simulation. Using the response profiles of 25 calibration sample mixtures of BB and CV, an IMOE was designed for BB analysis using angles of incidence in the range of 42° to 48°. The design of the IMOE is shown in Table I; it consists of 13 alternating layers of niobium pentoxide (Nb_2O_5) and silicon dioxide (SiO_2) on a BK-7 glass substrate, and is shown in Table 1. Other materials are also suitable for this design process. Nb_2O_5 and SiO_2 were selected because they are both produced in our laboratory and accurate optical constants for the materials produced in our deposition apparatus (a reactive sputtering system) have been measured via spectroscopic ellipsometry. The shift in the IMOE spectrum as the angle of incidence is varied from 42° to 48° is shown in Figure 3. The same calibration samples were utilized in the design of a 15-layer MOE using the conventional SVR algorithm at a 45° angle of incidence. For both designs, an optimal standard error of prediction (SEP) was calculated from 15 validation samples that were not included in the MOE/IMOE design process. The SEP is a measure of how well a MOE can predict future samples. It is defined by equation 9 below.

$$9. \qquad SEP = \sqrt{\frac{\sum_{i=1}^{p} (y_{i,val} - \hat{y}_{i,val})^2}{p}}$$

In equation 9, p is the number of validation samples, $y_{i,val}$ and $\hat{y}_{i,val}$ are the true and estimated values of the test sample concentrations respectively. A plot of the SEP for both MOEs versus angle of incidence clearly shows that the SEP for the modified SVR algorithm is relatively constant within the range of incident angles selected (Figure 4). On the other hand, the predictive performance of the MOE designed with the fixed-angle SVR algorithm sharply degrades when the angle of incidence is varied by even ±1.

The optimum SEP for the MOE designed with the fixed-angle SVR algorithm at 45° (0.4µM), is better than the average SEP for the MOE designed using the modified SVR algorithm (0.55µM). However, the loss in average predictive ability is more compensated by the robustness of the IMOE over multiple angles of incidence. Even slight variations (less than 1°) in the angle of incidence for a fixed-angle MOE may severely compromise its performance.

The rationale behind the ability to design angle-invariant IMOEs is as follows. As Figure 3 illustrates, the first-order effect of a change in the angle of incidence is to shift the IMOE spectrum to longer or shorter wavelength. Spectra can be represented by vectors in m-dimensional space, where m is the number of wavelengths in the spectrum. The IMOE spectrum can likewise be visualized as a vector in such a space. A shift of the IMOE spectrum to longer or shorter wavelengths corresponds to a rotation of the IMOE vector in this hyperspace around an axis defined by a vector of ones.

This picture of an IMOE vector is represented in three dimensions in Figure 5. In this Figure, the spectrum of an interferent is shown by the vector **b**. The interferent spectrum would have no projection on any of the vectors lying in the plane normal to **b**, and thus vectors in this plane would be candidates for the analysis of a chemical analyte, **a**, in the presence of **b**. For a two component mixture with an analyte vector that is not coincident with **b**, each of the vectors in the plane normal to **b** (the plane of the white ellipse in Figure 5) would work for the measurement of the analyte vector, **a**. The sole exceptions to this statement would be the two vectors in the plane that are orthogonal to both vectors. The remaining vectors in the plane would, of course, show different qualities of performance, depending on their overlap with the analyte vector, **a**.

The projection of a vector of ones onto the plane normal to the interferent vector represents an IMOE whose cone of rotation with varying angle of incidence is tangent to this plane. Such an IMOE is least subject to increased interference upon a change in the angle of incidence. The overlap of the IMOE vector with the analyte vector, **a**, may change when this occurs, thus changing the instrument gain for different angles of incidence. This effect will generally result in an "average" gain for a given range of angles of incidence. For a significant range of angles, the optimum IMOE spectrum would be one whose cone is not exactly tangent to the plane normal to the interferent, but which passes through the plane at two angles of incidence. This effect is observed in the results of Figure 4, where the SEP for 45° angle of incidence is a local maximum, with minima to either side corresponding to the angles at which the IMOE vector passes through a plane orthogonal to the spectral vector of the interference, CV.

CONCLUSIONS

We have described an algorithm enabling the design of IMOEs for multiwavelength operation by modeling of the angle-dependence of the IMOE spectrum during the design process. This opens the path toward chemical imaging systems based on the multivariate optical computing concept.

Chemical imaging devices that are based on simple optical computing elements may be a powerful yet simple alternative to current chemical imaging technology in certain applications. These devices promise substantially smaller, lighter instruments for imaging. In addition, the total absence of spectrometers and complicated data analysis could potentially extend imaging technology to everyday, non-specialist applications.

REFERENCES

1. P. Geladi, H. Grahn. "Multivariate Image Analysis," John Wiley and Sons Inc.: New York, 1996.

2. S. Bialkowski, Anal.Chem. 58, 2561-2563 (1986).

3. M.P. Nelson, J.F. Aust, J.A. Dobrowolski, P.G. Verly, M.L. Myrick, "Multivariate Optical Computation for Predictive Spectroscopy," Anal.Chem. 70, 73-82 (1998).

4. O. Soyemi, D. Eastwood, L. Zhang, H. Li, J. Karunamuni, P. Gemperline, R.A. Synowicki, M.L. Myrick, "Design and Testing of a Multivariate Optical Element: The First Demonstration of Multivariate Optical Computing for Predictive Spectroscopy," Anal.Chem. 73, 1069-1079 (2001).

5. A. Kasparov, V. Ryabenko, Pattern Recognit. Image Anal. 1, 347-354 (1991).

6. J.L. Vossen, K. Kern, "Thin-Film Processes," Academic Press: San Diego, 1991.

7. V.R. Costich, "Reduction of Polarization Effects in Interference Coatings," App.Opt. 9, 866-870 (1970).

8. A. Thelen, "Nonpolarizing Interference Filters Inside a Glass Tube," Appl.Opt. 15, 2983-2985 (1976).

9. Z. Knittl, H. Houserkova, "Equivalent Layers in Oblique Incidence: The Problem of Unsplit Admittance and Depolarization of Partial Reflectors," Appl.Opt. 21, 2055-2068 (1982).

10. C.M. de Sterke, C.J. van der Laan, H.J. Frankena, " Nonpolarizing Beamsplitter Design," Appl. Opt. 23, 595-601 (1983).

11. M. Gilo, "Design of Nonpolarizing Filters Inside a Glass Cube," Appl.Opt. 31, 5345-5349 (1992).

12. A. Thelen, "Nonpolarizing Edge Filters," J.Opt.Soc.Am. 71, 309-314 (1981).

13. A. Thelen, "Nonpolarizing Edge Filters: Part 2" Appl.Opt. 23, 3541-3543 (1984).

14. A.V. Tikhonravov, "Optical Coating Synthesis Using Optimal Conditions," Vest.Mosk.Univ.,Ser.3:Fiz.Astron. 23, 91-93 (1982).

15. G.W. DeBell, A.V. Tikhonravov, "Use of a New Synthesis Algorithm to Design Polarization Insensitive Optical Coatings," M.K. Trubetskov, Proc.SPIE. 2262, 187-193 (1994).

16. M.L. Myrick, O. Soyemi, H. Li, L. Zhang, D. Eastwood, "Spectral Tolerance Determination for Multivariate Optical Element Design," Fresenius J.Anal.Chem. 369, 351-355 (2001).

17. O. Soyemi, P. Gemperline, M.L. Myrick, "A Nonlinear Optimization Algorithm for Multivariate Optical Element Design," submitted to Appl.Spectr. (2001).

18 J.E. Dennis Jr., R.B. Schnabel, "Numerical Methods for Unconstrained Optimization and Nonlinear Equations," Prentice-Hall Inc.: Englewood Cliffs, NJ 1983.

Layer No.	Material	Layer Thickness (nm)
1	Nb_2O_5	97.76
2	SiO_2	68.87
3	Nb_2O_5	94.50
4	SiO_2	66.80
5	Nb_2O_5	57.72
6	SiO_2	49.04
7	Nb_2O_5	60.75
8	SiO_2	31.66
9	Nb_2O_5	90.12
10	SiO_2	22.29
11	Nb_2O_5	112.03
12	SiO_2	133.39
13	Nb_2O_5	81.59

Table 1. 13-Layer polarization insensitive MOE design for the determination of Bismarck Brown in a Binary Mixture with Crystal Violet
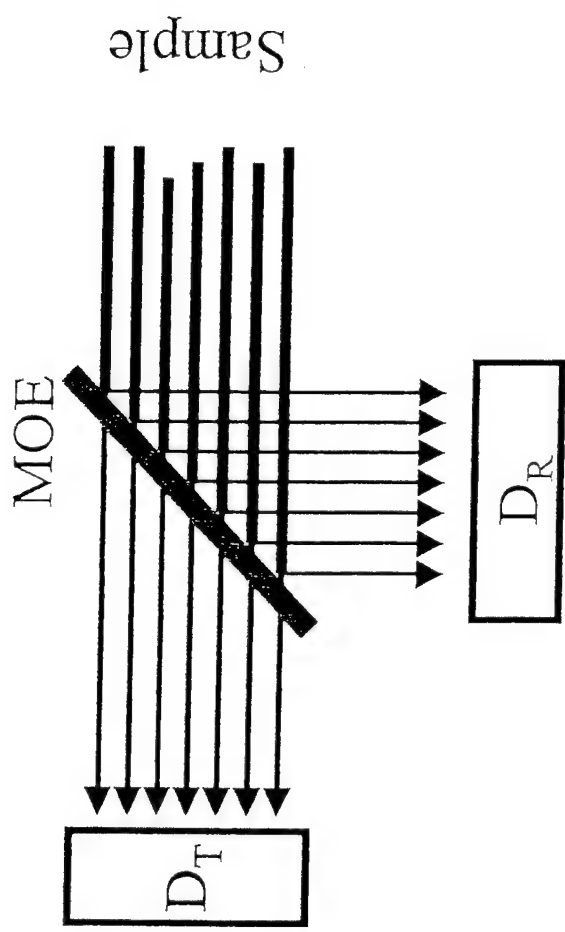
Figure 1. Concept for use of multivariate optical elements. DT and DR are detectors for transmitted and reflected light, respectively. MOE represents a multivariate optical element.
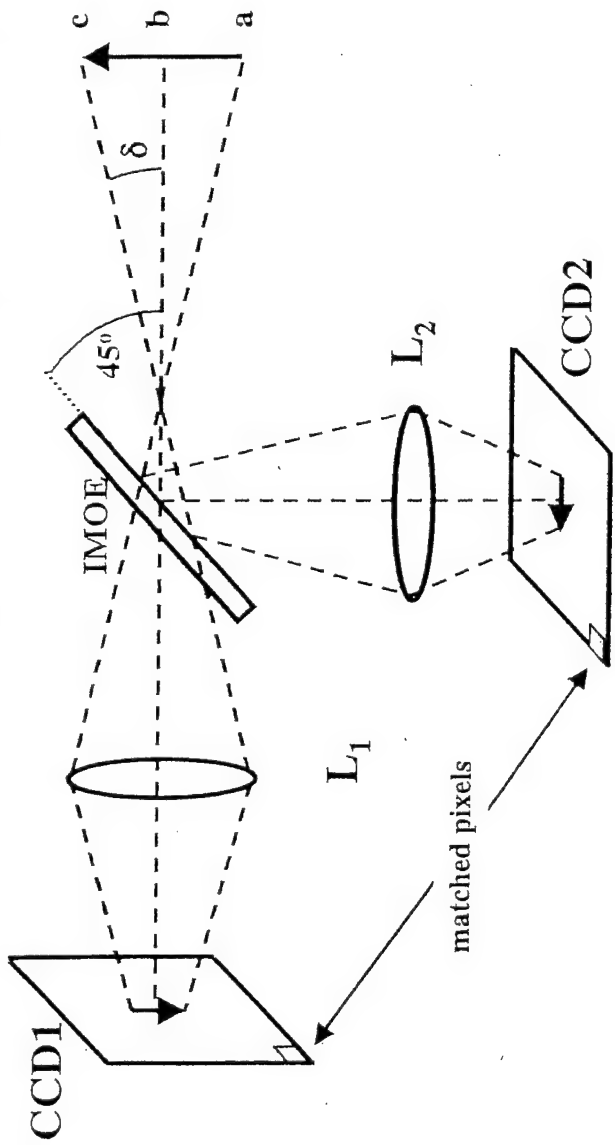
Figure 2. Schematic of a T-format multivariate optical computation device. Radiation from the sample is split by a multivariate element (MOE) as in Figure 1. L_1 and L_2 are focusing lens. CCD1 and CCD2 are charge-coupled detectors for transmitted and reflected light, respectively. Light paths marked a, b and c represent the maximum, mean and minimum angles of incidence of the light passing through the MOE. Pixel-by-pixel ... but computations are created by combining the detected light in the transmitted channel with that in the reflected channel. Pixels in both channels are matched together so that the portion of the source scene viewed by each is the same.

141
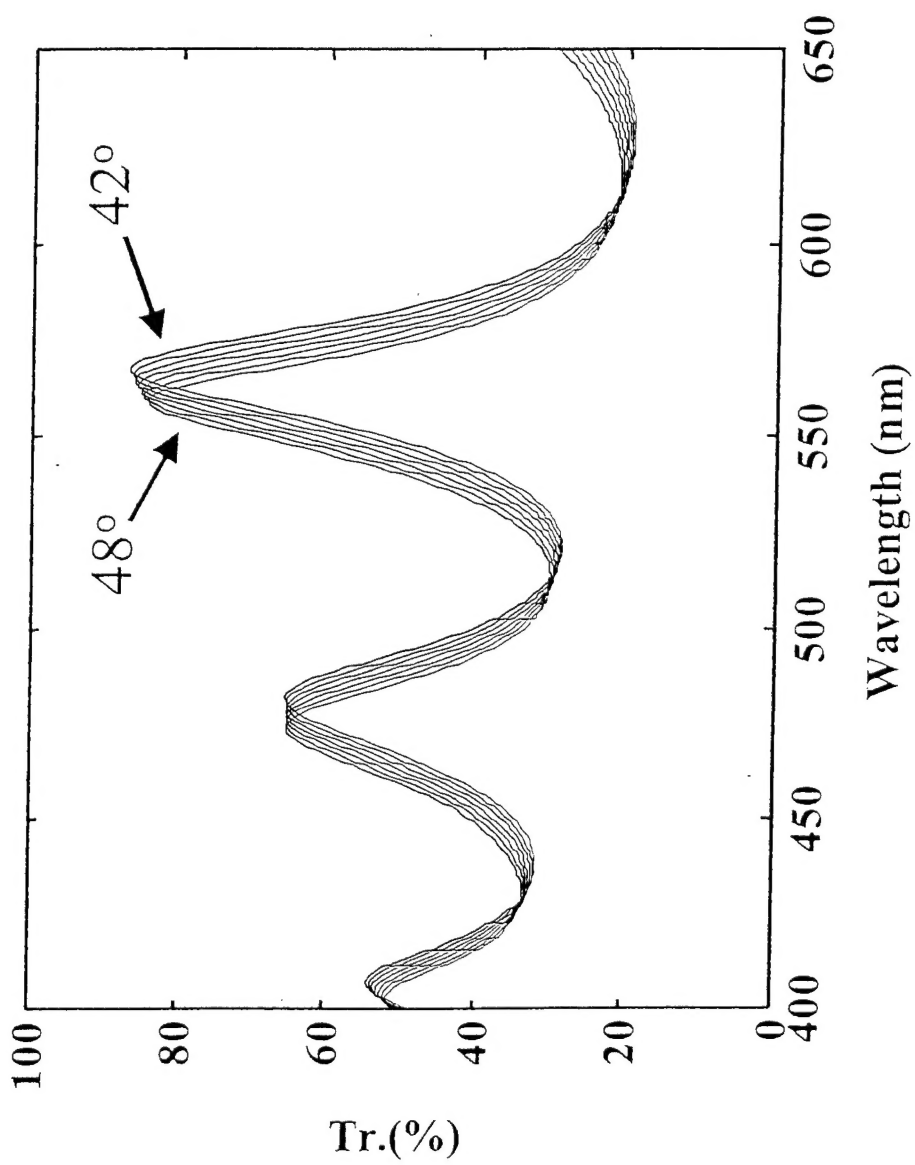
Figure 3. Transmittance spectra of a 13-layer MOE designed from the modified SVR algorithm at angles of incidence ranging from 42° to 48°.
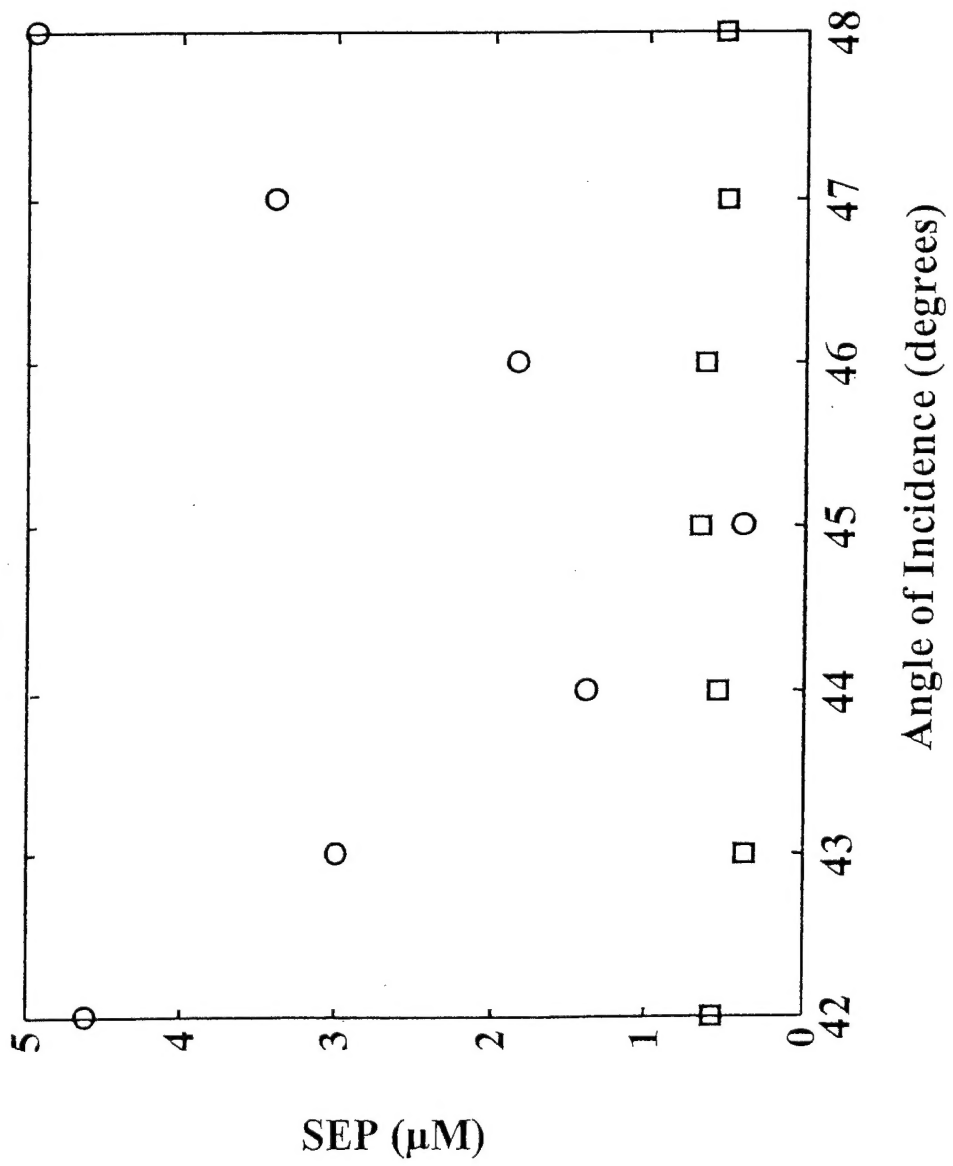
Figure 4. Comparison of the SEP for 15-layer MOE designed using the fixed-angle SVR algorithm (circles) with the MOE in Figure 3 (squares), at angles of incidence ranging from 42° to 48°.
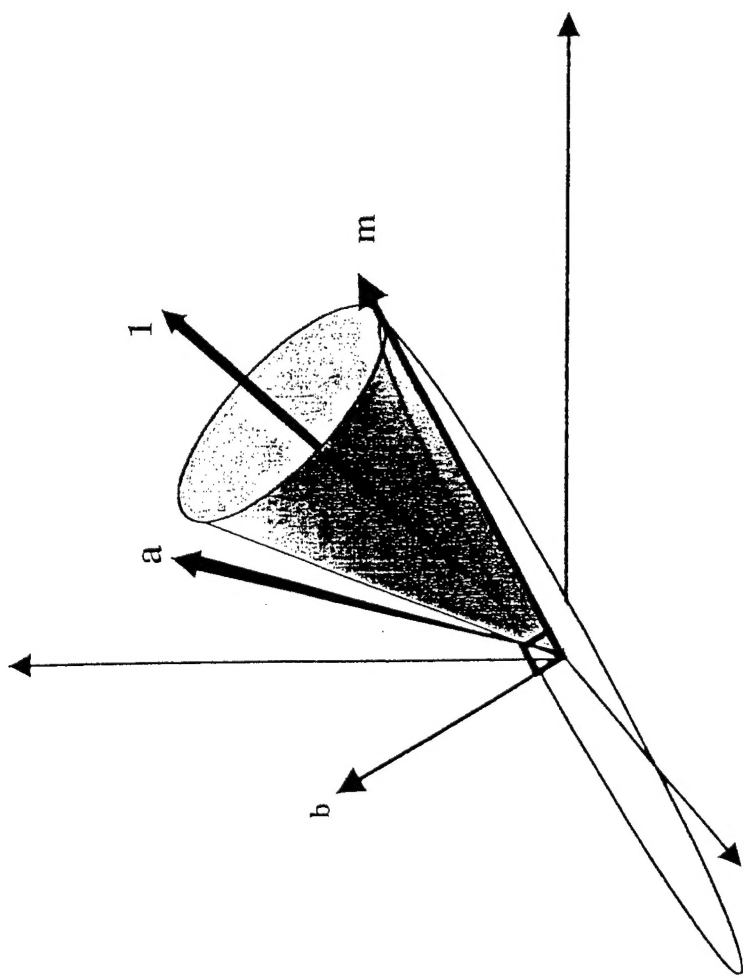
Figure 5. Vectorial illustration of an angle-insensitive IMOE spectrum. **l** = a vector of

ones. **a** = vector of an analyte. **b** = vector of an interfering species. **m** = vector

[...] The white circle is in a plane perpendicular to **b**.

[...] projection of **m** around **l**

144

LIST OF ORGANOPHOSPHORUS COMPOUNDS WHOSE SPECTRA HAVE BEEN MEASURED AT THE USC LABORATORY

Compound	MIR	NIR	Raman
Sand/white quartz (NIR)		X	
Methylphosphonic acid (NIR)		X	X
Dimethylmethylphosphonate	X	X	X
Methamidophos	X	X	
Trimetylphosphate	X	X	X
Dichlorvos	X	X	X
Hexamethylphosphoric triamide	X	X	X
Pinacolyl methylphosphonate	X	X	X
Dimethoate (NIR)		X	X
Dylox (NIR)		X	X
Dibrom	X	X	
Phorate	X	X	X
Prophos	X	X	X
Demeton O & S	X	X	
Disulfoton	X	X	X
Dyfonate	X	X	
Monocrotophos	X	X	X
Phosdrin	X	X	X
Dicrotophos	X	X	X
Terbufos	X	X	
Zinophos (NIR)		X	
Fenchlorphos (NIR)		X	X
Methylparathion (NIR)		X	X
Tetraethylpyrophosphate	X	X	
Tetraethyldithiopyrophosphate	X	X	
Tributylphosphorotrithioate	X	X	X
Trichloronate	X	X	
Carbophenothion	X	X	X
Chlorpyrifos (NIR)		X	X
Fensulfothion	X	X	
Parathion	X	X	X
Phosphamidon	X	X	X
Sulprofos (NIR)		X	X
Diazinon	X	X	
Ethion	X	X	X
Famphur (NIR)		X	X
Guthion (NIR)		X	
Imidan (NIR)		X	X
Malathion	X	X	X
Tetrachlorvinphos (NIR)		X	X
Chlorfenvinphos	X	X	
Leptophos (NIR)		X	X
Crotoxyphos	X	X	
EPN (NIR)		X	X
Guthion ethyl (NIR)		X	X
Coumaphos (NIR)		X	X
Dioxathion	X	X	X
Sulfometuron methyl (NIR)		X	X
Fenthion			X